TURBULENT EDDIES IN BOUNDARY LAYERS ON SMOOTH AND ROUGH FLAT PLATE

by

Shamsuzzaman Chowdhury

Prepared under

U. S. Army Research Grant DA-AMC-28-043-G20
U. S. Army Materiel Command
Washington 25, D. C.

FLUID MECHANICS PROGRAM
ENGINEERING RESEARCH CENTER
COLLEGE OF ENGINEERING

COLORADO STATE UNIVERSITY
FORT COLLINS, COLORADO

Technical Report

TURBULENT EDDIES IN BOUNDARY LAYERS ON SMOOTH AND ROUGH FLAT PLATE

by

Shamsuzzaman Chowdhury

Prepared under

U. S. Army Research Grant DA-AMC-28-043-G20
U. S. Army Materiel Command
Washington 25, D. C.

Fluid Mechanics Program
College of Engineering
Colorado State University
Fort Collins, Colorado

March 1966

CER65SC-EJP57

ABSTRACT OF THESIS

TURBULENT EDDIES IN BOUNDARY LAYERS
ON SMOOTH AND ROUGH FLAT PLATE

This study represents one in a series of boundary layer investigations which are undertaken in order to obtain a definition of the roughness characteristics of a surface from the turbulence structure in the boundary layer near the surface. It is attempted to discuss the effect of the roughness in the structure of the turbulent eddies found near the boundary by comparing space correlations and spectra which were measured in the boundary layer on smooth and rough flat plates.

The experimental investigations were made with a flat plate placed at a height of 2.0 ft. from the floor of a wind tunnel which had a 6 ft. x 6 ft. cross-section. The size of the plate used was 6 ft. x 3 ft. To obtain a rough surface condition, gravel which passed through a #7 sieve and are retained on a #8 sieve was glued to the surface of the aluminum plate. The density of the roughness material was 120 particles per square inch.

Mean velocity profiles were measured on six stations with ambient air velocity of 30 fps at a condition of zero pressure gradient which were obtained by constructing a false ceiling to the wind tunnel roof. The measurements were analyzed

in terms of the "wall law" and the "velocity-defect law" for smooth walls, and agreement with the work of other investigators was found. The logarithmic part of the velocity distribution curve for the rough boundary is shifted parallel to the smooth curve by an amount $\Delta u/u_* = 12$.

The turbulence signals were recorded on magnetic tape. They were obtained by using two single hot-wires, one of which was fixed in position and embedded in the plate surface and the other was mounted on a probe actuator whose position was varied freely in x, y and z directions with respect to the fixed probe. From these data, the turbulent intensities, turbulent spectra, total space correlations and filtered space correlations were determined electronically. Comparison of the results for smooth boundary with those for the rough boundary shows that the smooth surface eddy retains the correlation coefficients for a longer time than that of the rough surface case. The parameter to define the roughness characteristic in the velocity field from the measurement of space correlations was expressed in terms of L_{xs}/L_{xr} where L_{xs} and L_{xr} is the mean eddy size for smooth and rough boundary respectively.

Shamsuzzaman Chowdhury
Civil Engineering Department
Colorado State University
Fort Collins, Colorado
March 15, 1966

ACKNOWLEDGEMENTS

The writer wishes to express sincere gratitude to his major professor, Dr. Erich J. Plate, Associate Professor of Civil Engineering Department, for his encouragement and contributions have made this thesis possible.

The writer wishes to thank his research committee: Dr. Jack E. Cermak, Professor, Mr. Virgil A. Sandborn, Associate Professor of the Civil Engineering Department, and Dr. Patricia M. Prenter, Assistant Professor of Mathematics Department, for the time and valuable suggestions given in reviewing this thesis.

Appreciation is extended to those who assisted in the collection of data, drafting and typing the thesis: Mr. H. M. Tan, Mr. H. Shokouh, Miss H. Akari and Mrs. Mary Fox.

An expression of gratitude is given to the United States Army Materiel Command for the financial support under research grant DA-AMC-28-043-65-G20.

TABLE OF CONTENTS

Chapter		Page
	ABSTRACTS	ii
	ACKNOWLEDGEMENTS	v
	LIST OF TABLES	ix
	LIST OF FIGURES	x
	LIST OF SYMBOLS	xv
I	INTRODUCTION	1
II	REVIEW OF LITERATURE	3
	A. Mean Velocity Distribution on a Rough Flat Plate	3
	1. Smooth Surface	5
	2. Rough Surface	7
	B. Space-Correlation Distribution on Flat Plate	11
	1. Space Correlation	11
	2. Double Velocity Correlation	12
III	EXPERIMENTAL EQUIPMENT AND PROCEDURE	17
	A. Experimental Equipment	17
	1. Wind Tunnel	17
	2. Flat Plate	18
	a. Smooth surface	18
	b. Rough surface	19

TABLE OF CONTENTS (continued)

Chapter		Page
	3. Carriage	19
	4. Hot-Wire Anemometer	20
	5. Micromanometer	20
B.	Experimental Procedure	21
	1. Measurement of Pressure Gradient along the Flat Plate	21
	2. Measurement of Mean Velocity	23
	3. Hot-wire Probes	23
	a. Calibration of hot-wires	24
	b. Measurement of turbulent intensity	25
	c. Recording of turbulence intensity signals	26
	d. Frequency response of the recorder-amplifier	28
	4. Total Space Correlations	29
	a. Calibration of sum and difference circuit	30
	5. Filtered Space Correlations	31
	a. Calibration of filters (or spectrum analyzers)	31
	6. Error in Procedure	32

TABLE OF CONTENTS (continued)

Chapter		Page
IV	ANALYSIS OF EXPERIMENTAL DATA	34
	A. Mean Velocity Field	34
	1. Wall Law	35
	2. Velocity Defect-Law	35
	3. Development of δ along the Smooth Plate	36
	4. Determination of Shear Velocity (u_*) . .	39
	a. Logarithmic law of velocity distribution method	40
	b. Momentum integral equation method.	40
	B. Turbulence Field.	44
	1. Turbulent Intensity	44
	2. Space Correlation Measurements	45
	a. Total space correlation measurements	45
	b. Filtered space correlation measurements	47
V	CONCLUSIONS AND RECOMMENDATIONS	51
	BIBLIOGRAPHY.	55
	APPENDIX - A	58
	Calculation of Total Space Correlations	58
	Calculation of Filtered Space Correlations . . .	60
	APPENDIX - B TABLES.	62
	APPENDIX - C FIGURES	66

LIST OF TABLES

Table		Page
1.	Basic data for smooth flat plate (velocity field). .	62
2.	Basic data for rough flat plate (velocity field). . .	63
3.	Comparison of the values of δ , u_* and R_e . . .	64
4.	Eddy sizes for smooth and rough flat plates . . .	65

LIST OF FIGURES

Figure		Page
1.	Plan view of wind tunnel	66
2.	Test section geometry	67
3.	Plan of smooth and rough flat plate	68
4.	Cross-section elevation of smooth and rough flat plate	69
5. a.	Carriage used for mean velocity data recording .	70
b.	Carriage used for space correlation data recording	70
6. a.	Calibration of two hot-wires (against pitot tube) .	71
b.	Calibration of hot-wires (one against the other) .	71A
7.	Non-dimensional plot of pressure distribution along the flat plate	72
8.	False wind tunnel ceiling to obtain zero pressure gradient on flat plate	73
9.	The total pressure tube	74
10. a.	Experimental arrangement for calculation of turbulent intensities	75
b.	Experimental arrangement for calibration of sum and difference circuit	75
11.	Details of the space correlation measuring probes	76
12.	Experimental arrangement for recording of turbulence signals	77

LIST OF FIGURES (continued)

Figure		Page
13.	Experimental arragement for frequency response of tape recorder-impendance matching amplifier	78
14.	Experimental arrangement for total correlation measurements	79
15.	Experimental arrangement for filtered correlation measurements	80
16.	Turbulent boundary layer profiles at zero pressure on smooth and rough flat plate	81
17.	Universal velocity distribution for turbulent layers on smooth and rough flat plate	82
18.	Universal plot of turbulent boundary layer profiles at zero pressure on flat plate	83
19.	Variation of form factor with distance	84
20.	Determination of slope(m) from values of δ and θ (C_L) on smooth plate	85
21.	Comparison of artificially and naturally developed boundary layer thickness	86
22.	Development of boundary layer thickness	87
23.	Distribution of shear velocity along C_L	88
24.	Development of momentum thickness	89
25.	Development of displacement thickness	90
26.	Development of wall friction with Reynolds number	91

LIST OF FIGURES (continued)

Figure		Page
27.	Velocity defect law on smooth flat plate	92
28.	Velocity defect law on rough flat plate	93
29.	Effect of roughness on universal turbulent velocity profiles	94
30.	Distribution of turbulence intensities on smooth flat plate	95
31.	Distribution of turbulence intensities on rough flat plate	96
32.	Diagramatic sketch of the flow model in the wall layers of the fully developed turbulent boundary layer after Kline and Runstadler	97
33.	Non-dimensional longitudinal space correlations on flat plate, f(x) vs x	98
34.	Non-dimensional transverse space correlations on flat plate, f(y) vs y.	99
35.	Non-dimensional vertical space correlation on flat plate, f(z) vs z	100
36.	Dimensional longitudinal space correlation on flat plate, R(x) vs x	101
37.	Dimensional transverse space correlations on flat plate, R(y) vs y	102
38.	Dimensional vertical space correlations on flat plate, R(z) vs z	103

LIST OF FIGURES (continued)

Figures		Page
39.	Surfaces of iso-correlations on x-y plane, R_1 .	104
40.	Surfaces of iso-correlations on x-y plane, R_2 .	105
41.	Surfaces of iso-correlations on y-z plane, R_3 .	106
42.	Picture of the eddy structure in (x-y-z) plane on smooth and rough flat plate	107
43.	Non-dimensional longitudinal filtered space correlations on flat plate, R(n) vs x, n = 20 c/s	108
44.	Non-dimensional longitudinal filtered space correlations on flat plate, R(n) vs x, n = 100 c/s	109
45.	Non-dimensional longitudinal filtered space correlations on flat plate, R(n) vs x, n = 200 c/s	110
46.	Dimensional longitudinal filtered space correlations on flat plate, R'(n) vs x, n = 20 c/s . .	111
47.	Dimensional longitudinal filtered space correlations on flat plate, R'(n) vs x, n = 200 c/s . .	112
48.	Non-dimensional spectrum of turbulence signal (#1) on flat plate for x = 0.0", 0.40", 0.80" and 1.50"	113
49.	Non-dimensional spectrum of turbulence signal (#2) on smooth flat plate for x = 0.0", 0.40", 0.80" and 1.50".	114

LIST OF FIGURES (continued)

Figure		Page
50.	Non-dimensional spectrum of turbulence signal (#2) on rough flat plate for x = 0.0", 0.40", 0.80" and 1.50"	115
51.	Non-dimensional spectrum of turbulence signal (#1) on smooth flat plate for z = 0.06", 0.08", and 0.10"	116
52.	Non-dimensional spectrum of turbulence signal (#1) on rough flat plate for z = 0.06", 0.08" and 0.10"	117
53.	Dimensional spectra of turbulence signal (#2) on smooth flat plate	118
54.	Dimensional spectra of turbulence signal (#2) on rough flat plate	119

LIST OF SYMBOLS

Symbol	Definition	Dimension
A, A', A'_1, A'_2	Constant	
A_3	Amplitude of sine wave	volt
B, B_1, B_2	Constant	
C, C_1, C_2,	Constant	
C_3, C_4, C_5	Constant	
c_f	Local skin friction	
D, D_1	Constant	
E_1	Constant	
f	Function	
$f(r)$	Definition of space correlation measurements. Eq. (59)	
$f(x)$	Longitudinal space correlation	
$f(y)$	Transverse space correlation	
$f(z)$	Vertical space correlation	
g, g_1, g_2	Function	
G, G_1, G_2	Constant	
h	Function	
Δh	Difference between dynamic and static pressure head	mm of Hg.
i	Instantaneous value of current	amp.
$\bar{I}_{ma}$	Mean current in milliampere	ma.

LIST OF SYMBOLS (continued)

Symbol	Definition	Dimension
j	Overheating ratio $j = R_w - R_a / R_a$	
k_r	Mean height of the roughness elements	in.
k, k_1, k_2	Constant	
K_1	Constant	
L_{xs}	Mean value of large eddy size in x-direction on smooth surface	in.
L_{xr}	Mean value of large eddy size in x-direction on rough surface	in.
m	Exponent used in Eq. (41)	
m_1	Slope of straight portion of logarithmic plotting of u/u_a vs z	
p_d	Dynamic pressure	lb/ft^2
p_s	Static pressure	lb/ft^2
Q, Q_1, Q_2	Rms value of the instantaneous velocity fluctuation	volt
R_a	Wire resistance at fluid temperature	ohm.
R_e	Reynolds number	
R_{e*}	Roughness Reynolds number	
$R(x)$	Dimensional longitudinal space correlation	$(ft/sec.)^2$

LIST OF SYMBOLS (continued)

Symbol	Definition	Dimension
$R(y)$	Dimensional transverse space correlation	$(ft/sec.)^2$
$R(z)$	Dimensional vertical space correlation	$(ft/sec.)^2$
R_w	Wire resistance	ohm.
$R(n)$	Longitudinal filtered space correlation, Eq. (60)	
$R'(n)$	Dimensional longitudinal filtered space correlation, $R'(n) = \overline{u'_{1(n)}\ u'_{2(n)}}$	$(ft/sec)^2$
R_1	Surfaces of iso-correlation in x-y plane	
R_2	Surfaces of iso-correlation in x-z plane	
R_3	Surfaces of iso-correlation in y-z plane	
R	Double velocity total space correlation, $R = \overline{u'_1\ u'_2}$	$(ft/sec)^2$
u	Instantaneous velocity component	ft/sec
u'	Turbulence velocity fluctuation	ft/sec
u_a	Free stream or ambient velocity	ft/sec
u_*	Shear velocity	ft/sec

LIST OF SYMBOLS (continued)

Symbol	Definition	Dimension
$\sqrt{\overline{u'^2}}$	Root-mean square value of the velocity fluctuation	ft/sec
V, V_1, V_2	Rms value of the instantaneous velocity fluctuation	volt
x , y , z	Coordinate system with origin at the beginning of the leading edge for mean velocity data and at the center of Station 3 for space correlation data, x is the longitudinal, y is the transverse and z is the vertical distance	in. or ft.
δ	Boundary layer thickness	in.
δ_s	Sublayer thickness	in.
δ^*	Displacement thickness	in.
θ	Momentum thickness	in.
τ	Shearing stress	lb/ft^2
τ_o	Wall shearing stress	lb/ft^2
μ	Dynamic viscosity	$(lb\ sec)/ft^2$
ρ	Density	$slug/ft^3$
ρ_a	Air density	$slug/ft^3$
ν	Kinematic viscosity	ft^2/sec
α	Temperature coefficient	
β	Exponent used in Eq. (17)	
γ_w	Specific weight of water	lb/ft^3

CHAPTER I

INTRODUCTION

There are numerous problems yet to be solved in fluid mechanics. Among them, one of the most important problems is to study the effect of roughness on the turbulent boundary layer. A mathematical solution is inaccessible to this problem due to the number of unknown parameters involved. Experimental investigations have been done by some researchers to find a solution to some aspects of the problem. A systematic and complete knowledge of the effect of the roughness characteristics on turbulent boundary layer is valuable for the accurate estimation of the skin friction, drag of ships, airplane bodies and lifting surfaces, etc.

The characterization of the roughness effect in a turbulent boundary layer involves a large number of parameters because of the great variety of possible geometrical forms of surface roughnesses. The complexity of the problem is reduced to a certain degree, when one single type of roughness element is considered. The flow on the surface with one single type of roughness element still does not depend only on the form and height of rough elements, but also on the density. Consideration is confined to geometrically similar roughnesses and the significant parameter is then reduced to one; this one being the height of the roughness element denoted

by k_r . The influence of k_r on the turbulence structure in a turbulent boundary layer is most pronounced near the boundary, and a definition of the roughness characteristic by a suitable parameter based on a measure of the turbulent structure appears feasible.

The main purpose of this study is to determine the difference of the structure of the turbulence field of smooth and rough flat plates from turbulent correlations and to compare the correlations with the measures of roughness based on the mean velocity profiles. For this, mean velocity profiles were measured as well as turbulence fluctuations which were recorded on magnetic tape, along smooth and rough surfaces on a flat plate. The mean velocity profiles give a measure of the roughness characteristic in terms of k_r and/or $\Delta u/u_*$, while the space correlations of turbulence fluctuations might give another measure, for the roughness perhaps in integral scale. An attempt was made to obtain an empirical relation between these two measurements.

The results of the mean velocity distributions are compared with those of other investigators. Correlation results for smooth and rough surfaces are compared in this study.

CHAPTER II

REVIEW OF LITERATURE

A review of literature pertinent to the present study is presented in this chapter. The problem of this study is to define a measure of the roughness characteristic of a boundary layer of the velocity field adjacent to the boundary from the turbulent correlations. This requires investigation of two problems: (a) mean flow on rough boundaries - which will yield the well known measure of the roughness in k_r and/or $\Delta u/u_*$, and (b) space correlation measurements from which another measure might be defined. A relation between these two measures can possibly be established empirically.

The review of literature in the light of the present problem is discussed under two main headings:

A. Mean Velocity Distribution on a Rough Flat Plate

B. Space-Correlation Distribution on Flat Plate

A. Mean Velocity Distribution on a Rough Flat Plate

The flow past a stationary thin flat plate set parallel to the flow is considered. The flat plate was sharpened at the leading edge to avoid any sudden lateral deflection of the approaching fluid. As the air flows past the leading edge, there develops a boundary layer which begins at the leading edge and grows in thickness. The initial boundary layer will be laminar. A transition region is reached where

the flow changes from laminar to turbulent, with a consequent sudden thickening of the boundary layer. The location of the transition region from laminar to turbulent boundary layer is defined approximately by the value of $R_e = u_a x/\nu$, between 2×10^5 and 10^6. In the turbulent boundary layer, viscosity is important only very near the wall where the frictional shearing stresses $\tau = \mu \partial u/\partial z$ in the boundary layer are considerable because of the large velocity gradient. Further away from the boundary, however, the viscous shearing stresses are very small compared with the apparent turbulent stress. The flow field of fluid far from the boundary can be divided into two regions: the thin boundary layers near the wall, in which friction must be taken into account; and the region outside the boundary layer, where the friction forces are small and they may be neglected.

The definition of boundary layer is, to a certain extent, arbitrary because the transition from the velocity in the boundary to that outside of it takes place asymptotically. The boundary layer thickness δ is frequently defined as the distance from the boundary to the point at which the actual velocity is within 1% of local mainstream velocity. This can be expressed by a relation

$$\delta = 0.99\, u_a \qquad (1)$$

Schlichting (24) gives a relation for the boundary layer thickness as a function of x and u_a as

$$\delta \sim \sqrt{\frac{\mu x}{\rho u_a}} = \sqrt{\frac{\nu x}{u_a}} \qquad (2)$$

The mean velocity distribution of the boundary layer differs, depending on the surface characteristics.

1. Smooth Surface:

The velocity distribution in the boundary layer on a smooth flat plate can be described by using two universal laws, the "wall law" and "velocity-defect law". The "wall law" pertains to the region close to the wall where the effect of viscosity is directly felt and the "velocity-defect law" pertains to the bulk of shear layer where viscous forces become negligible. The wall law as explained by Rotta (21) can be stated as follows:

It is generally assumed that the mean velocity distribution near the wall is completely determined by the magnitude of the shear stress at the wall, τ_o, the density ρ, the kinematic viscosity ν, and the distance z from the wall. This can therefore be expressed in dimensionless form by

$$\frac{u}{u_*} = g\left(\frac{u_* z}{\nu}\right) \qquad (3)$$

where

$$u_* = \sqrt{\frac{\tau_o}{\rho}} \qquad (4)$$

is the friction velocity and g is a universal function of $z u_* / \nu$. The functional equation, Eq. (3), is the law of the wall. In the laminar sublayers it takes the special form

$$\frac{u}{u_*} = \frac{z u_*}{\nu} \tag{5}$$

which arises from the circumstance that the sublayer is so thin that shear stress τ therein is constant and equal to τ_o. The range of z over which Eq. (3) is valid must be established by experiment.

According to Schubauer and Tchen (26), the argument leading to the velocity-defect law is that the reduction in velocity $(u_a - u)$ at a distance z is the result of the tangential stress at the wall, dependent on the distance δ to which the effect has diffused from the wall. This may be written in dimensionless form by the relation

$$\frac{u_a - u}{u_*} = h\left(\frac{z}{\delta}\right) \tag{6}$$

Eq. (6) is the velocity-defect law. From the results of the other investigators, the turbulent boundary layer shows that the variables u/u_* and $z u_*/\nu$ not only correlate the data in the laminar sublayer, but also the correlation extends well out to the turbulent field that was also correlated by the variables $(u_a - u)/u_*$ and z/δ. This overlapping of the two methods of correlation shows some relationship must exist between two distinct sets of parameters used. Therefore, in the overlapping

region in which both laws are valid, the functions g and h must be logarithms. Thus, in the overlap zone the Eqs. (3) and (6) may be written as

$$\frac{u}{u_*} = A \text{ Log } \left(\frac{z\, u_*}{\nu} \right) + C \qquad (7)$$

and $$\frac{u_a - u}{u_*} = - A \text{ Log } \left(\frac{z}{\delta} \right) + D \qquad (8)$$

where $A = 2.3/k$ and k, C and D are experimentally determined constants. The constant k is independent of the nature of the wall (whether smooth or rough), its value is 0.40 and C = 8.5 (for completely rough condition), given by Schlichting (24).

The validity of the defect law extends right to the region of the wall flow, provided that the thickness of the sublayer δ_s is sufficiently small compared with the total thickness of boundary layer δ. Since δ cannot be exactly defined, Rotta (21), proposed the introduction of the dimensionless wall distance $z\, u_*/\delta^* u_a$ instead of z/δ. With this, Eq. (8) may be written as

$$\frac{u_a - u}{u_*} = - A \text{ Log } \left(\frac{z\, u_*}{\delta^* u_a} \right) + D_1 \qquad (9)$$

2. Rough Surface:

The wall law and velocity-defect law can also be applied to describe the velocity distribution on a rough surface but their form has to be modified.

Considering the boundary layer over a flat plate with the surface uniformly covered by roughness elements of size small

compared to with the boundary layer thickness δ , Rotta (21) explained that there exists a layer of constant mean shear stress adjacent to the wall, where the motion is entirely determined by the magnitude of τ_o , ρ , ν and the scale and geometry of the roughness. With the geometrically similar roughnesses, the effect of roughness is determined by a representative length scale, say k_r . The Eq. (3) can be expanded to

$$\frac{u}{u_*} = g_1 \left(\frac{z\, u_*}{\nu} , \frac{k_r\, u_*}{\nu} \right) \tag{10}$$

It is generally accepted that the direct influence of the surface roughness is felt only near the wall, and that further away from the wall, but still within the region of constant stress, the flow pattern is independent of the roughness and viscosity. The Eq. (7) can be expressed for a rough surface by the relation

$$\frac{u}{u_*} = A \, \text{Log} \, \frac{z\, u_*}{\nu} + C_1 \tag{11}$$

where $C_1 = g_2 (k_r\, u_* / \nu)$ and A is the same as in Eqs. (7) and (8).

The velocity-defect law as expressed by Eq. (8) holds true for rough as well as smooth surfaces, provided the roughness elements are not so large that the origin of z becomes difficult to determine. This is shown by experimental results of other investigators, Hama (10) and Clauser (2).

Another form of the wall law equation for rough surface as suggested by Clauser (2) is

$$\frac{u}{u_*} = A \text{ Log } \left(\frac{z\, u_*}{\nu} \right) + C - \frac{\Delta u}{u_*} \qquad (12)$$

An important characteristic of the roughness effect is: that, if the surface roughness elements are large enough so that the laminar sublayer completely disappears, then the inner layer must become independent of the viscosity. Eq. (12) shows that for this to occur $\Delta u/u_*$ must be of the form

$$\frac{\Delta u}{u_*} = A \text{ Log } \frac{k_r\, u_*}{\nu} + C_2 \qquad (13)$$

This equation applied only for values $k_r\, u_*/\nu$ for which the surface is fully rough. The downward shift $\Delta u/u_*$ between wall laws for smooth and rough surfaces has been shown by a number of investigators, namely Bhaduri (1), Clauser (2), Schlichting (24), and others, in their respective studies. Sayre and Albertson (23), in the study of open channel flow, found that velocity distribution changed not only with the roughness height but there exists also a considerable effect of spacing of roughness elements on the velocity distribution on rough boundary. They attempted to relate the size, shape and spacing of the roughness elements by a single parameter.

The flow over a rough surface must depend upon the size, shape and distribution of roughness elements and upon the friction velocity. Thus, it should be expected that near a wall having a given roughness pattern, the velocity profile should be correlatable by using parameters u/u_*, $z\, u_*/\nu$ and $k_r\, u_*/\nu$ in which k_r is the size of the roughness.

Equation (12) shows that $\Delta u / u_*$ represents the vertical shift of the logarithmic curve caused by roughness. This shift is a function of roughness, Reynolds number $R_{e*} = k_r u_* / \nu$ as shown in Eq. (13). This function must be determined by experiments. Clauser (2), Hama (10), Schlichting (24) and other investigators have done work on rough surfaces. Some of the results on rough surface, obtained by different investigators in Colorado State University, Fluid Mechanics Laboratory, are summarized as follows:

Name	Type of Roughness	Velocity Used	Reference Equation (smooth surface)	$\frac{\Delta u}{u_*}$
Chanda	Crushed Stones between 0.25" to 0.35"	35 fps	$\frac{u}{u_*} = 5.6 \text{ Log } \frac{z u_*}{\nu} + 4.9$ (Moore)	10.75
Bhaduri	Wooden strip of $\frac{1}{4}$"x$\frac{1}{4}$"x6 ft spaced 3.0" apart	12 fps	$\frac{u}{u_*} = 5.6 \text{ Log } \frac{z u_*}{\nu} + 5.4$ (Stevenson)	12.50
Quraishi	Flexible plastic strip of 0.25" wide, 0.01" thick and 4" high	20 fps	$\frac{u}{u_*} = 5.6 \text{ Log } \frac{z u_*}{\nu} + 5.4$ (Stevenson)	19.10

A considerable quantity of experimental data has been collected by Hama (10), shown in Fig. (29), on various types of roughness. It shows the behavior of different kinds of roughness through the range smooth, partially rough and fully rough conditions. The limits of such ranges can be judged from this figure. It will be noted that

for values of R_{e*} below approximately 12, the vertical shift $\Delta u/u_*$ approaches zero. The limit below which the surface is smooth appears to be at $R_{e*} \cong 4$.

The mean velocity distribution in turbulent boundary layer can also be correlated by using the relation

$$\frac{u}{u_a} = f\left(\frac{z}{\delta}\right) \tag{14}$$

In case of flat plate, the relation expressed by Eq. (14) applies over a limited range of Reynolds number.

B. Space-Correlation Distribution on Flat Plate

The measurement of roughness characteristics adjacent to the boundary in a turbulent flow, with the aid of space correlations method, is discussed under this heading. Before discussing the space correlation distribution on the flat plate, some background of the problem will be given. This can be discussed under the headings: (1) space correlation and (2) double velocity correlation.

1. Space Correlation:

The knowledge of space correlation theory for describing the isotropic field of turbulence structure has been used by Lin (16), Pasquill (17) and others. The fundamental theory was originated by Taylor. The space correlation method of describing turbulent fluid motion on boundary layer can be summarized as follows:

Investigation of turbulent motion shows that the velocity and pressure at a fixed point in space do not remain constant with time but perform very irregular fluctuations of high frequency. The photographic pictures of this irregular motion of turbulent flow have been shown in any standard text book of fluid mechanics. The lumps of fluid which perform such fluctuations in the direction of flow and at right angles to it consists of macroscopic fluid balls of varying small size, called the eddies.

Considering the fact that turbulent motion consists of eddies of a more or less definite range of sizes, it can be explained that the size of the eddies would be more realistically formulated in terms of differences in velocity existing instantaneously between two points in the field. The statistical expression of the knowledge of the eddy size is provided by space correlation between the velocities at two points at a specified distance apart. If the eddy sizes are large compared with distance, the correlation coefficients will tend to be high, and vice versa.

2. Double Velocity Correlation:

In order to obtain a definition to calculate the double velocity correlation, let the turbulent components u_1' and u_2' in a velocity field be measured instantaneously at two points; one of which is fixed, and other is varied in distance x from it. Then the longitudinal correlation coefficient $f(x)$ is defined by the relation

$$f(x) = \overline{u'_1 \, u'_2} \Big/ \sqrt{\overline{u'^2_1}} \cdot \sqrt{\overline{u'^2_2}} \tag{15}$$

where u'_1 , u'_2 , $\sqrt{\overline{u'^2_1}}$ and $\sqrt{\overline{u'^2_2}}$ are the velocity fluctuations and root-mean-square values of velocity fluctuations in longitudinal direction at two points in fluid flow, respectively. The correlation coefficient will decrease with increase of distance x. The transverse correlation coefficient f(y) can similarly be defined by the relation

$$f(y) = \overline{u'_1 \, u'_2} \Big/ \sqrt{\overline{u'^2_1}} \cdot \sqrt{\overline{u'^2_2}} \tag{16}$$

where u'_1 and u'_2 are the velocity fluctuations in y direction. The correlation coefficient decreases fast to zero with increasing x and the quantity which is characteristic of scale of turbulence is given by the relation

$$L_x = \int_0^{\beta} f(x) \, dx \tag{17}$$

It is a measure of lumps of fluid which move together as a unit and, thus, describes the size of the larger eddies.

Favre (5), Townsend (27), Willmarth (29), and Wills (28) are among those who have done some experimental investigation to describe the behavior of turbulent flow near the boundary. Their investigations were limited to the case of smooth surface only. Favre (5), in his study of space correlation measurement, found that

the longitudinal and transverse correlation fall to zero faster as the value of Reynolds' number decreases. Similar reasoning given by Liepman for the measurement of double velocity correlation in z direction.

Townsend (27) infers that the correlation falls off much more rapidly in the y and z directions than in the x direction, and the component eddies must be considerably elongated in the x direction. Favre (5), in the investigation of characteristic of the structure of the turbulent flow near the smooth boundary, compares the results of autocorrelation and longitudinal space correlation in a boundary layer and shows that, in the central zone of the boundary layer, i. e., $z/\delta \approx 0.25$, the curve of space correlations versus time correlations coincide.

In the investigation of the form of the large eddies of turbulent motion, Grant (9) measured the double velocity correlation tensor at a number of positions in the wake of a circular cylinder and in a flat plate boundary layer. He concludes that in the wake, the correlations at large values of separation are explained in terms of a pair of vortices, side by side and rotating in opposite directions and in the boundary layer over flat plate the correlations measured have been found to be highly anisotropic and consistant with the presence of vortex pair eddies.

Several authors such as Townsend (27), Favre (5), Kline and Rundstadler (22), Grant (9) and others have made an attempt to explore the mechanism of the wall flow in the turbulent velocity field with the help of turbulent eddies. Measurements of various components of double velocity space correlation function carried out by Grant (9) show that the size of the eddies in the x direction are large compared with eddies in y and z directions, which are comparable with the distance of the wires from the wall. In order to bring into agreement these results with well-established similarity law of the wall, Townsend (27), distinguishes between the total turbulent motion and the part responsible for the Reynolds shear stress. The shape of the correlation function suggests that the motion may be like a two-dimensional jet, originating at the edge of viscous layer, with its surrounding induced flow. This is supplemented and to some extent supported by visual observations of eddy structure as shown in Fig. (32), given by Kline and Rundstadler (22). No definite information concerning why the observed pattern actually exists is available by Townsend (27) and by Kline and Rundstadler (22). The instability of the flow near the outer edge of the sublayer and the action of the outer flow are certainly decisive elements.

From the review of literature, the following conclusions can be drawn concerning this present study.

(a) The mean velocity distribution on turbulent boundary layer can satisfactorily be expressed by the two universal laws - the

wall law (the variables u/u_* and $z\,u_*/\nu$), in the inner part of velocity profile and velocity-defect law (the variables $(u_a - u)/u_*$ and z/δ), in the outer part of the velocity profile. The two laws are correlated in the overlapping zone by a logarithmic function.

(b) In case of rough surface, the wall laws show a downward shift of the straight line section of the logarithmic curve expressed by the parameter $\Delta u/u_*$.

(c) The measurements of space correlation functions of longitudinal, transverse and vertical directions of longitudinal velocity fluctuations in a boundary layer on a flat plate have shown that when two points in a flow continually have related fluid structure, then their correlation should, in general, be high whereas on the other hand, two points having entirely different structures can be expected to have a considerably lower correlation.

(d) A comparison of the eddies over rough and smooth boundaries has as yet not been made.

(e) The magnitude of the correlation coefficients in the direction of the motion of an eddy and also perpendicular to this direction will depend upon the structure of the eddy.

CHAPTER III

EXPERIMENTAL EQUIPMENT AND PROCEDURE

In this chapter, the experimental equipment and procedure of the tests made for this study are described. The experiments required measuring the mean velocity profiles and recording the turbulence intensity fluctuations on a magnetic tape, and evaluating the recordings.

A. Experimental Equipment:

The experimental equipment consists of the (1) wind tunnel, (2) flat plates with smooth and rough surface, (3) carriage, (4) hot-wire anemometers and (5) micromanometers. A brief description for each of the instruments is given below.

1. Wind Tunnel:

The experiments were performed in a low-speed wind tunnel located in the Fluid Dynamics and Diffusion Laboratory, Colorado State University, Fort Collins, Colorado.

The tunnel is a closed circulating type with a test section of 30 ft. length, 6 ft. width, and 6 ft. height. The free stream turbulence level u'/u_a is kept within $\pm$ 2% by an inlet contraction ratio 4:1 and a damping screen. Air flow in the tunnel is moved by a constant speed pitch controlled fan. The mean velocity in the test

section can be varied from 3 fps to 75 fps approximately. A free stream velocity of 30 fps was used for the experiments. There is no arrangement for temperature control in the tunnel. A thermometer showed that the temperature varied from 70° F at the beginning of the test run to 90° F after a few hours of operation. The temperature was recorded at the beginning and end of each experiment. A schematic diagram of the wind tunnel is shown in Fig. (1).

2. Flat Plate:

The flat plate used for the experiment was made of aluminum. It is 6 ft. long, 3 ft. wide and 3/8 inch thick. The plate was mounted on a steel stand at a height of 2 ft. parallel to the floor of the tunnel, as shown in Fig. (2).

For the purpose of measuring the pressure along the plate, two lines of pressure taps were made and they are placed at a distance of 6 inches on either side of center line. These pressure taps were connected by 3/16 inch (internal diameter) plastic tubes, as shown in Fig. (4). The plastic tubes were brought outside of the tunnel for measuring pressure along the plate.

The experiments were performed for two different surfaces.

a. Smooth surface:

The original finished surface of the flat plate was used for this case. A 4 inch wide strip of sand paper (grid 36) was attached

at a distance of one inch from the leading edge along the total width of the plate, to establish a turbulent flow and to thicken the boundary layer. Also, a plastic tube of 1/16 inch (internal diameter) was fixed along the width of the plate (cutting one side) to improve the pressure gradient. A plan view of the smooth surface flat plate is shown in Fig. (3) and a cross-sectional elevation of it is shown in Fig. (4).

b. Rough surface:

The surface of the flat plate was made rough by placing one layer of angular sand of fractions passed through #7 sieve* and retained on #8 sieve. The roughness materials were placed uniformily on the plate, as shown in Figs. (3) and (4). The density of the roughness materials was about 120 particles per square inch.

3. Carriage:

A carriage as shown in Fig. (5a) was used for vertical movement of the total pressure tube of 0.035 inch outside diameter. The probe was fixed on a rod which was connected to a micrometer scale. Attached to the carriage was a small one rpm-ac motor with a driving mechanism by which the probe can be moved and positioned at any desired height. The control of this mechanism was

---

* A. S. T. M. Specifications of U. S. Standard Sieve Series was used.

outside the tunnel. The distance is measured from the position of the probe to that of the plate surface. A height of 0.025 inch was attained for each revolution of the motor.

The carriage as shown in Fig. (5b) was used for positioning the hot-wire probe #1. The vertical position of the probe was attained manually.

4. Hot-Wire Anemometer:

The turbulent velocity was measured with a model IIHR, type 3A, twin-channel hot-wire anemometer. The instrument worked on the principle of constant-temperature. A tungsten wire of 0.0002 inch diameter and 0.05 inch long was used as a detecting element. The amplifier of the hot-wire anemometer contains a linearizing stage.

By applying King's empirical equation

$$\frac{i^2 R_w \alpha}{j} = C_3 + C_4\sqrt{u} \qquad (18)$$

calibration of hot-wire was obtained. A typical linearized calibration curve in the form of $\bar{I}_{ma}$ vs u is given in Fig. (6a). The details of the Eq. (18) is given by Habbard (12).

5. Micromanometer:

An equibar type 120, electronic manometer, which operates over eight full scale ranges from 0.01 mm to 30 mm of mercury,

was used for pressure measurement along the plate, calibration of the hot-wires, measurement of the mean velocity, and adjustment of the ambient velocity. The instrument gives accurate results within an operating temperature varying from 40^{o} F to 95^{o} F. The accuracy of the result can be obtained within ± 0.3% full scale of selected range.

B. Experimental Procedure

The experimental procedure can be discussed under the following headings:

1. Measurement of Pressure Gradient along the Flat Plate
2. Measurement of Mean Velocity
3. Hot-wire Probes
   a. Calibration of hot-wires
   b. Measurement of turbulent intensity
   c. Recording of turbulence intensity signals
   d. Frequency response of recorder-amplifier
4. Total Space Correlations
   a. Calibration of sum and difference circuit
5. Filtered Space Correlations
   a. Calibration of filters

1. Measurement of Pressure Gradient along the Flat Plate:

The static pressure was measured with a transonic equibar 120, electronic manometer on two lines, on either side of the

central line as shown in Fig. (3). In case of smooth surface, the pressure tap #11 was used as a reference line. A pressure distribution curve for smooth surface is shown in Fig. (7).

In case of rough surface, the use of pressure tap #11 as a reference line proved unsatisfactory, i. e., it gave uneven distribution of pressure along the plate. Assuming that the static pressure at the ambient flow is the same as that within the flow, the pressure along the plate was measured by using two pitot tubes; one placed in the free stream at height of 2 ft. from the plate surface and its position was behind the plate, and the other at a height of 4 inches from the top of the roughness materials. The latter was moved along center line corresponding to the position of the pressure taps. The pressure difference between two lines was directly read in mm of Hg from the manometer. The final calculation of pressure distribution was made with reference to the reading of pressure tap #11. A pressure distribution curve for rough surface is shown in Fig. (7).

The experiments were to be performed at a pressure gradient of zero. To attain this, the shape of the wind tunnel ceiling was changed by mounting a specially shaped false ceiling onto the tunnel ceiling. The shape of the false ceiling was found by trial and error. Details of the shape of the ceiling are shown in Fig. 8. The maximum magnitude of pressure gradient is about $\pm$ 0. 193 x 10^{-5} psi/in , which within experimental error can be considered as zero pressure gradient.

2. Measurement of Mean Velocity:

The mean velocity for different stations, as shown in Figs. (3) and (4) was measured by a total pressure tube, shown in Fig. (9), and the Transonic, Equibar type 120, electronic manometer. The static pressure was measured with the pressure tap right at the testing stations for the smooth surface, and with the static holes of the pitot tube placed in the free stream in case of rough surface. The output of the electronic manometer voltage corresponding to pressure difference was plotted on the y-axis of the x-y plotter. A voltage proportional to the position was applied to the other axis of the x-y plotter.

The velocity was then determined in terms of the difference of the dynamic pressure and static pressure in accordance with the formula

$$u = \sqrt{\frac{2(p_d - p_s)}{\rho_a}} = \sqrt{\frac{2\,\gamma_w\,\Delta\,h}{\rho_a}} = C_5\sqrt{\Delta h}\ \text{fps} \qquad (19)$$

where Δh is the reading from x-y plotter in mm of mercury height and C_5 is a constant which has been determined to be 54 at normal temperature.

3. Hot-wire Probes:

The most important tool for the space correlations study is the hot-wire. The accuracy of the experimental results depends on the proper and systematic way of using the hot-wire, according to

the instructions given in the manual. The calibration of the hot-wire and its use for measuring the turbulent intensity and recording the turbulent intensity signals on magnetic tape are discussed under separate headings as follows.

a. Calibration of hot-wires:

Two hot-wires were used for the recording of the turbulence signals simultaneously on a magnetic tape. Both hot-wires were calibrated at the beginning and at the end of the experiment against a pitot tube placed in the free stream. Two calibration curves were obtained each time. The significance of the calibration procedure of the hot-wire is very important to obtain a linearized characteristics of the hot-wire in the mean velocity field. In all computations of turbulence the slope A' of the calibration curve of $\overline{I}_{ma}$ vs u are used. Therefore, for the accuracy of the experimental results, it is essential to obtain the calibration curve accurately.

The technique of the calibration procedure can be explained as: The first calibration curve was obtained by placing the floating probe, i. e., probe #1 in the free stream with the pitot tube at the same height and the other probe, i. e., probe #2 which was placed at a height of 0. 04 inch from the floor of the plate. The pitot tube was connected to the electronic manometer and the two probes were connected to the two channels of the hot-wire anemometer. A

calibration curve, as shown in Fig. (6a), was obtained with $\overline{I}_{ma}$ vs u. $\overline{I}_{ma}$ was recorded from the hot-wire anemometer and u was calculated by using Eq. (19) with Δh read from electronic manometer for different velocities. The second calibration curve was obtained by placing probe #1 at the same height as probe #2 and at sufficient distance apart to avoid any flow disturbance. At the beginning, the value of $\overline{I}_{ma}$ for both probes was made the same at the maximum velocity, then the velocity was changed from minimum to maximum. $\overline{I}_{ma}$ was recorded for each velocity and plotted $\overline{I}_{ma_1}$ vs $\overline{I}_{ma_2}$. A calibration curve for smooth surface is shown in Fig. (6b).

b. Measurement of turbulent intensity:

The root mean square values of the velocity fluctuation in the direction of the mean flow was measured at six stations along the center line of the flat plate which are shown in Fig. (3).

The hot-wire was connected to the hot-wire anemometer. The output of the hot-wire anemometer was then connected to the rms meter which was connected to the y axis of the x-y plotter. Voltage corresponding to the velocity fluctuation component was plotted on the y axis of the plotter and the voltage proportional to the probe position was applied to the other axis of the plotter.

The intensity of the turbulence $\sqrt{\overline{u'^2}}$, in a turbulent flow is calculated by using the formula

$$u' = \sqrt{\overline{u'^2}} = \frac{A'}{B}\sqrt{\overline{e^2}} \tag{20}$$

where A' is the slope of the calibration curve of the hot-wires, shown in Fig. (6a). With the experimental equipment shown in Fig. (10a), the turbulent intensities $\sqrt{\overline{u_1'^2}}$ and $\sqrt{\overline{u_2'^2}}$ are calculated by using the Eq. (20) written in the following form

$$u_1' = \sqrt{\overline{u_1'^2}} = \frac{A_1'}{B}\sqrt{\overline{e_1^2}} \tag{21}$$

and

$$u_2' = \sqrt{\overline{u_2'^2}} = \frac{A_2'}{B}\sqrt{\overline{e_2^2}} \tag{22}$$

where $\sqrt{\overline{e_1^2}}$ and $\sqrt{\overline{e_2^2}}$ are the rms-meter reading in volts, and B is the conversion factor obtained by passing a current I (in ma) through a resistor of 50,000 ohms using the relation

$$E = B\, I_{ma} \tag{23}$$

i.e., $$E = 50{,}000 \times I \times 10^{-3} = 50\, I \tag{24}$$

B is found to be 50. Knowing the values of A_1', A_2' and B, the turbulent intensities $\sqrt{\overline{u_1'^2}}$ and $\sqrt{\overline{u_2'^2}}$ can be obtained by using Eqs. (21) and (22).

c. Recording of turbulence intensity signals:

In order to obtain space correlation measurements, the two turbulent intensity signals from the hot-wires placed in the velocity field in the tunnel were recorded simultaneously on a magnetic tape

using a Sanborn 2000 tape recorder. Two hot-wires, as shown in Fig. (11), were used. Probe #2 was fixed at the center line and at the center of station 3 on the floor of the plate at a height $z' = 0.04$ inch above the smooth surface and above the top of roughness materials in case of rough surface. Probe #1 was fastened to the carriage and its position can be varied in x , y and z directions. The two probes were connected to the two channels of the IIHR type 3A, hot-wire anemometer. Output of the hot-wire anemometer was connected to the rms-meter and to the tape recorder through the impedance matching amplifier of the hot-wire anemometer. Since only a maximum of one volt rms can be recorded by the magnetic tape recorder, the outputs of the hot-wire amplifiers were reduced to ± 0.53 volts at the beginning of data recording by using the attenuator of the hot-wire anemometer. This value was checked several times and recorded during the experiment. A complete instrumental set-up is shown in Fig. (12).

In order to revert back to the original turbulent intensities, i. e., $\sqrt{\overline{u_1'^2}}$ and $\sqrt{\overline{u_2'^2}}$ from the output of the tape recorder, a relation must be set up between these two. This requires two things: first, the frequency response of the recorder-amplifier must be determined and secondly, the d-c gain of the arrangement must be found.

d. Frequency response of the recorder-amplifier:

For determination of the recorder-amplifier frequency response, turbulence signals are replaced by regular sine waves of a known frequency and amplitude by using an oscillator as shown in Fig. (13). The sine wave is put into the tape recorder through the amplifier unit of the hot-wire anemometer. For a particular value of Q, the rms value of the input to the impedance matching amplifier, different values of V , the rms value of the output of Mincom tape recorder are obtained by changing the frequency of the sine wave. Results show a linear relationship exists between Q and V within the frequency range from 16 to 2,000 c/s .

Gain of the system:

The gain of the recorder-amplifier arrangement can be expressed by the relation

$$\frac{V}{Q} = G \tag{25}$$

i. e., for two different signals, Eq. (25) can be written as

$$\frac{V_1}{Q_1} = G_1 \tag{26}$$

and

$$\frac{V_2}{Q_2} = G_2 \tag{27}$$

A relation can be established between V_1 and V_2, the output of the tape recorder and u_1' and u_2', the turbulence signals. Equating Eqs. (21) and (26), the following relation is obtained

$$V_1 = G_1 \, Q_1 = \frac{G_1 \, B}{A_1'} \sqrt{\overline{u_1'^2}} = \frac{G_1 \, B}{A_1'} \, u_1' \tag{28}$$

Similarly,

$$V_2 = G_2 \, Q_2 = \frac{G_2 \, B}{A_2'} \sqrt{\overline{u_2'^2}} = \frac{G_2 \, B}{A_2'} \, u_2' \tag{29}$$

where G_1 and G_2 are obtained from frequency response curve of the arrangement and V_1 and V_2 are measured by rms-meter from the output of the tape recorder.

4. Total Space Correlations:

Measurement of total space correlation has a great significance of this present study. This gives us some information about the structure of turbulent eddy near the smooth and rough boundaries. For the accuracy of the experimental results, the space correlation measurements require careful attention. Experimental arrangement for the total space correlation measurement is shown in Fig. 14. The total space correlations in longitudinal, transverse and in vertical directions have been calculated by using the Eq. (59) as given in appendix - A. The term $\overline{u_1' \, u_2'}$ is measured by using the sum and difference circuit. This instrument is designed by the Colorado State University electronic shop. It was used to add and

subtract the two recorded turbulent intensity signals. The sum and difference circuit was calibrated every time before the space correlation measurements were taken. Description of the calibration procedure is given below.

a. Calibration of sum and difference circuit:

The sum and difference circuit instrument was calibrated by using two sine waves which were equal in amplitude and frequency. Two sine waves of 300 Hz and one volt peak-to-peak as observed on an oscilloscope were generated by a sine wave generator and placed into the sum and difference circuit, shown in Fig. (10b). The rms value of the individual wave and the sum and difference of these two sine waves was measured by a rms-meter connected to the output of the sum and difference circuit. Theoretically, the results should give the following:

(i) when two sine waves $A_3 \sin t$, are added

$$V_{rms} = \sqrt{\frac{1}{2\pi} \int_0^{2\pi} (2 A_3 \sin t)^2 \, dt} = \sqrt{2}\, A_3 \tag{30}$$

(ii) when two sine waves are subtracted

$$V_{rms} = \sqrt{\frac{1}{2\pi} \int_0^{2\pi} (A_3 \sin t - A_3 \sin t)^2 \, dt} = 0 \tag{31}$$

(iii) when using one sine wave

$$V_{rms} = \sqrt{\frac{1}{2\pi} \int_0^{2\pi} A_3^2 \sin^2 t \, dt} = \frac{A_3}{\sqrt{2}} \tag{32}$$

where A_3 is the half peak-to-peak voltage of oscilloscope and V_{rms} is the output voltage of the sum and difference circuit measured by rms-meter. The results for two sine waves of different amplitudes and frequencies show a maximum of 5% error.

5. Filtered Space Correlations:

Like total space correlation, the filtered space correlation measurements are equally important in this present study. Measurement of filtered space correlations provide us the information about the size of the individual turbulent eddy structure in the turbulent flow near the smooth and rough boundaries. Experimental arrangements for the measurement of filtered space correlation is shown in Fig. (15). Filtered space correlations were calculated by using Eq. (60), given in appendix - A. The term $\overline{u'_{1(n)}\ u'_{2(n)}}$ was obtained in the same way as discussed for calculation of total space correlations. The two recorded turbulent intensity signals were put into the filters for screening out the particular frequency signals and calculate the correlation of those particular frequency signals. The two filters were calibrated before the measurement of the filtered space correlations. The procedure for calibration is described below.

a. Calibration of filters (or spectrum analyzers):

Two filters were used. Filter #1, identified as 1/3 octave filter set of type 1609; and filter #2, identified as audio frequency spectrum recorder, type 2311, manufactured by B and K Co.

Two sine waves of 300 Hz and amplitude of one volt peak-to-peak as indicated by the reading on an ocilloscope were passed through the filters. The output of the filters were then connected to the sum and difference circuit. The rms value of the individual, of the sum and of the difference of the two sine waves was passed through the frequency range from 16 to 2000 Hz of the filters and was measured by the rms-meter. The results of the filtered correlations calculated by using two sine waves show a maximum of ± 8% error.

6. Error in Procedure:

An account of over-all error in experimental procedure which might possibly be entered during the experiment should be discussed to justify the accuracy of the experimental results of the present study. The most possible steps of the procedure where error can be entered are the recording of turbulence intensity signals and the electrical instruments for analyzing the data.

In the first case, some error might enter during the recording of turbulence signals from the hot-wires which were placed in the velocity field inside the tunnel due to the inaccurate placing of the hot-wire probe #1, because the horizontal and vertical positions of the probe #1 were made manually. The error expected in the calibration of hot-wire is negligible. Chances of additional error, due to the disturbance of the flow caused by

entering the tunnel after every five minutes to fix the position of probe #1, cannot be ruled out.

The maximum error expected from the electrical equipment for analyzing the experimental data is about ± 8% as discussed in the calibration of sum and difference circuit and filters. This error is within the limit of experimental error in a study of turbulent flow.

CHAPTER IV

ANALYSIS OF EXPERIMENTAL DATA

The description of the experimental results will be given in this chapter. The experimental data is divided into two groups, the mean velocity data and the space correlation data. From the mean velocity data, the measure of the roughness effect in terms of $\Delta u/u_*$ is established. From the space correlations of filtered signals inferences are drawn on the eddy structure and an attempt is made to express the measure of the roughness effect in terms of L_{xs} / L_{xr} where L_{xs} and L_{xr} are defined as the measure of scale of turbulence for smooth and rough surfaces respectively.

A. Mean Velocity Field

Vertical velocity profiles were obtained at six stations on center line and six inches on either side of the center line. The data were taken with a total pressure tube on both the smooth and rough surfaces, using an air velocity of 30 fps. The mean velocity data are presented in one of the following forms:

$$\frac{u}{u_a} = f\left(\frac{z}{\delta}\right) \tag{33}$$

$$\frac{u}{u_*} = g\left(\frac{z\, u_*}{\nu}\right) \tag{34}$$

and

$$\frac{u_a - u}{u_*} = h\left(\frac{z}{\delta}\right) \tag{35}$$

A brief discussion of the Eqs. (33, 34, and 35) are given, referring to related figures. The detailed discussion will be taken up later.

A plot of u/u_a versus z/δ , shown in Fig. (16), shows that the turbulent mean velocity profiles do not coincide but form a family of profiles for different Reynolds number and degree of roughness of the wall. This result agrees with Clauser (2), Hama (10), and others.

1. Wall Law:

Eq. (34) lead to the well known "wall law". A plot of the wall law in Fig. (17), shows that when the wall is smooth and laminar sublayer exists, the sublayer is so thin that the shearing stress τ is constant. From this, it can be said that u is proportional to z , i.e., $u/u_* = zu_*/\nu$. Above the sublayer region logarithmic function is the best to describe the velocity distribution.

2. Velocity Defect-Law:

Eq. (35) lead to the well known velocity defect law. By using ordinate $(u_a - u)/u_*$, with the consideration of skin friction coefficient c_f , the two-parameter family of turbulent profiles as shown in Fig. (16), can be reduced to a single universal curve as shown in Fig. (18). The same argument has been given by Clauser (2). The curve in Fig. (18), shows that it was not valid near the wall. This can be explained by saying that the flow immediately

adjacent to the wall depends on absolute velocity, but the plot has been made by considering velocity defect (u_a - u) or relative velocity.

3. Development of δ along the Smooth Plate:

The boundary layer thickness δ is one of the important parameters whose use for the plotting of the Figs. (16, 18, 27, 28, 30 and 31) is significant in this study. The accuracy of the experimental results depends on the accurate estimation of δ. There is no definite mathematical relation by which δ can be calculated accurately but few approximate methods exist and are extensively used by other investigators.

In this experiment two methods have been used to calculate δ, one is the power law method and the other is from its definition, Eq. (1). The power law method of calculating δ has been used only to check the results of δ using Eq. (1). The values of δ, for both smooth and rough surfaces calculated by using Eq. (1), are given in Tables (1) and (2). They compare satisfactorily.

The validity of the power law for velocity distribution in turbulent flow is generally accepted. Although it does not strictly hold in the vicinity of the boundary, it describes the velocity distribution in the whole boundary layer very satisfactorily and it is easy for mathematical application.

The general formula of the power law given by Schubaner and Tchen (26) is

$$\frac{u}{u_a} = \left(\frac{z}{\delta}\right)^{\frac{m}{2-m}} \tag{36}$$

By definition, the displacement thickness δ^* and momentum thickness θ are

$$\delta^* = \int_o^{\delta} \left(1 - \frac{u}{u_a}\right) dz \tag{37}$$

and

$$\theta = \int_o^{\delta} \frac{u}{u_a}\left(1 - \frac{u}{u_a}\right) dz \tag{38}$$

From Eqs. (36, 37 and 38), the relation for form factor H is obtained as

$$H = \frac{\delta^*}{\theta} = \frac{2 + m}{2 - m} \tag{39}$$

The Von Karman's momentum integral equation at zero pressure gradient and at u_a = constant, gives a relation

$$\frac{\tau_o}{\rho u_a^2} = \frac{d\theta}{dx} = \frac{c_f}{2} \tag{40}$$

From Eqs. (40 and 38) and with Blasius law of resistance, a relation for δ obtained as

$$\delta \propto x^{\frac{1}{m+1}} = E_1 x^{\frac{1}{m+1}} \tag{41}$$

where E_1 is a constant whose value is assumed to be .0834 for $u_a x/\nu$ up to 1.07×10^6, in this experiment. Derivation of Eqs.

(39, 40, and 41) can be obtained in any standard text book of fluid mechanics. The form parameter H is calculated by using the relation $H = \delta^*/\theta$, the value of which is given in Tables (1 and 2), for both smooth and rough surfaces and a plot is shown in Fig. (19). The values of H vary from 1.36 to 1.38 in smooth cases, except in Station 1.

The parameter m, as calculated by Eq. (39) is within the range of 0.316 to 0.305. Accordingly, the velocity profile follows 5.41 ~ 5.55th power law and both θ and δ^* follow 0.759 ~ 0.766th power parabola. The plot θ or δ versus x on logarithmic paper should appear to be a straight line with a slope of approximately 0.763.

Since the boundary layer in this experiment was artificially thickened by sand paper (36 grit) placed at the front part of the plate, the slope of the plot of (θ and δ^*) versus x, in logarithmic paper, shown in Fig. (20) gives only 0.57 in place of 0.763. The virtual origin must therefore be estimated. To obtain this, a plot of θ versus $(x_o + x)$ on logarithmic paper has been made first. From this, the slope is measured for different values of x_o. From this plotting of x_o vs slope, the virtual origin is found at a distance of 15.5 inches upstream of the plates leading edge, corresponding to the slope 0.763. Then Eq. (41) must be modified to read

$$\delta = E_1 (15.5 + x)^{0.763} \qquad (42)$$

where x is in inches.

Boundary layer thickness δ, calculated by using Eq. (42) and with the definition, Eq. (1) are in close agreement as shown in Fig. (21). The artificially thickened boundary layer approaches naturally developed boundary layer asymptotically as it advances further downstream. Both naturally developed boundary layers (calculated) from Eq. (42) and artificially thickened boundary layer (actual) are plotted in Fig. (21) for comparison.

It is observed that from Station 2 onward, the difference between the naturally and artificially developed boundary layers is appreciably small, whereas at Station 1 the difference is large. Data for Station 1 is not reliable and are discarded for analysis.

4. Determination of Shear Velocity (u_*):

The shear velocity u_* is another important parameter used in the analysis of the mean velocity data. It plays a very important role to describe the overlapping zone of turbulent velocity profile by logarithmic function for both wall law and velocity-defect law, the plotting of which is shown in Figs. (17, 27 and 28). It is,therefore, necessary to calculate u_* accurately in order to obtain an accurate experimental result. Shear velocity has been calculated by using two methods: (a) logarithmic law of velocity distribution method and (b) momentum integral equation method.

a. Logarithmic law of velocity distribution method - It is assumed that in the vicinity of the boundary the logarithmic law of velocity distribution is valid:

$$\frac{u}{u_*} = 5.75 \log z + C_1 \tag{43}$$

The plotting of u/u_a versus $\log z$ should then appear in the form

$$\frac{u}{u_a} = m_1 \log z + C_2 \tag{44}$$

where m_1 is the slope of the straight line portion of u/u_a vs $\log z$. Equating the Eqs. (43 and 44), a relation is obtained as

$$u_* = \frac{m_1 u_a}{5.75} \tag{45}$$

Using Eq. (45), the shear velocity u_* for both smooth and rough surfaces have been calculated. The values of u_* are given in Tables (1 and 2). They are plotted in Fig. (23).

b. Momentum integral equation method - The friction velocity $u_* = (\tau_o / \rho)^{\frac{1}{2}}$ can be computed by means of the two-dimensional momentum integral equation for zero pressure gradient. Applying the momentum principle to an elementary length of boundary layer, a relation is obtained as in Eq. (40) which can be written in different form as

$$u_* = u_a \sqrt{\frac{d\theta}{dx}} \tag{46}$$

The values of u_* obtained by using Eq. (46) are a bit higher than the values obtained by using Eq. (45), shown in Table (3). This is probably the effect of the artificially thickened boundary layer.

The values of θ and δ^* for smooth and rough surfaces are calculated accurately by area integration methods in accordance with their definitions as given by Eq. (37 and 38). They are given in Tables (1 and 2) and plotted as functions of x in Figs. (24 and 25).

One important thing to note here is the determination of the origin of measuring vertical distance from the rough surface. It lies anywhere from the deepest valley to the crest of the roughness materials. The origin can be shifted until the logarithmic portion of the velocity profile appears to be a straight line.

From the non-dimensional plotting of u/u_* versus $z u_*/\nu$ as shown in Fig. (17), two significant facts are noted. First, a comparison of the correlation schemes in terms of u/u_* and $z u_*/\nu$ for outer profile and inner profile on a smooth surface showed that an overlapping region esists where the profile is logarithmic in character. Secondly, the outer portion of the profile is valid for both smooth and rough surfaces, including the overlapping region. It follows from these two facts that the inner portion for rough surface must have a logarithmic region with the same logarithmic slope, as in the case of smooth surface. When $z u_*/\nu < 13$, the surface is aerodynamically smooth and the inner velocity profile follows a relation $u/u_* = z u_*/\nu$, where a linear relationship between u and z exists. The inner logarithmic law for velocity distribution in a turbulent boundary layer over a rough surface can be written as

$$\frac{u}{u_*} = 5.75 \log \frac{z u_*}{\nu} + 6.25 - \frac{\Delta u}{u_*} \qquad (47)$$

The value of $\Delta u/u_* = 12.0$. The quantity $\Delta u/u_*$ shows the effect of the rough surface which causes the velocity distribution for smooth surface to shift vertically downward. The absolute value of $\Delta u/u_*$ depends on the type and magnitude of roughness and is a function of $k_r u_*/\nu$ where k_r is the roughness height. A relation exists between $\Delta u/u_*$ and $k_r u_*/\nu$ as given in Eq. (13). When the right-hand side of Eq. (13) becomes dominant for large values of $k_r u_*/\nu$, then $\Delta u/u_*$ becomes proportional to $\log k_r u_*/\nu$ with a constant of proportionality equal to A and fully developed rough flow is obtained and the wall law equation for a smooth surface can best be compared with the equation given by Stevenson as

$$\frac{u}{u_*} = 5.6 \log \frac{z u_*}{\nu} + 5.4 \qquad (48)$$

The present experimental data agree satisfactorily with Eq. (48) over most of the boundary layer.

The wall shear τ_o is affected by u_a, δ and ν in the case of turbulent boundary layers over rough surfaces and it is also influenced by Reynolds number. According to Clauser (2) and Hama (10) it is known that the velocity distribution as shown in Fig. (16), of a two-parameter family for Reynolds number and roughness, can be reduced to form a single parameter family curve by using the

parameter c_f, the local skin friction. To attain this it is necessary to measure all velocities relative to the ambient velocity u_a, i. e., $(u_a - u)$. Non-dimensional plotting of $(u_a - u)/u_*$ versus (z/δ) in logarithmic paper are shown in Figs. (27 and 28). It is noted from these figures that velocity-defect law can equally be applied to both smooth and rough surfaces. Clauser (2) stated that if two profiles, having widely different values of Reynolds number and roughness have the same skin friction coefficient c_f, they will have identical non-dimensional velocity profiles. The experimental results in this study confirm this.

It is observed that the outer part of the curve in Figs. (27 and 28) differs from the logarithmic law which occupies most of the part. The velocity distribution on the outer part can be given by an empirical formula given by Hama (10) as

$$\frac{u_a - u}{u_*} = 9.8 \left(1 - \frac{z}{\delta}\right)^2 \qquad (49)$$

and the logarithmic part of the velocity distribution can be expressed by the relation

$$\frac{u_a - u}{u_*} = -5.75 \log \frac{z}{\delta} + 2.35 \qquad (50)$$

Eq. (49) connects smoothly with logarithmic part at $z/\delta \sim 0.14$. Experimental results for velocity-defect law best agree with Hama (10).

B. Turbulence Field

In the turbulent flow field, the turbulence intensity of velocity fluctuation $\sqrt{\overline{u'^2}}$ was measured for two different purposes, using hot-wire measurement technique. First, u' component of velocity fluctuation, was recorded along with mean velocity data by using single hot-wire at six different stations, to plot u'/u_a vs z/δ . Secondly, for space correlation measurement, turbulent velocity fluctuations u'_1 and u'_2 at two points in the velocity field were recorded on magnetic tape. Two hot-wires were used for this case. All data for space correlation measurements were taken between Stations 3 and 4, on the flat plate for both smooth and rough surfaces. Turbulence field data are explained in details under two main headings: (1) Turbulent intensity and (2) Space correlation measurement.

1. Turbulent Intensity:

The turbulent intensity of velocity fluctuation $\sqrt{\overline{u'^2}}$ in the boundary layer was measured for both smooth and rough surfaces of the flat plate. Non-dimensional plots of u'/u_a versus z/δ for both smooth and rough surfaces are shown in Figs. (30 and 31). The figures show that the absolute maximum intensity exhibit with the maximum value of u' fluctuation which occurs very close to the wall just outside the wall layer region. For a smooth surface, the experimental results have been compared with Klebanoff (14) and the curve shows nearly the same trends and location of maximum

value of u'. Fig. (31) shows that for rough surface, the value of u'/u_a decreases with distance. The shape of the curve in Fig. (31) is similar as found for all stations, in agreement with findings of Hinze (11), Klebanoff (14) and Bhaduri (1). It is compared with Bhaduri's data, in Fig. (31). The experimental curve shows higher values of u'/u_a close to the wall. This is due to the air velocity being higher in this experiment than that used by Bhaduri (1).

2. Space Correlation Measurements:

The analysis of the correlation data is divided into two parts: (a) total space correlation measurements and (b) filtered space correlation measurements.

a. Total space correlation measurements:

In order to describe a structure of the turbulent flow, the space correlation between the velocity fluctuation components at two separated points in the flow is determined. The space correlations express the coherence of neighboring fluid elements at distances apart. The double velocity space correlations have been calculated from the definition given in Eq. (59), in the appendix - A, where u'_1 and u'_2 are the instantaneous value of the mean velocity fluctuation. The non-dimensional plots of f(x) vs x, f(y) vs y and f(z) vs z are given in Figs. (33, 34 and 35). It is observed from these figures that the value of space correlations is high near the origin and decreases as the value of x, y and z are increased. When the

separation distance between the two hot-wires by which correlation measurements have been made is zero, i.e., $x = y = z = 0$ and time, $t = 0$, then by definition $f(x) = 1$. At the origin the experimental results shows that $f(x) \neq 1$, the reason for this is that the origin, z_1, the vertical distance between two hot-wires is not zero but 0.02 inches. It is noted in the Figs. (33, 34, and 35) that at large values of x, y and z, the negative correlations occur which in case of f(x) persist for large distances. The negative values of correlations can be attributed to return flow of the turbulent eddies. The magnitude of correlation coefficients f(x), for both smooth and rough surfaces are positive at small values of x, but at large values of x both show negative correlation with not much difference in magnitude. For smooth case, the shape of the experimental curves for f(x) and f(z) are similar to those obtained by Favre (5) and Hinze (11). Results of space correlation for both smooth and rough surfaces are compared in each case and it is observed that the values of f(x) and f(z) for the smooth surfaces are higher than the values in the case of rough surface. In the case of f(y), the smooth surface result gives lower value than the rough surface results. The plots of f(y) and f(z) show that correlation values fall very rapidly which indicates that the size of the energy containing eddy structure is smaller in y and z directions than in x direction. The individual turbulence signal for rough surface shows

a higher value than the smooth surface which produces higher non-dimensional values of space correlations. This has been shown by calculating the dimensional values of space correlations, R(x), R(y) and R(z). Plots of the dimensional double velocity correlations, R(x, y, z) vs (x, y, z) are shown in Figs. (36, 37, and 38). Surfaces of iso-correlations R_1, R_2 & R_3, in x-z, x-z and y-z planes are shown in Figs. (39, 40, and 41). These figures have been drawn by taking a constant value of non-dimensional space correlation in different planes. With the information from the Figs. (39, 40, and 41), a reasonable inference can be made about the structure of the turbulent eddy on both smooth and rough surfaces. This is shown in Fig. (42). Fig. (42) is drawn by taking non-dimensional value of space correlations in x, y and z planes. The values of R_1 and R_3 in x and z directions are higher in smooth surface than that of rough surface; but in y direction, the value of R_2 is opposite.

b. Filtered space correlations measurements:

The recorded turbulence signals u'_1 and u'_2 were played back and passed through the filters in order to measure the individual eddy structure. Only longitudinal space correlation data have been analyzed by this method. For each value of x, (0.0", 0.2", 0.4", 0.6", 0.8", 1.0", 1.5", and 2.0") the turbulence signals were put into the filters and the correlations are calculated for a frequency (n) range of 16-2000 Hz by using the Eq. (60) of the

appendix - A. Filtered space correlations have been calculated for several frequencies, but few of them are presented here. Non-dimensional plotting of R(n) versus x for frequencies 20, 100 and 200 are shown in Figs. (43, 44 and 45). It is observed that the non-dimensional values of correlation for smooth surface are higher than that of rough surface for each individual frequency of turbulence. The dimensional plottings of R'(n) vs x are shown in Figs. (46 and 47). The figures show that rough surface has higher values of R'(n) than that of smooth surface. Filtered space correlations measurement gives a very interesting results. At low frequency the eddy structure is well preserved for a longer distance in longitudinal direction. As the frequency increases, the space correlation curves approaches zero at a shorter distance and the negative values of the space correlations increases. The negative value is due to the back flow created by the different velocity components at the fixed probe. Similar reasoning was given by Grant (9), for negative value of space correlations. Non-dimensional plot of filtered space correlations, given in Figs. (43, 44, and 45), confirms about the eddy structure for both smooth and rough surfaces as shown in Fig. (42).

The spectral functions of turbulence energy F(n) are obtained as function of the frequency n, for each individual signal on smooth and rough surfaces. Non-dimensional plottings of F(n) vs n are shown in Figs. (48, 49 and 50). The areas of the curves F(n) have

been chosen so as to be equal for common intervals of frequencies. Results show close agreement with Favre (5) and Townsend (27). In vertical direction, for different values of z (0. 06", 0. 08" and 0. 10"), the turbulence spectra have also been calculated. The non-dimensional plottings of F(n) vs n are shown in Fig. (51 and 52). The results agree with other investigators. Dimensional value of the turbulence energy spectrum are calculated for signal #2 for different values of x and semi-logarithmic plottings are shown in Figs. (52 and 54). It is observed from Figs. (53 and 54), that the energy contained in the turbulence signal for rough surface in the lower frequency range is high which indicates the presence of high turbulence level. Results of Figs. (53 and 54), cleraly justify the results of non-dimensional and dimensional plottings of filtered space correlations as shown in Figs. (43-47). It can also be inferred from this that at lower frequency range rough surface contain more large turbulent eddy than that of smooth surface. But the turbulent eddy structure changes as the frequency increases and at high frequency range both become nearly the same. With this, it can be predicted that there exist a certain relationship between eddy structure of smooth and rough surfaces.

Finally, the size of the eddies for different frequencies are calculated from non-dimensional plotting of correlation coefficients by using Eq. (60) of the appendix - A, for both smooth and rough surfaces. The values of the upper limit β of the integral in Eq. (17) are taken from the point where positive part of the filtered space

correlation curves are zero, this is an assumption. Equal assumptions have been made by several other investigators. The values for both smooth and rough surfaces are obtained by measuring the area under the curve of filtered space correlation for different frequencies by planimeter and the results are shown in Table 4. There is a large difference in the measure of L_{xs} and L_{xr}, as is evident from the results. It, therefore, appears feasible to trace the roughness effect in the measures of L_{xs} or L_{xr}, if it can be shown that

(i) L_{xs} can be suitably non-dimensionalized to be valid for all smooth boundaries.

(ii) If there exists a unique L_{xr}, also suitably non-dimensionalized, for each roughness.

However, these provisions can not be proved from the data of this study, which used one roughness pattern only, and more extensive experiments are required for this purpose.

Kline (22), concludes in his study of double velocity correlations, that if a turbulent eddy is transported by flow having a relatively low turbulence level, it will retain higher space correlation values than will be the same eddy moving through highly turbulent surroundings. The experimental results of the space correlation in this study confirms this.

CHAPTER V

CONCLUSIONS AND RECOMMENDATIONS

As a result of the present study of the experimental investigation of turbulent eddies in a boundary layer on smooth and rough flat plates, the following conclusions can be made. The conclusions can be divided into two main groups:

A. Velocity Field

1. The velocity-defect law is universal for both smooth or rough surfaces, in agreement with the consideration of Clauser (2) and Hama (10).

2. The velocity distributions of the boundary layer are described by two universal laws - the wall law and the velocity-defect law and the intermediate region common to the two, in which the velocity profile is logarithmic.

3. The roughness effect can be expressed by using the parameter $\Delta u/u_*$, which is defined as the vertical shift of the logarithmic curve caused by roughness. For a geometrically similar roughness, the quantity $\Delta u/u_*$ is a function of the Reynolds number based on the roughness height $k_r u_*/\nu$ alone, and is directly related to the increase in surface resistance which the roughness produces.

B. Space Correlations

1. Space correlations fall more rapidly in the y and z directions, i. e., at right angles to the direction of the mean flow, than in the direction x, i. e., parallel to the mean flow. The component eddies are much more elongated in the x direction. This is true for both smooth and rough surfaces.

2. The turbulence level near a smooth surface is lower than near a rough surface. But, near the smooth surface the turbulent eddies transported by the flow retain higher space correlation values than that of the eddies moving through the highly turbulent surroundings near the rough surface.

3. The turbulent eddy structure is relatively well preserved in the case smooth surface, but in the case of rough surface, the presence of highly turbulent surroundings rapidly distort the turbulent eddy structure.

4. The measure of the roughness effect by using the parameter L_{xs} / L_{xr} is possible if L_{xs} and L_{xr} can suitably be non-dimensionalized and large number of experimental data are used for different roughness elements.

5. The turbulent eddy structure varies greatly in the lower frequency range, obtained from filtered space correlation measurements and turbulence energy spectrum, for both smooth and rough boundaries.

6. The non-dimensional plotting of space correlation as shown in Fig. (42), shows the difference which exist between the turbulent eddy structure on both smooth and rough boundaries. In smooth boundary the eddy structure is much stiffer in x and z planes than that of rough boundary eddy structure.

C. Suggestions for Further Study

The experimental results in this study are limited to one fixed velocity, i. e. , 30 fps and a particular type of surface roughness elements. Before attempting to make a generalized conclusion, it is necessary to extend the investigation to the following:

1. Use different velocities.

2. Use different types of roughness elements with varying parameters.

3. Space correlation measurements for the range of low frequencies, i. e. , 0 $\longrightarrow$ 16 c/s should be made.

4. In order to get a complete picture of the structure of the turbulent flow motion, the space-time correlation measurements must be made.

5. Space-time correlation measurements of wall pressure fluctuation should be made to get the information about the influence of turbulent eddies near the wall in turbulent motion.

6. Arrangement for the positioning of the floating probe in the wind tunnel must be made from outside the tunnel.

7. Extensive space-correlation measurements must be made near 1" distance in x direction.

BIBLIOGRAPHY

BIBLIOGRAPHY

1. Bhaduri, S., Mass Diffusion from a Point Source in a Turbulent Boundary Layer Over a Rough Surface. Ph. D. Dissertation, Colorado State University, Fort Collins, Colorado, 1963, 169 p.

2. Clauser, F. H., The Turbulent Boundary Layer. Advances in Applied Mechanics, 4:1-51, Academic Press, New York, 1956.

3. Clauser, F. H., Turbulent Boundary Layer in Adverse Pressure Gradients. Journal of the Aeronautical Sciences, 21:91-108, 1954.

4. Davis, P. O. A. L., Fisher, M. J. and Barratt, M. J., Characteristics of the Turbulence in the Mixing Region of a Round Jet. Journal of Fluid Mechanics, 15:337-367, 1963.

5. Favre, A., Gaviglio, J. and Dumas, R., Some Measurements of Time and Space Correlation in Wind Tunnel. U. S. National Advisory Committee for Aeronautics. Technical Memorandum 1370, 1955, 21 p.

6. Favre, A. and Gaviglio, J., Repartitions Spectrales De Correlations Spatio-Temporelles De Vitesses, En Couche Limite Turbulence. France Office National d'Etudes et de Recherches Aerospatiales ONERA-TP-164, 1964, 33 p.

7. Favre, A. J., Review on Space-Time Correlations in Turbulent Fluids. Journal of Applied Mechanics, 32:241-257, 1965.

8. Ferri, A., Kuchemann, D. and Sterne, L. H. G. (eds.), Progress in Aeronautical Sciences, 2:1-220, Pergamon Press, New York, 1962.

9. Grant, H. L., The Large Eddies of Turbulent Motion, Journal of the Fluid Mechanics, 4: 149-192, Part 2, 1958.

10. Hama, F. R., Boundary Layer Characteristics for Smooth and Rough Surfaces. Transactions of the Society of Naval Architects and Marine Engineers, 62:333-358, 1964.

11. Hinze, J. O., Turbulence: An Introduction to the Mechanism and Theory. McGraw-Hill Book Company, Inc., New York, 1959, 586 p.

12. Hubbard, P. G., Operating Manual for the IIRH Hot-Wire and Hot-Film Anemometers. State University of Iowa, Studies in Engineering. Bulletin No. 37, 1957, 34 p.

13. Klebanoff, P. S. and Diehl, Z. W., Some Features of Artificially Thickened Fully Developed Turbulent Boundary Layer with Zero Pressure Gradient. U. S. National Advisory Committee for Aeronautics. Technical Note, 2475, 1951, 55 p.

14. Klebanoff, P. S., Characteristics of Turbulence in a Boundary Layer with Zero Pressure Gradient. U. S. National Advisory Committee for Aeronautics. Report 1247, 1955, 19 p.

15. Landweber, L., Re-analysis of Boundary Layer Data on a Flat Plate. Report on Contract No. 1161(01), AD-245-541, Iowa Institute of Hydraulic Research, 1960, 17 p.

16. Lin, C. C., Statistical Theories of Turbulence. Princeton University, Princeton, New Jersey, 1961, 60 p.

17. Pasquill, F., Atmospheric Dissufion: The Dispersion of Wind-borne Material from Industrial and other Sources. D. Van Nostrand Company, Ltd., London, 1962, 297 p.

18. Plate, E. J., Operation and Maintenance of the Low Speed Precision Wind Instrument Test Facility. Final Report Under Contract, DA-29-040-ORD-2346, Colorado State University, Fort Collins, Colorado, 1962, CER62EJP10, 72 p.

19. Plate, E. J. and Cermak, J. E., Investigation to Develop Wind Tunnel Techniques for Measuring Atmospheric Gaseous Diffusion in Model Vegetative Surfaces. Colorado State University, Fort Collins, Colorado, 1963, CER63-EJP-JEC28, 158 p.

20. Plate, E. J. and Sandborn, V. A., An Experimental Study of Turbulent Boundary Layer Structure. Final Report on U. S. Army Grant DA-SIG-36-039-62-G24, Colorado State University, Fort Collins, Colorado, CER64-EJP-VAS37, 46 p.

21. Rotta, J., On the Theory of Turbulent Boundary Layer. U. S. National Advisory Committee for Aeronautics. Technical Memorandum 1344, 1953, 50 p.

22. Runstadler, P. W., Kline, S. J. and Reynolds, W. C., An Experimental Investigation of the Flow Structure of the Turbulent Boundary Layer. Report MD-8, Department of Mechanical Engineering, Stanford University, Stanford, California, 1963, 308 p.

23. Sayre, W. W., The Effect of Roughness Spacing in Ridig Open Channels. Colorado State University, Fort Collins, Colorado, 1959, CER59WWS31, 78 p.

24. Schlichting, H., Boundary Layer Theory. McGraw-Hill Book Company, Inc., New York, 1955, 535 p.

25. Schlichting, H., Experimental Investigation of the Problem of Surface Roughness. U. S. National Advisory Committee for Aeronautics. Technical Memorandum 283, 1937, 42 p.

26. Schubauer, G. B. and Tchen, C. M., Turbulent Flow. Princeton University Press, Princeton, New Jersey, 1961, 123 p.

27. Townsend, A. A., The Structure of Turbulent Shear Flow. Cambridge University Press, London, 1956, 315 p.

28. Wills, J. A. B., On Convection Velocities in Turbulent Shear Flows. Journal of Fluid Mechanics, 20:417-432, 1964.

29. Willmarth, W. W. and Wooldridge, C. E., Measurements of the Fluctuating Pressure at the Wall Beneath a Thick Boundary Layer. University of Michigan, College of Engineering, Aerodynamics Laboratory, ORA Report 02920-1-T, 1962, 32 p.

30. Wooldridge, C. E. and Willmarth, W. W., Measurements of the Correlation Between the Fluctuating Velocities and Fluctuating Wall Pressure in Thick Turbulent Boundary Layers. University of Michigan, College of Engineering Aerodynamics Laboratory, ORA Report 02920-2-T, 1962, 85 p.

APPENDIX - A

APPENDIX - A

A detailed description for the deduction of formula for the calculation of total space correlations and filtered space correlations is given here.

Calculation of Total Space Correlations

The instantaneous output of the tape recorder is put into the sum and difference circuit and the output of it is then connected to rms-meter. This is shown in Fig. (14). The sum and difference of the two instantaneous turbulence signals can be expressed by the mathematical relations

$$S = \sqrt{\overline{(k_1 V_1 + k_2 V_2)^2}} \tag{51}$$

and,

$$D = \sqrt{\overline{(k_1 V_1 - k_2 V_2)^2}} \tag{52}$$

The result of the frequency response of sum and difference circuit, as discussed in Chapter 3-B3(d), shows that $k_1 = k_2 = K_1$. With this information, the Eqs. (51) and (52) reduce to

$$S = K_1 \sqrt{\overline{(V_1 + V_2)^2}} \tag{53}$$

and,

$$D = K_1 \sqrt{\overline{(V_1 - V_2)^2}} \tag{54}$$

Introducing the values of V_1 and V_2 from Eqs. (28 and 29), the Eqs. (53 and 54) can be written as

$$S = K_1 \sqrt{\left(\frac{G_1 B}{A'_1} u'_1 + \frac{G_2 B}{A'_2} u'_2 \right)^2} \tag{55}$$

and, $$D = K_1 \sqrt{\left(\frac{G_1 B}{A'_1} u'_1 - \frac{G_2 B}{A'_2} u'_2 \right)^2} \tag{56}$$

From Eqs. (55) and (56) it follows

$$S^2 - D^2 = 4 K_1^2 \left(\frac{G_1 G_2 B^2}{A'_1 A'_2} \right) \overline{u'_1 u'_2} \tag{57}$$

Dividing Eq. (57) by the product of Eqs. (28) and (29), the result obtained is

$$\frac{S^2 - D^2}{V_1 \cdot V_2} = \frac{4 K_1^2 (\overline{u'_1 u'_2})}{\sqrt{u'^2_1} \cdot \sqrt{u'^2_2}} \tag{58}$$

The total correlation coefficient defined by

$$f(r) = \frac{\overline{u'_1 u'_2}}{\sqrt{u'^2_1} \cdot \sqrt{u'^2_2}} = \frac{S^2 - D^2}{4 K_1^2 (V_1 \cdot V_2)} \tag{59}$$

Calculation of Filtered Space Correlations

Two filters, one identified as 1/3 octane filter set of type 1609 and the other identified as audio frequency spectrum recorder of type 2311, manufactured by B and K Co., are used to calculate the correlation coefficients. The purpose of the use of spectrometers is to yield the correlation of each individual frequency signal, which the total turbulence signals consists of, by filtering. The two instantaneous signals from the tape recorder are put into the sum difference circuit through spectrometers, as shown in Fig. (15). These spectrometers employed a filter range from 16 to 2,000 c/s. The filtered correlation is calculated by using the relation

$$R(n) = \frac{\overline{u'_{1(n)}\, u'_{2(n)}}}{\sqrt{\overline{u'^{2}_{1(n)}} \cdot \sqrt{\overline{u'^{2}_{2(n)}}}} = \frac{S^2 - D^2}{4 K_1^2 \left(v_{1(n)} \cdot v_{2(n)}\right)} \qquad (60)$$

where $v_{1(n)}$ and $v_{2(n)}$ are the rms value measured at the output of the filters. To obtain the absolute value of the output of filters, $v_{1(n)}$ and $v_{2(n)}$ are multiplied by factors B_1 and B_2. This can be expressed by the relations

$$V_{1(n)} = v_{1(n)} B_1 = v_{1(n)} \frac{V_1}{\text{Lin } C_1} \qquad (61)$$

$$V_{2(n)} = v_{2(n)} B_2 = v_{2(n)} \frac{V_2}{\text{Lin } C_2} \qquad (62)$$

where $V_{1(n)}$ and $V_{2(n)}$ are the absolute magnitude of filters output. V_1 and V_2 are the rms-volts of the turbulence signals measured at the output of the tape recorder. Lin C_1 and Lin C_2 are the rms-volts of the turbulence signals measured at the output of the filters.

APPENDIX - B

TABLES

Table 1. Basic data for smooth flat plate (velocity field).

x ft.	u_a fps	δ in.	δ^* in.	θ in.	$H = \delta^*/\theta$	m_1	$u_* = \frac{m_1 u_a}{5.75}$	c_f
1.00	30.55	0.89	0.119	0.0856	1.390	0.264	1.40	0.00413
2.00	30.50	1.25	0.168	0.122	1.375	0.228	1.21	0.00315
3.00	29.45	1.58	0.208	0.152	1.370	0.224	1.145	0.00304
4.00	30.75	1.88	0.241	0.175	1.375	0.221	1.182	0.00296
5.00	30.75	2.16	0.279	0.204	1.370	0.218	1.165	0.00298
6.00	30.70	2.40	0.308	0.226	1.360	0.216	1.520	0.00282

Table 2. Basic data for rough flat plate (velocity field).

x ft.	u_a fps	δ in.	δ^* in.	θ in.	$H = \delta^*/\theta$	m_1	$u_* = \frac{m_1 u_a}{5.75}$	c_f
1.00	30.23	0.80	0.246	0.120	2.05	0.432	2.265	0.01120
2.00	30.15	1.26	0.334	0.176	1.90	0.401	2.100	0.00971
3.00	30.25	1.70	0.426	0.229	1.81	0.383	2.020	0.00887
4.00	29.47	2.00	0.497	0.280	1.78	0.372	1.915	0.00833
5.00	30.15	2.42	0.590	0.333	1.77	0.365	1.915	0.00806
6.00	30.15	2.75	0.661	0.375	1.77	0.360	1.900	0.00793

Table 3. Comparison of the values of δ , u_* and R_e

x ft.	δ in.		u_* fps		$R_e = u_a x/\nu$	
	Smooth Surface		Smooth Surface		Smooth Surface	Rough Surface
	Cal. by Eq. (1)	Cal. by Eq. (42)	Cal. by Eq. (45)	Cal. by Eq. (46)		
1.0	0.89	1.04	1.40	1.82	1.48×10^5	1.46×10^5
2.0	1.25	1.37	1.21	1.66	2.94×10^5	2.91×10^5
3.0	1.58	1.67	1.145	1.50	4.27×10^5	4.39×10^5
4.0	1.88	1.95	1.182	1.48	5.94×10^5	5.70×10^5
5.0	2.16	2.23	1.165	1.37	7.41×10^5	7.28×10^5
6.0	2.40	2.45	1.152	1.25	8.90×10^5	8.73×10^5

Table 4. Eddy sizes for smooth and rough flat plates.

n c/s	L_{xs} in.	L_{xr} in.	$\Delta = L_{xs}/L_{xr}$
16	27.53	24.44	1.13
20	28.08	23.47	1.20
25	26.45	19.43	1.36
32	23.59	19.60	1.20
40	17.22	14.45	1.19
64	10.98	6.41	1.71
80	9.41	4.83	1.95
320	2.05	0.62	3.31

APPENDIX - C

FIGURES

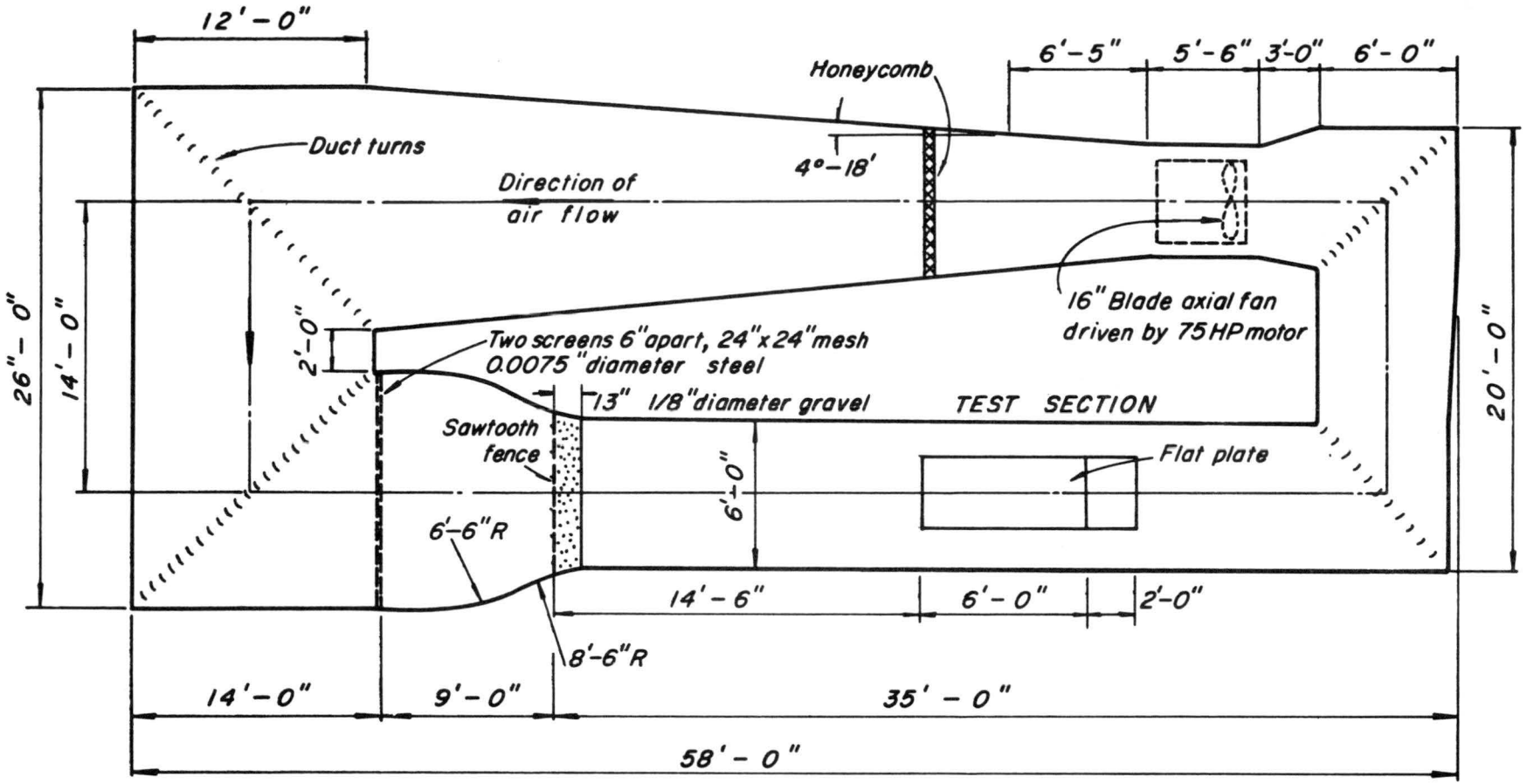

Fig. 1 Plan view of wind tunnel

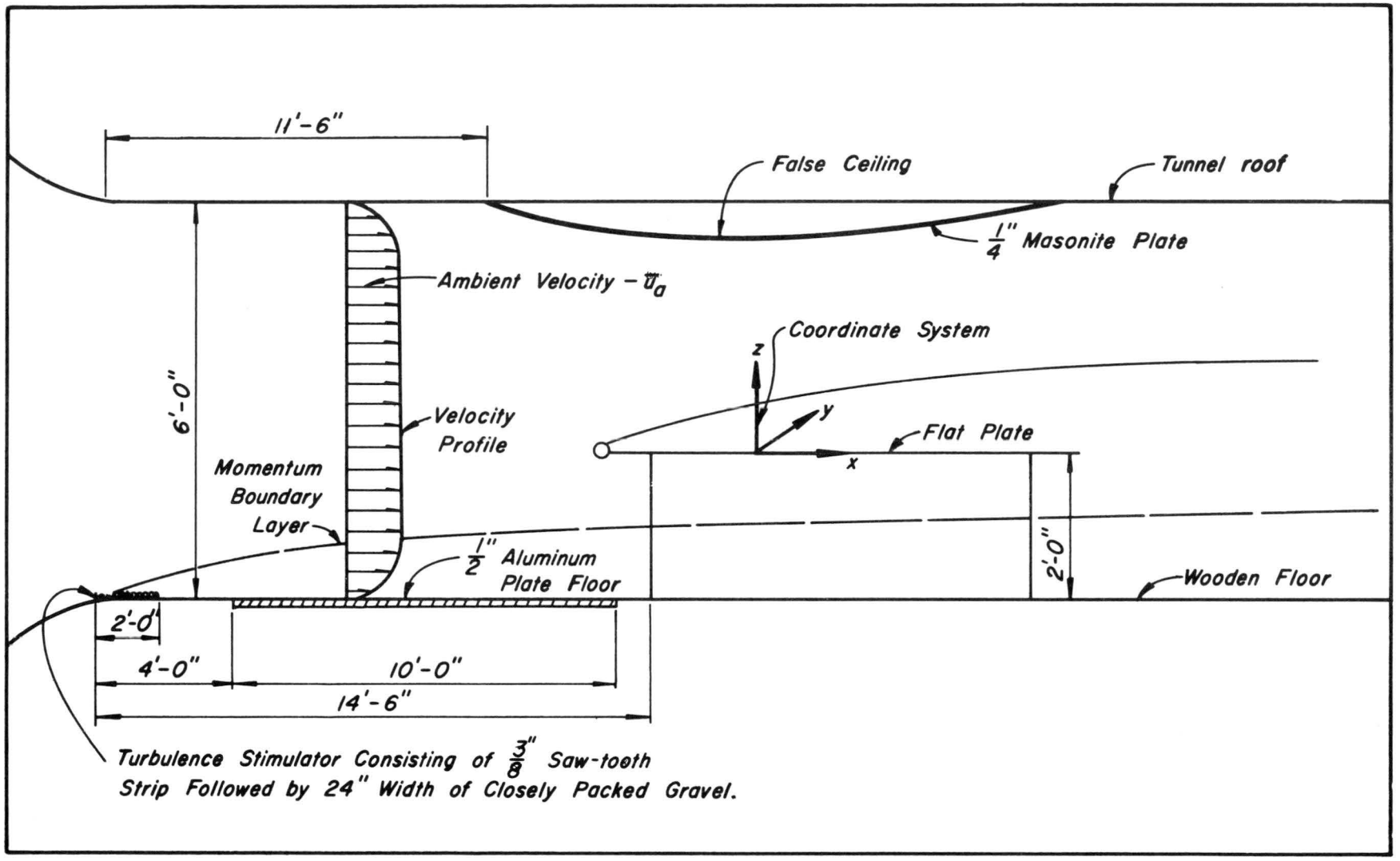

Fig. 2 Test section geometry.

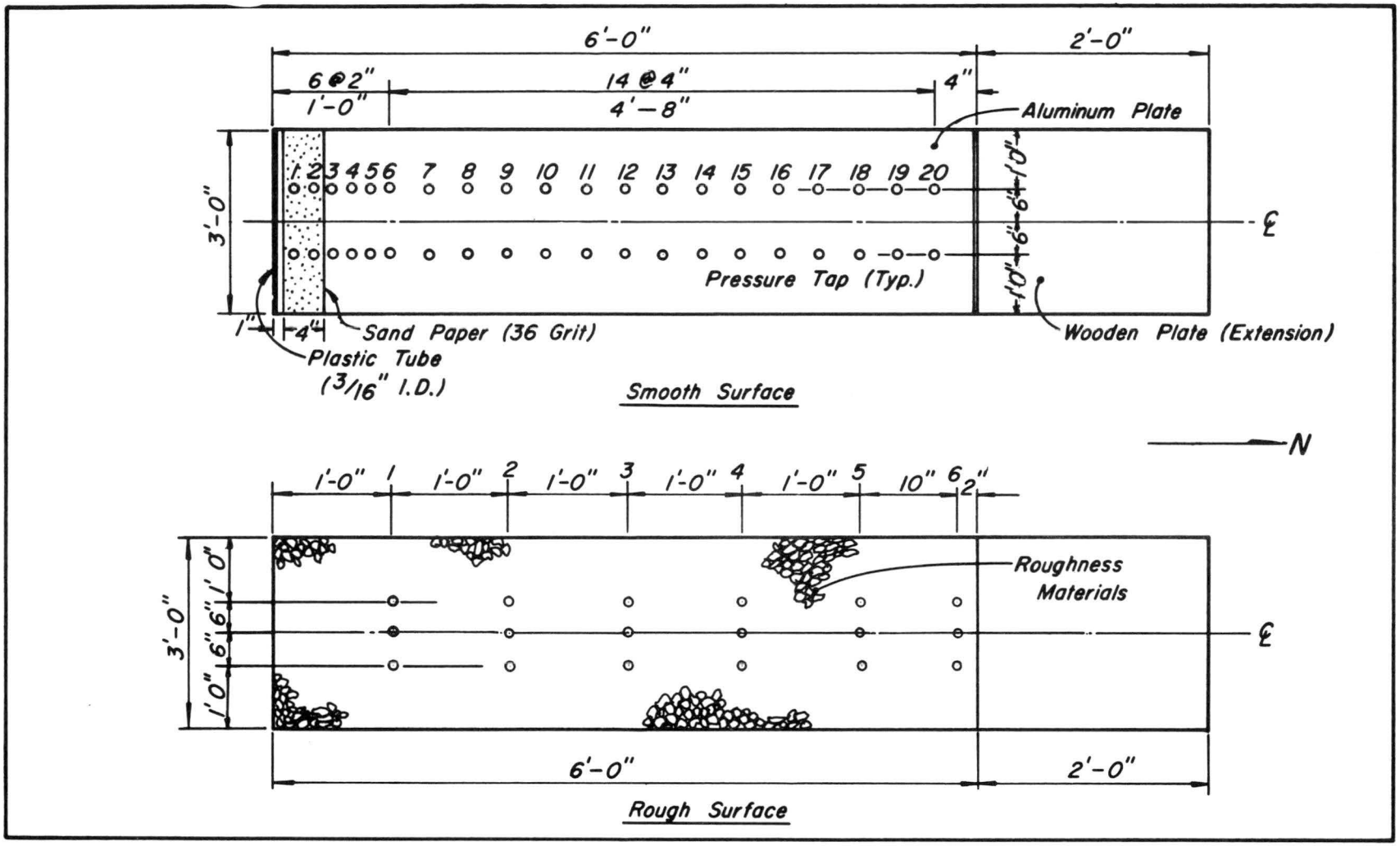

Fig. 3 Plan of smooth & rough flat plate.

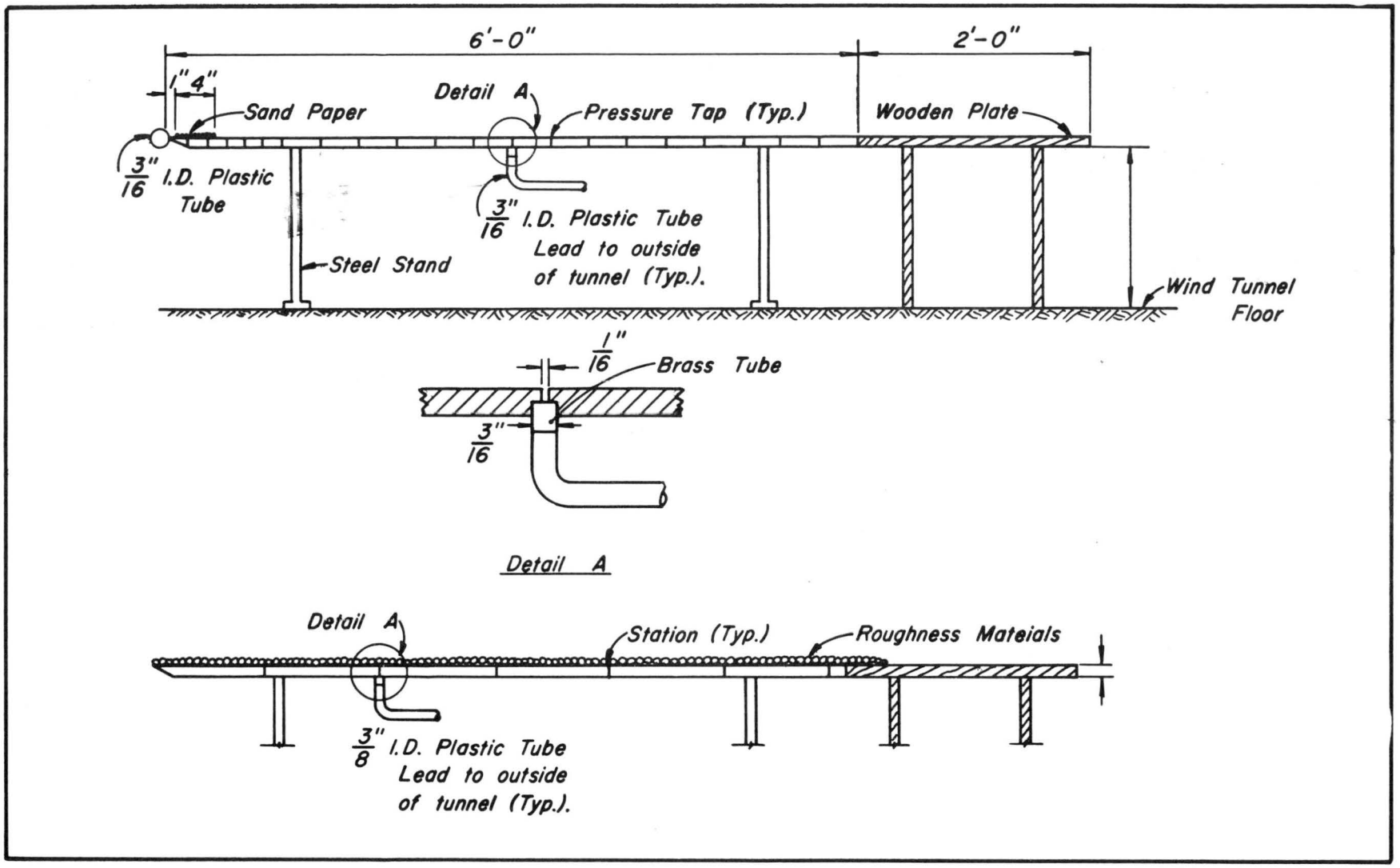

Fig. 4 Cross-sectional elevation of smooth & rough flat plate

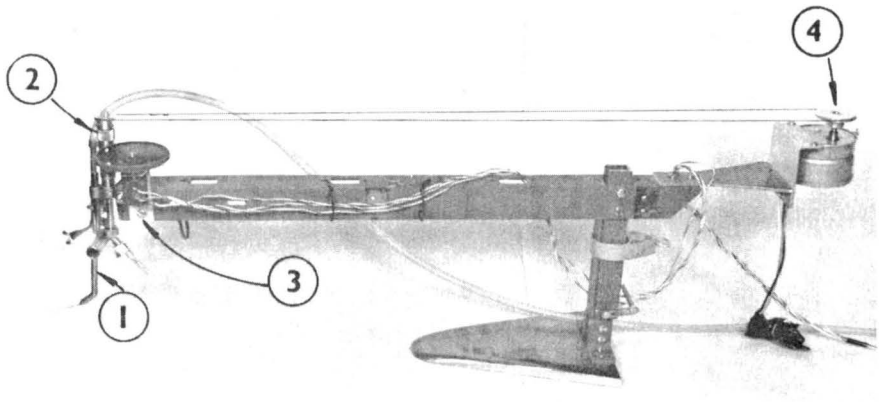

Fig. 5a. Carriage used for mean velocity data recording. (1) Total pressure tube, (2) Micrometer scale, (3) Potentiometer, (4) 1-rpm a-c motor.

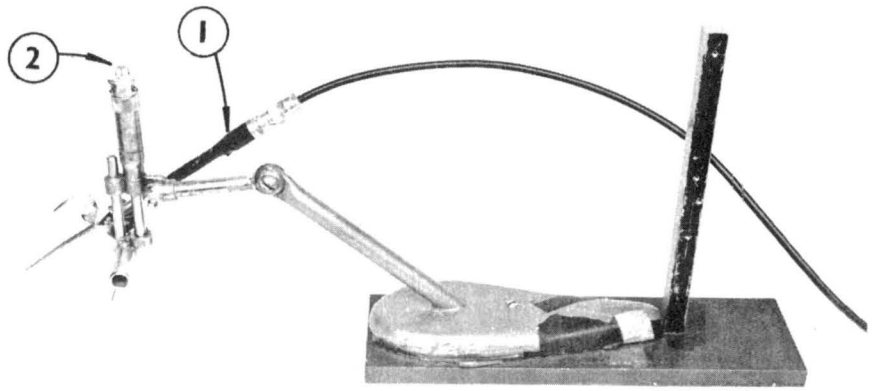

Fig. 5b. Carriage used for turbulence signal recording. (1) Floating probe (#1), (2) Micrometer scale.

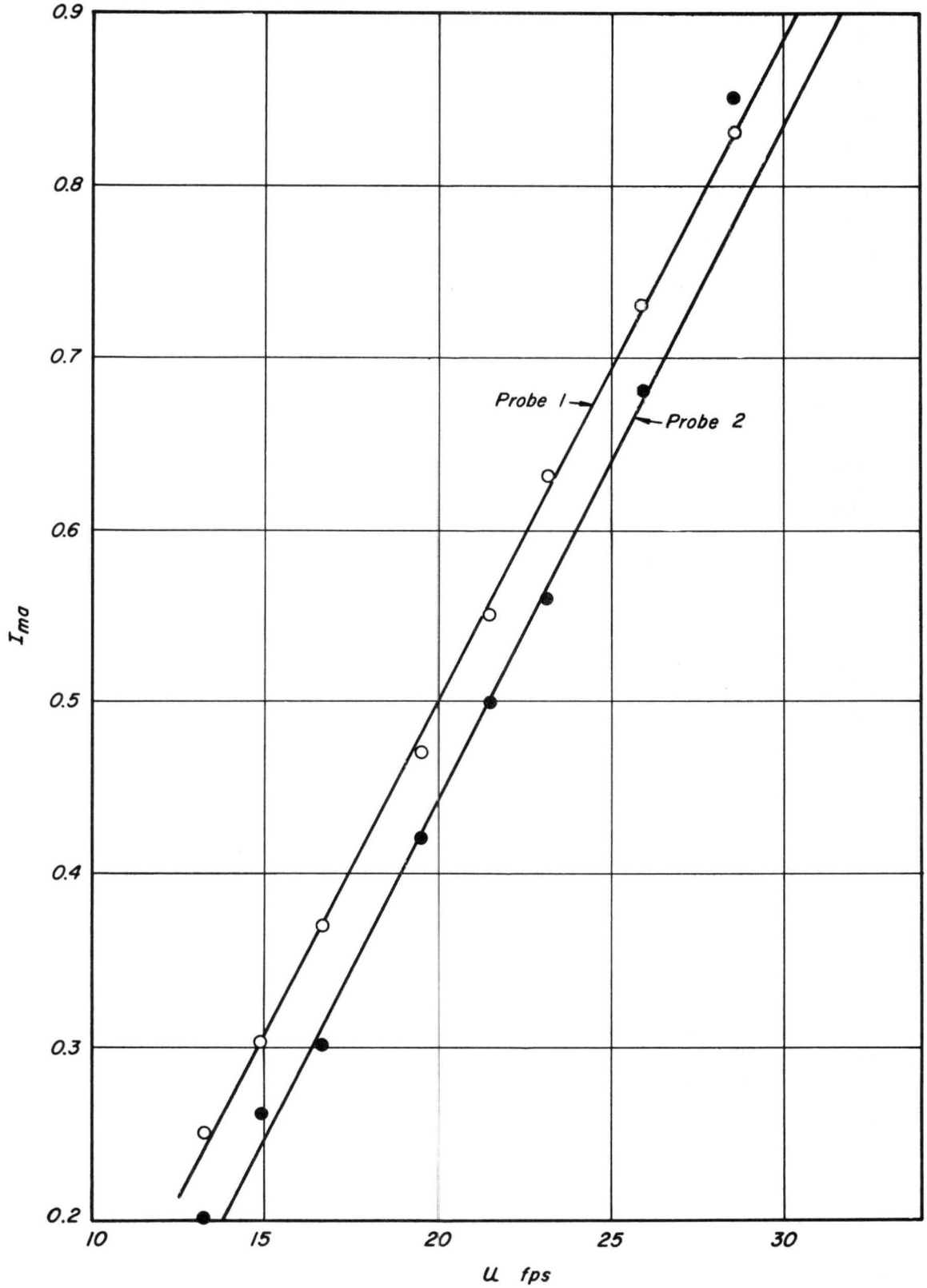

Fig. 6a Calibration of hot wires
(against pitot tube)

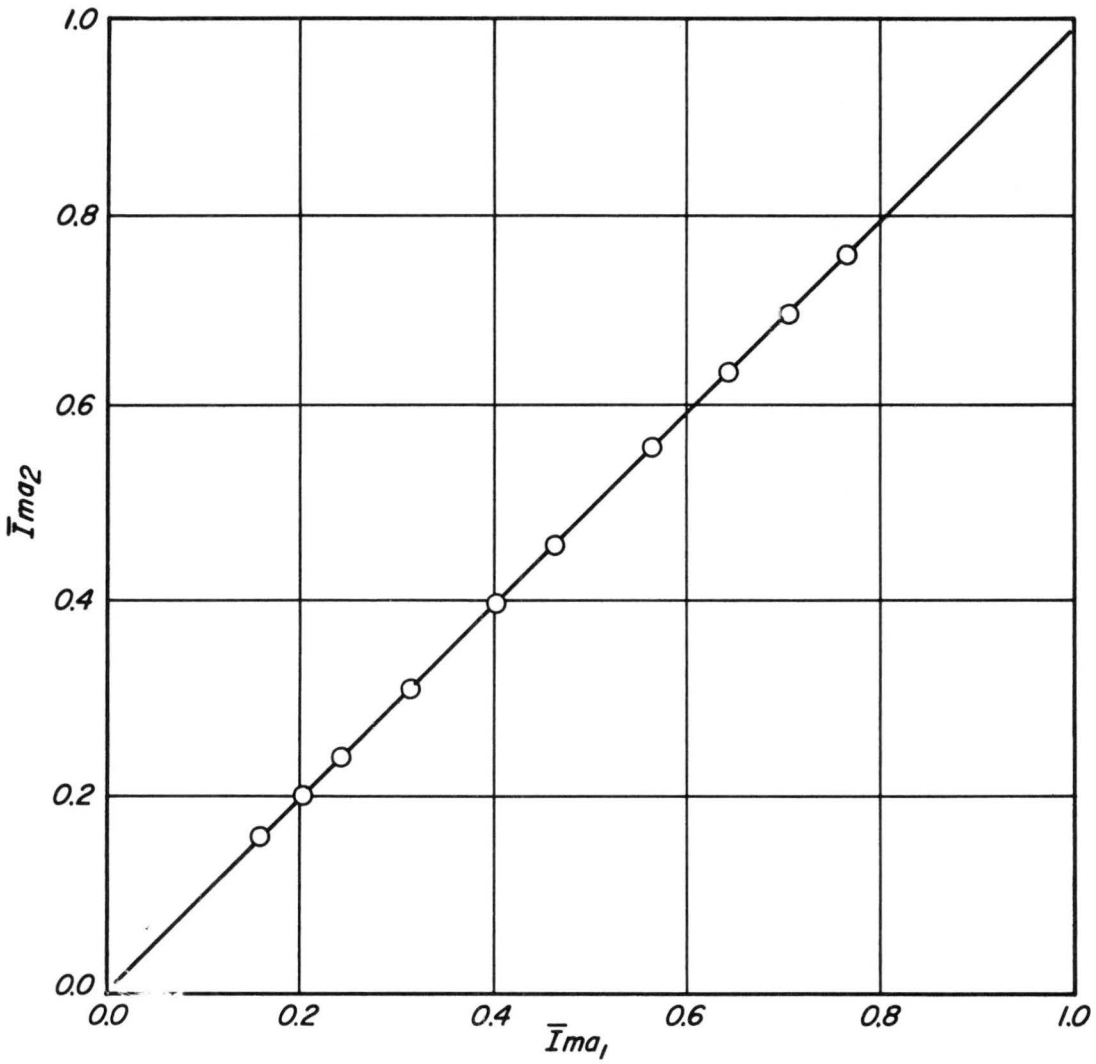

Fig. 6 b Calibration of hot - wires.
(one against the other)

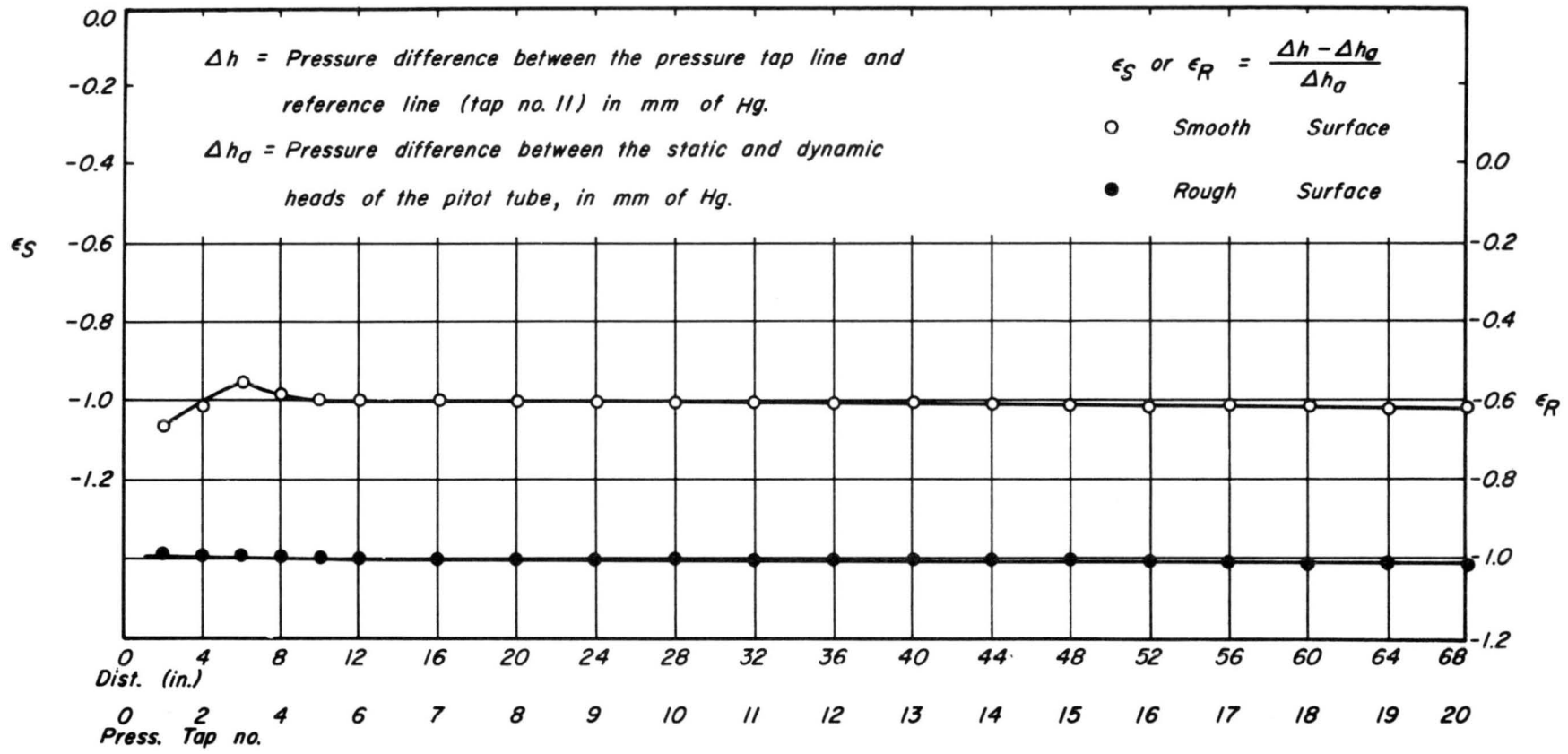

Fig. 7 Non−dimensional plot of pressure distribution along the flat plate.

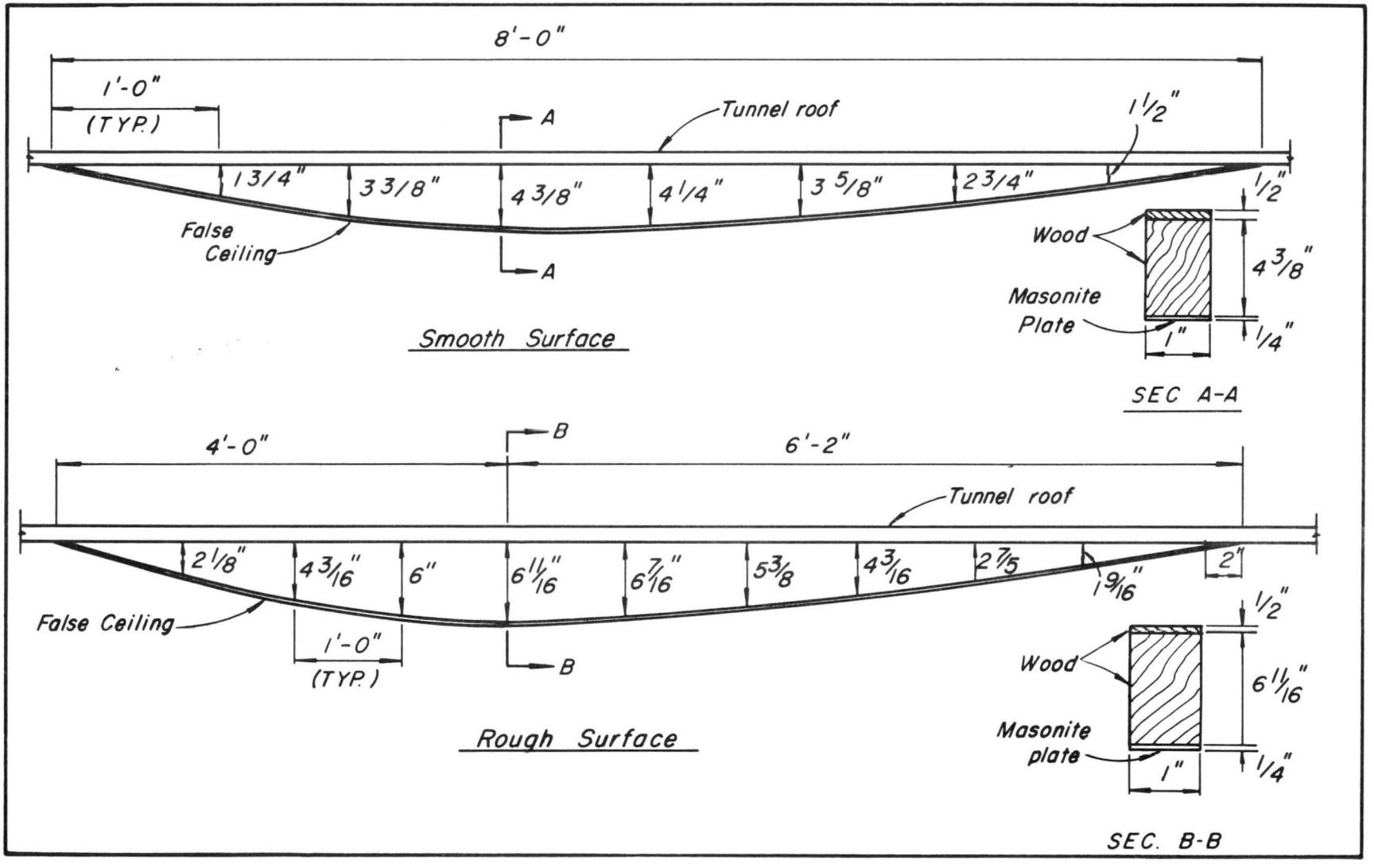

Fig. 8 False wind tunnel ceiling to obtain zero pressure gradient on flat plate

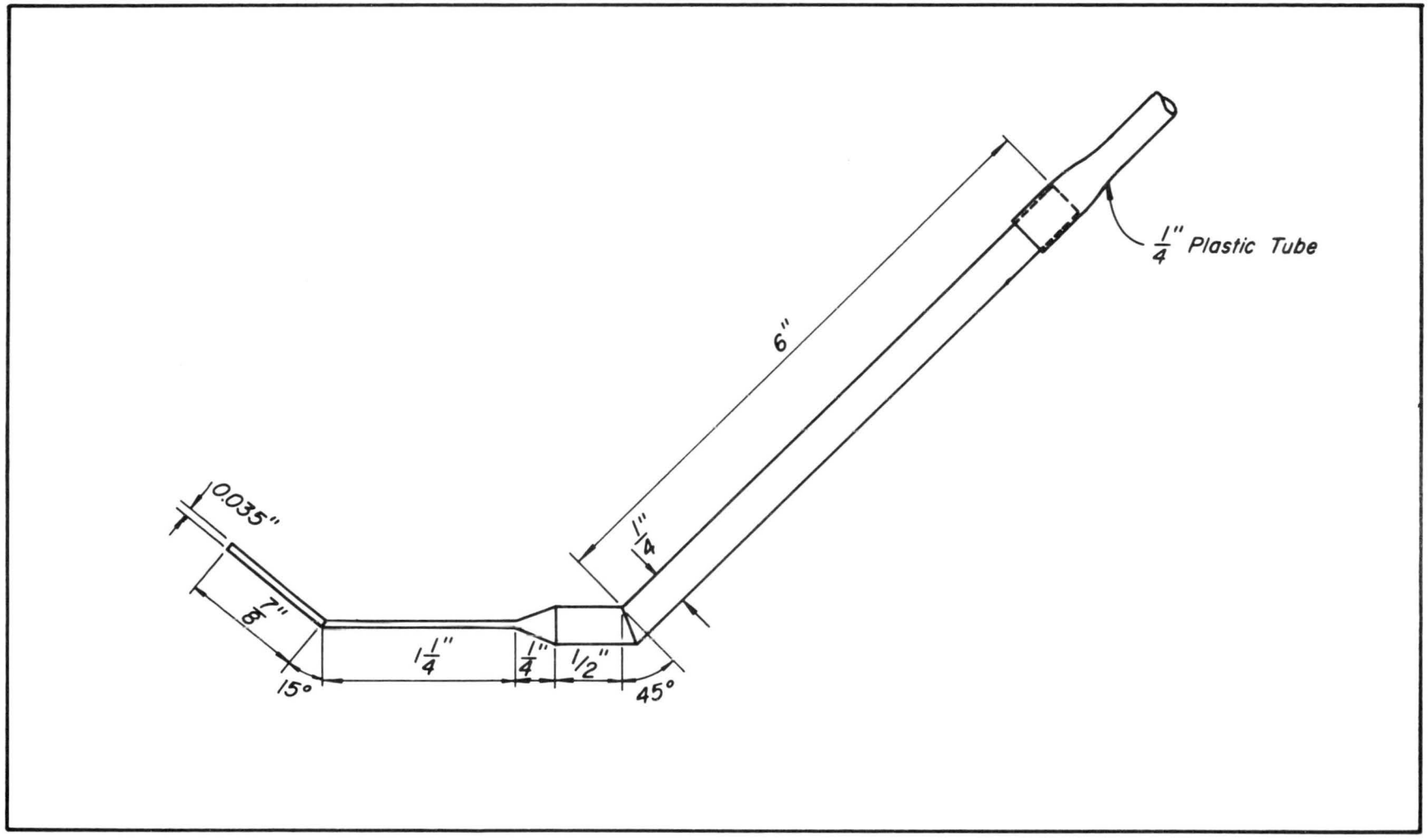

Fig. 9 The total pressure tube

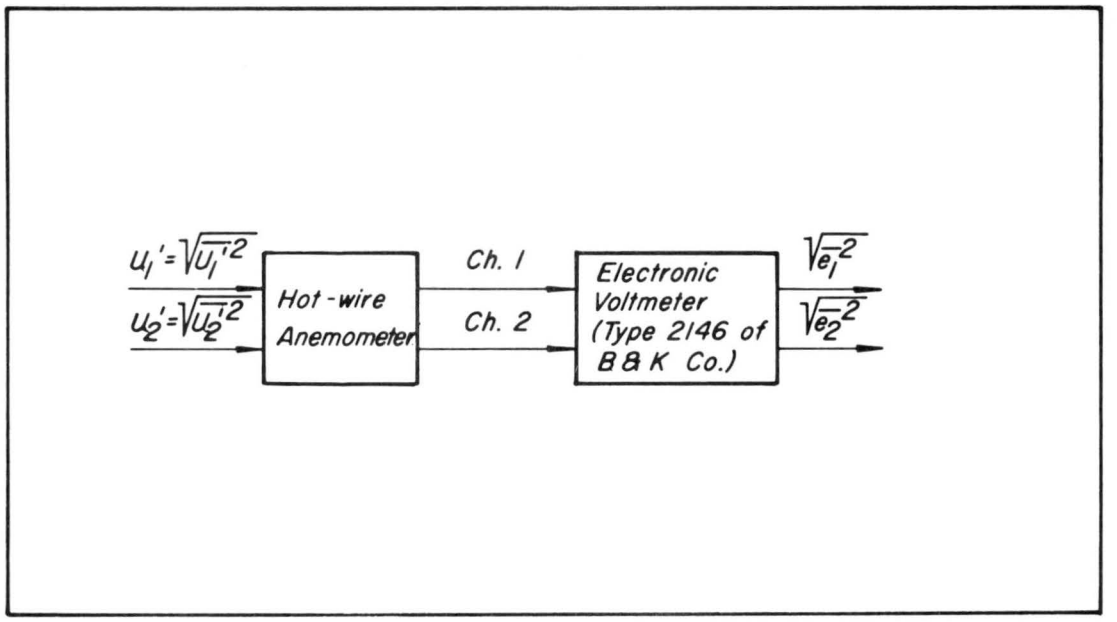

Fig. 10a Experimental arrangement for calculation of turbulent intensities

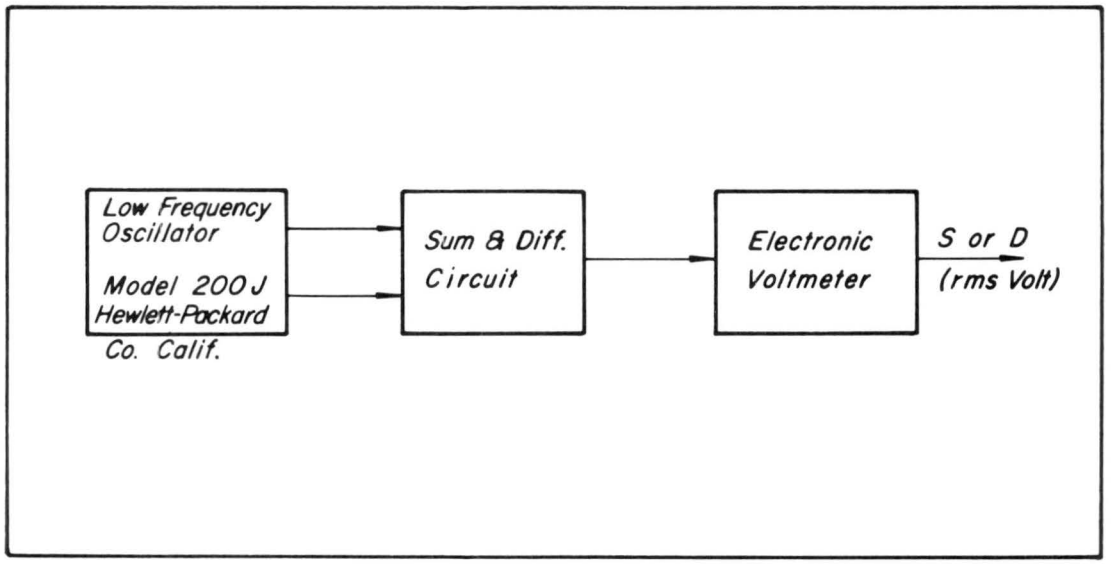

Fig. 10b Experimental arrangement for calibration of sum & diff. circuit

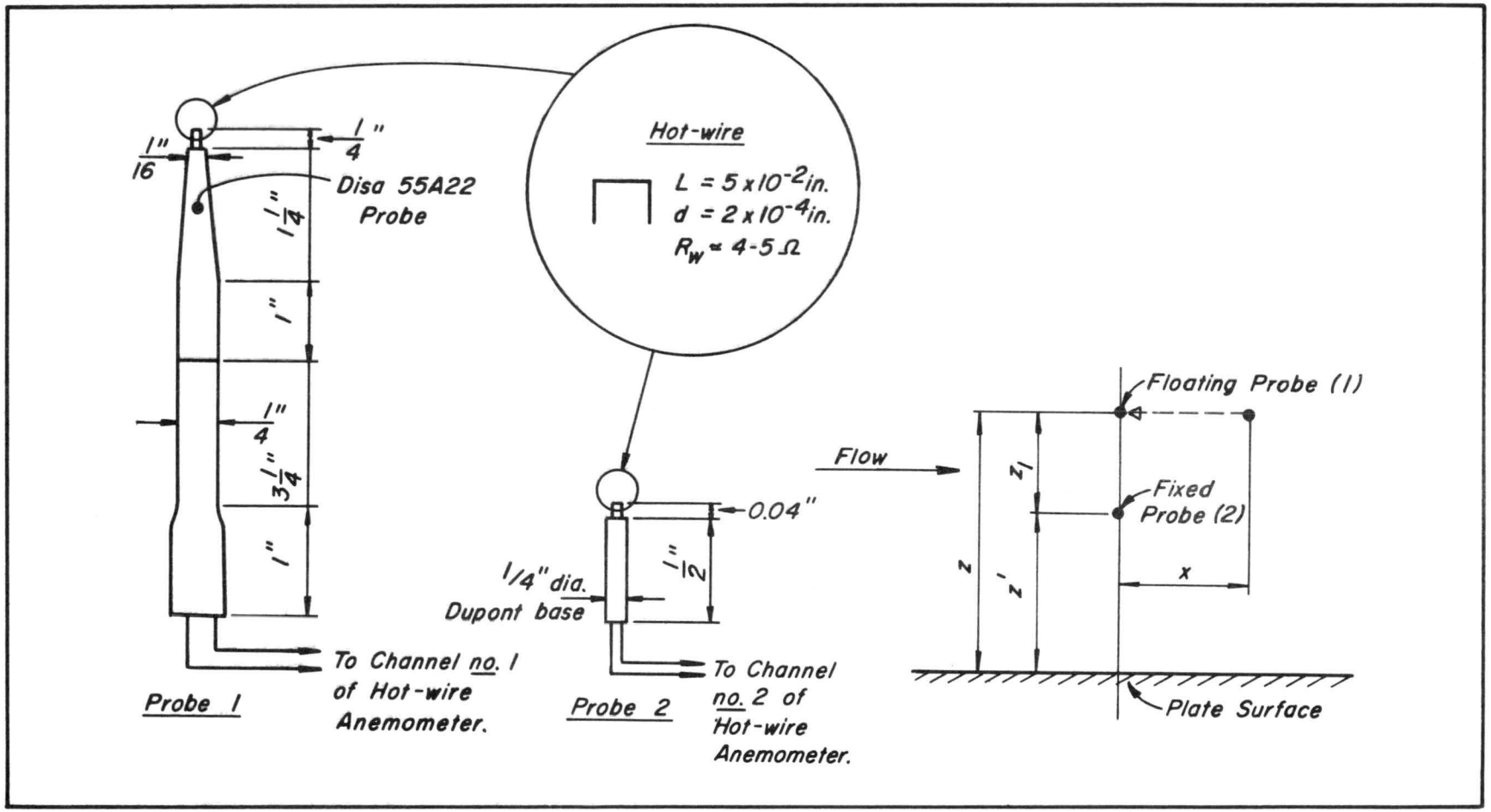

Fig. 11 Details of the space correlations measuring probes

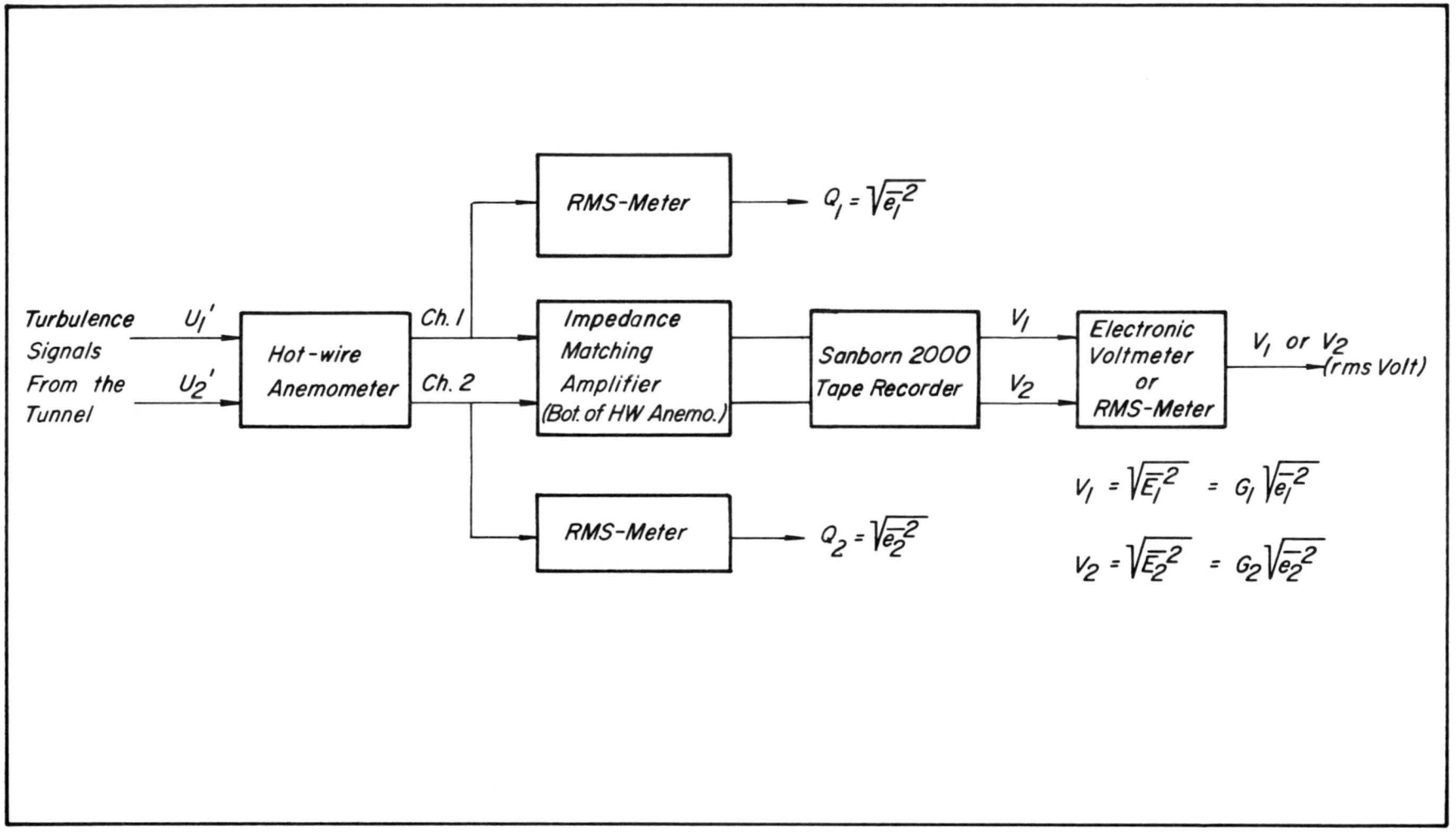

Fig. 12 Experimental Arrangement for recording of turbulence signals

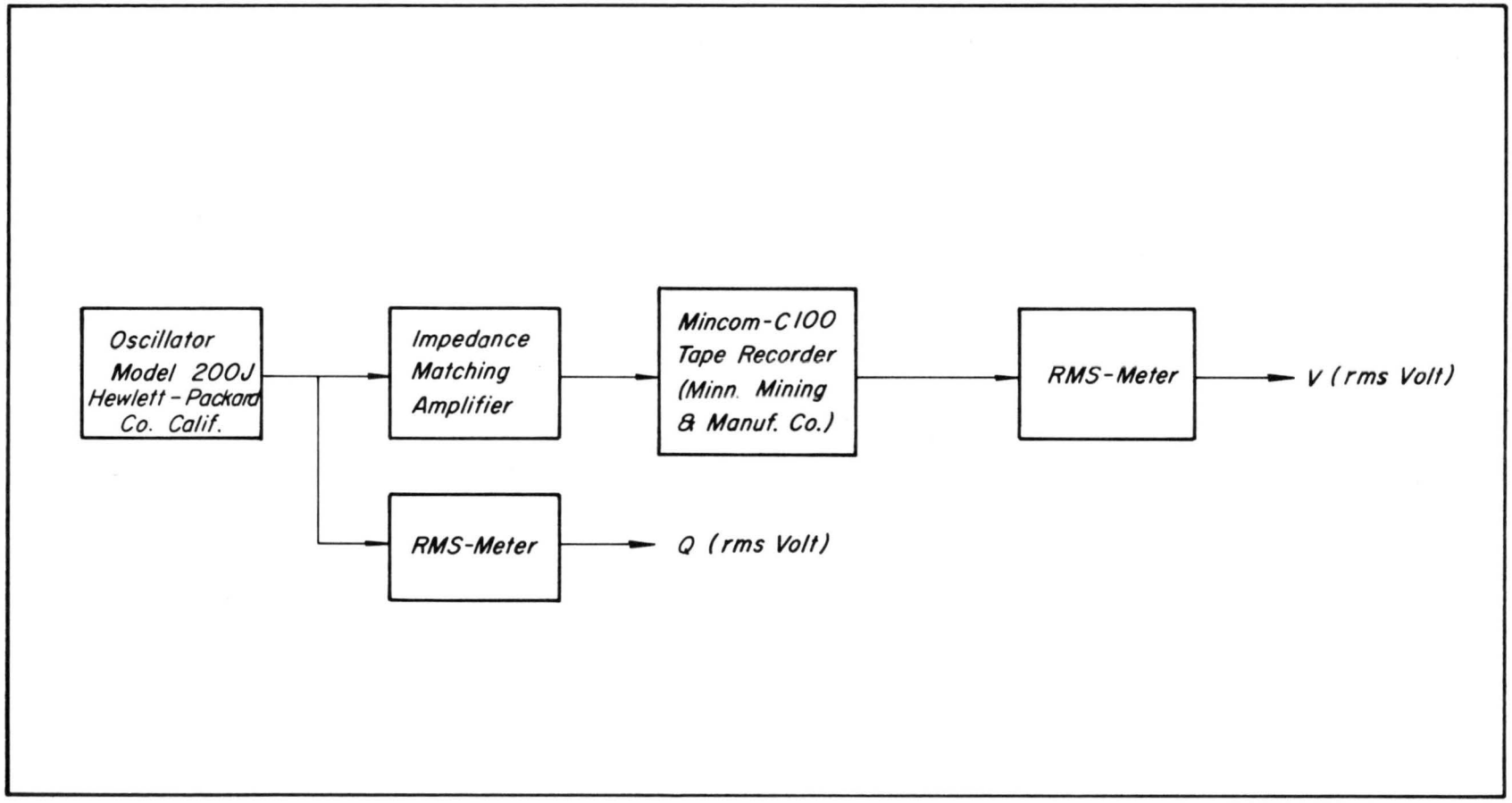

Fig. 13 Experimental arrangement for frequency response of tape recorder – impedance matching amplifier.

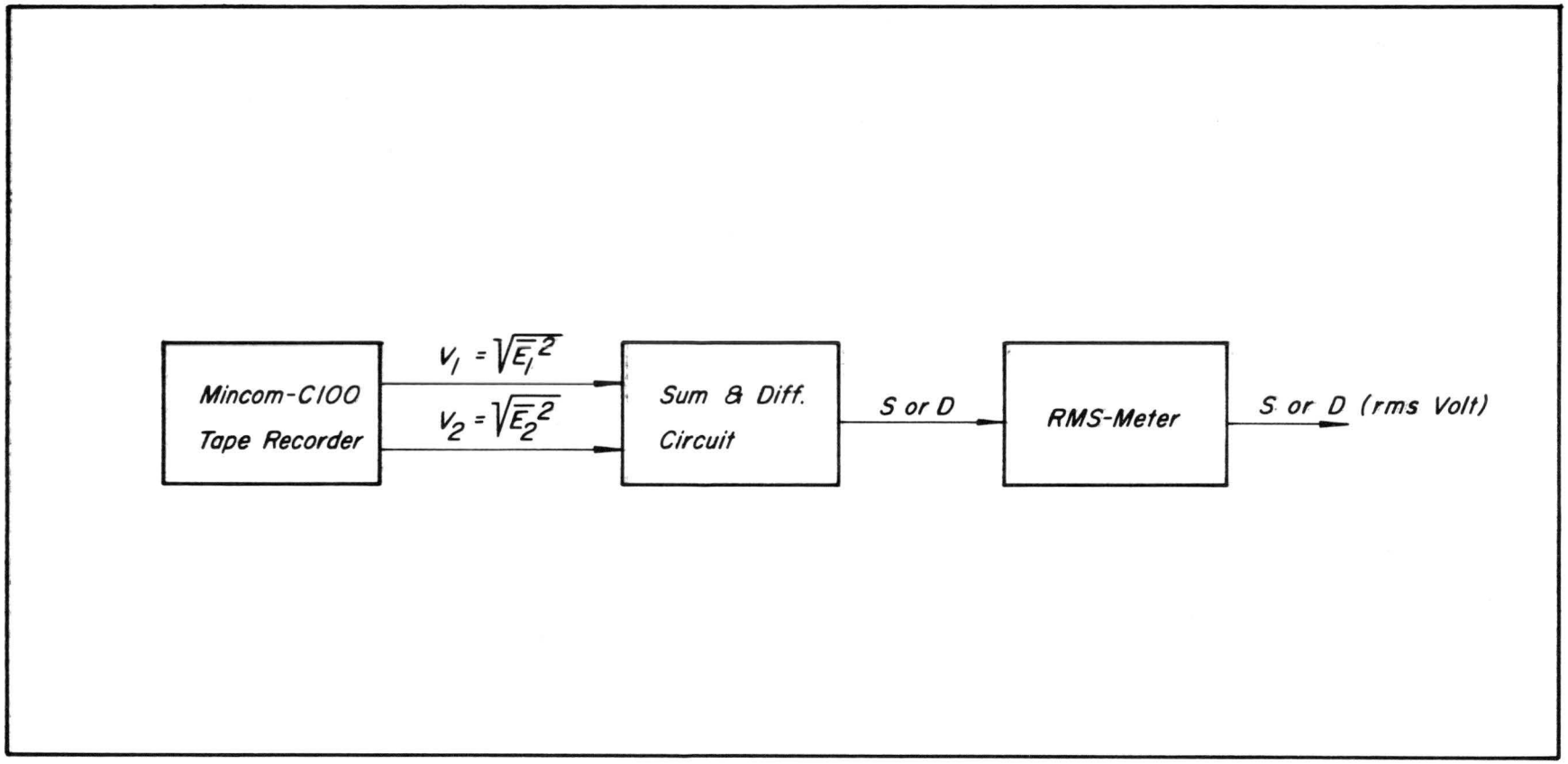

Fig. 14 Experimental arrangement for total correlations measurements.

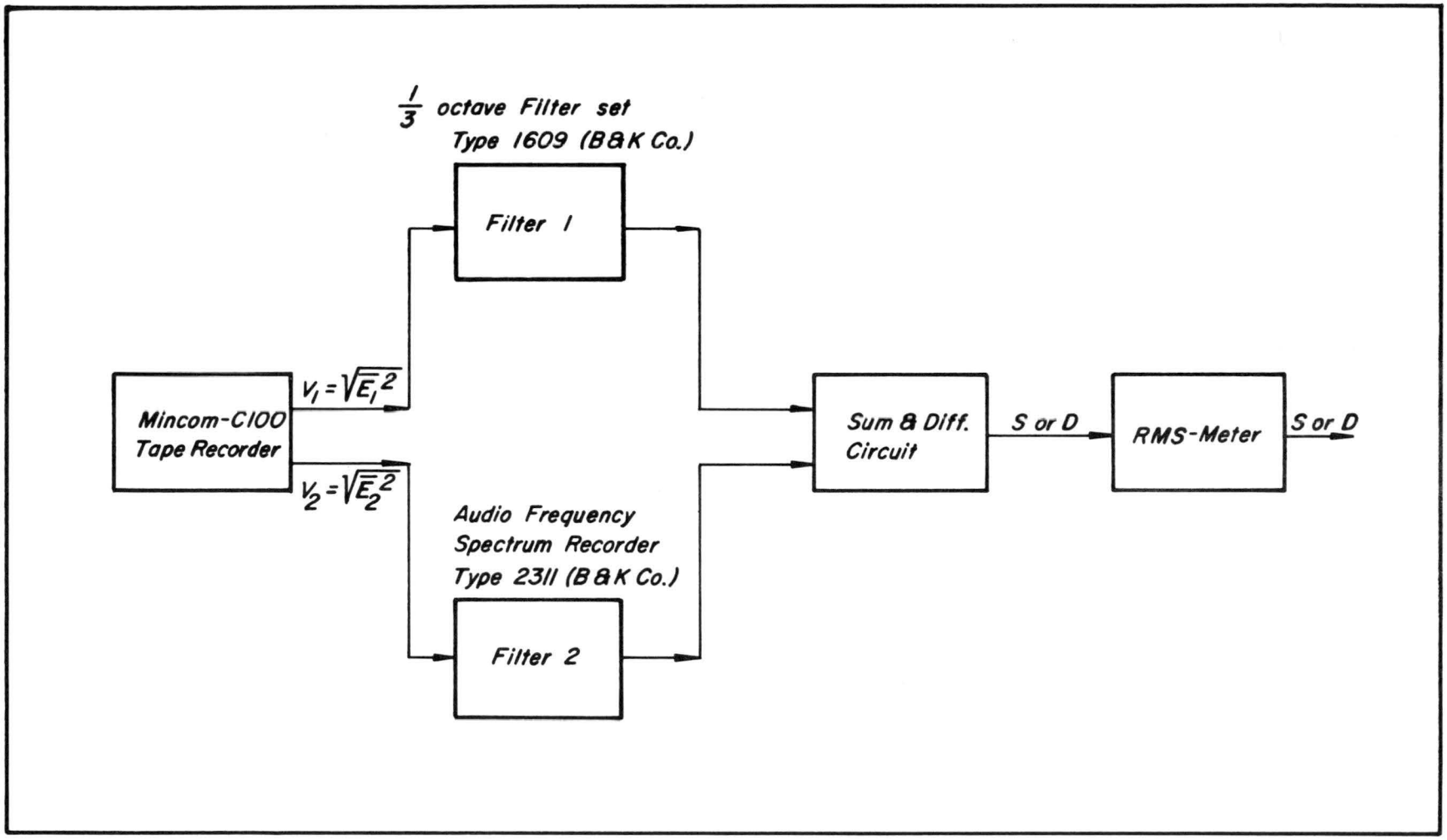

Fig. 15 Experimental arrangement for filtered correlations measurments.

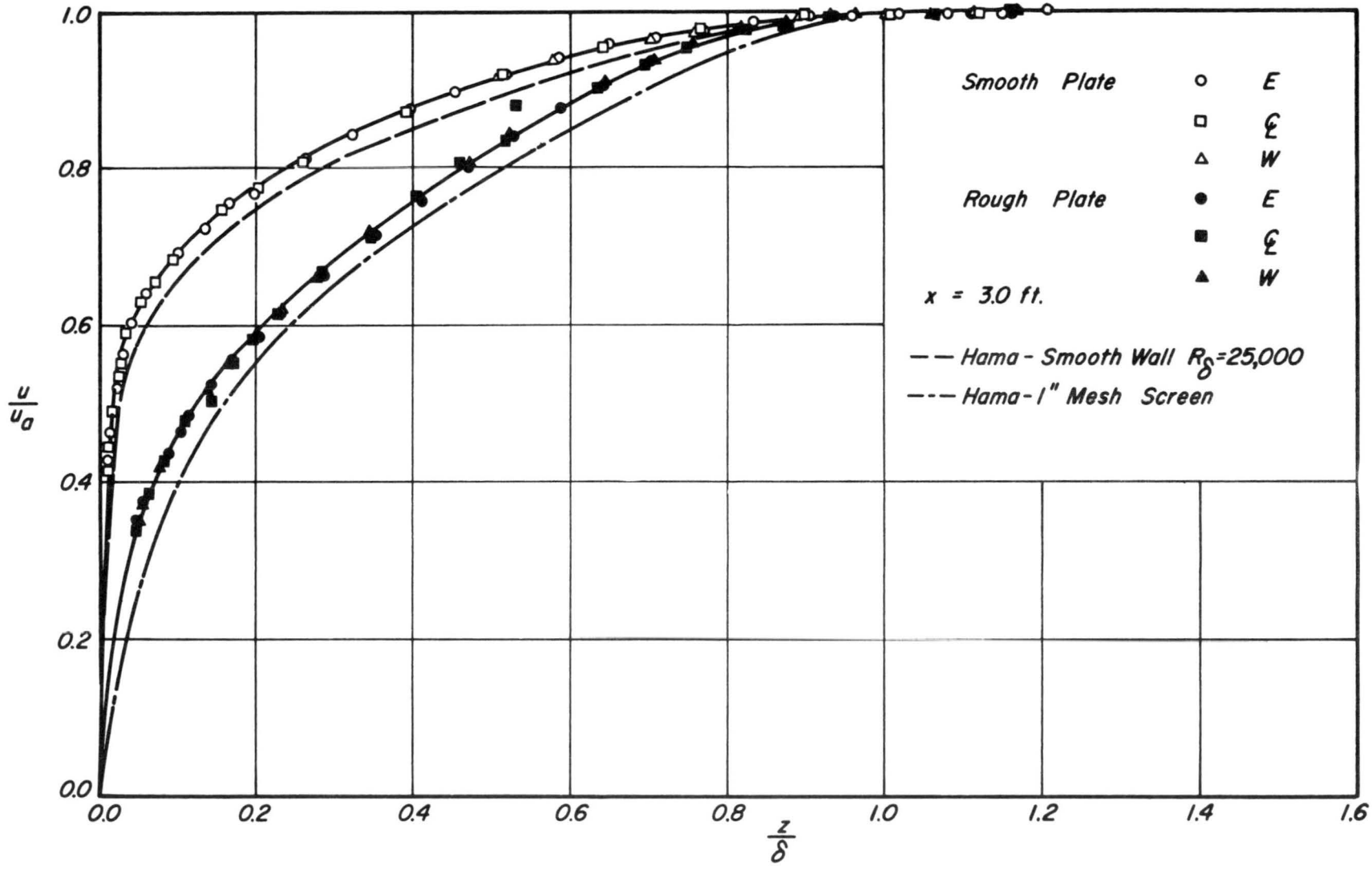

Fig. 16 Turbulent boundary layer profiles at zero pressure on smooth & rough flat plate.

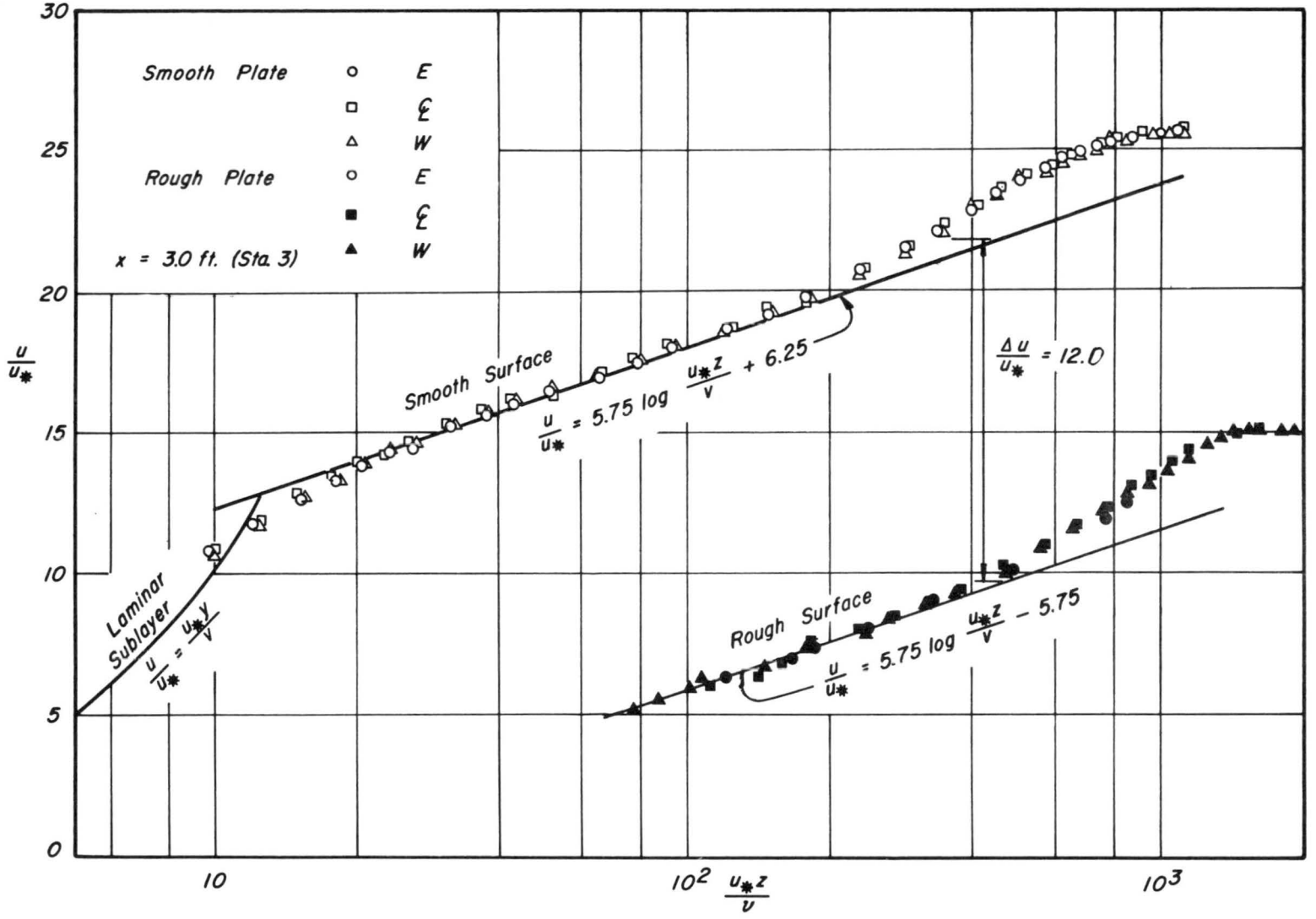

Fig. 17 Universal velocity distribution for turbulent layers on smooth & rough flat plate.

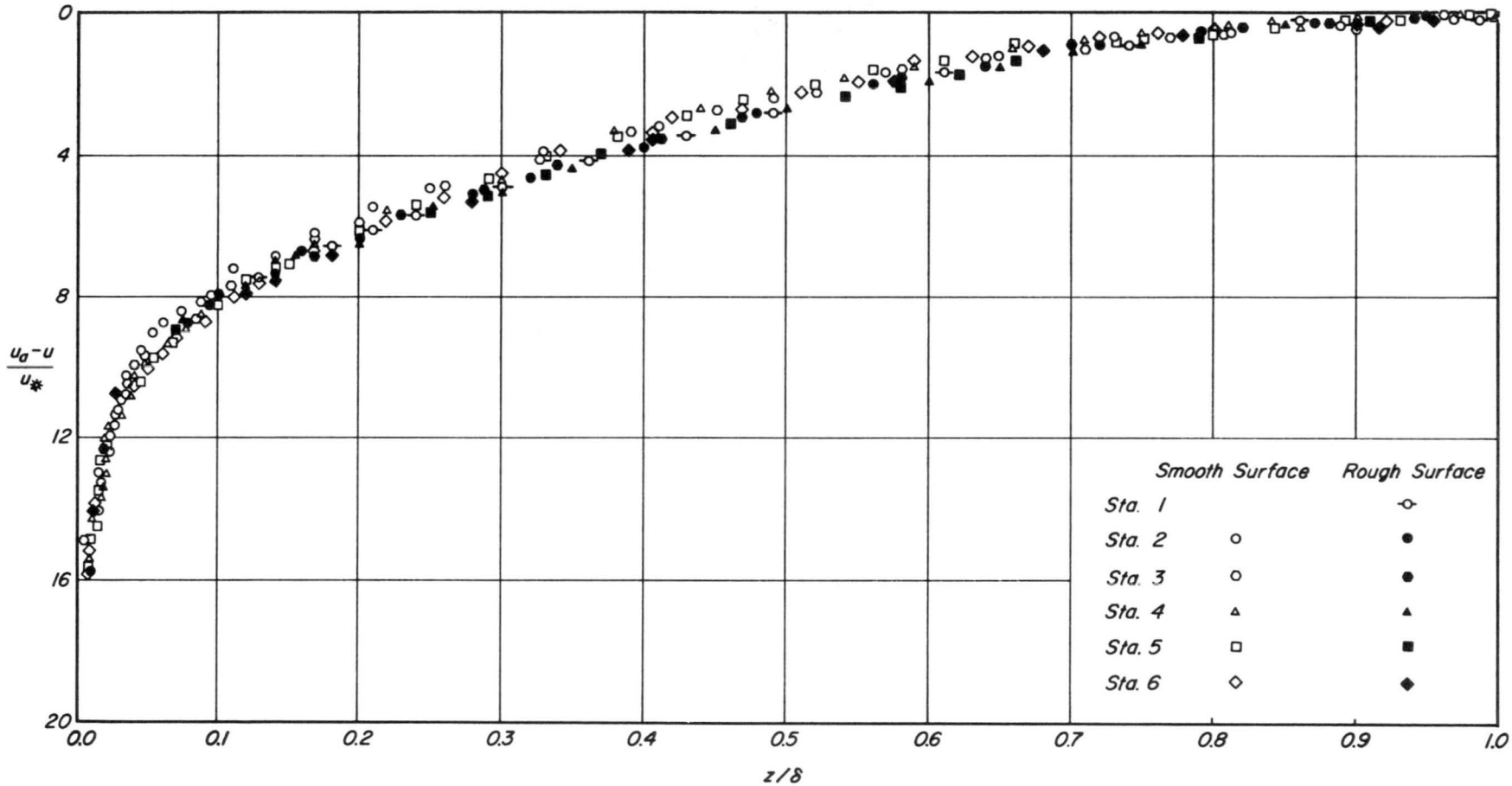

Fig. 18 Universal plot of turbulent boundary layer profiles at zero pressure on flat plate.

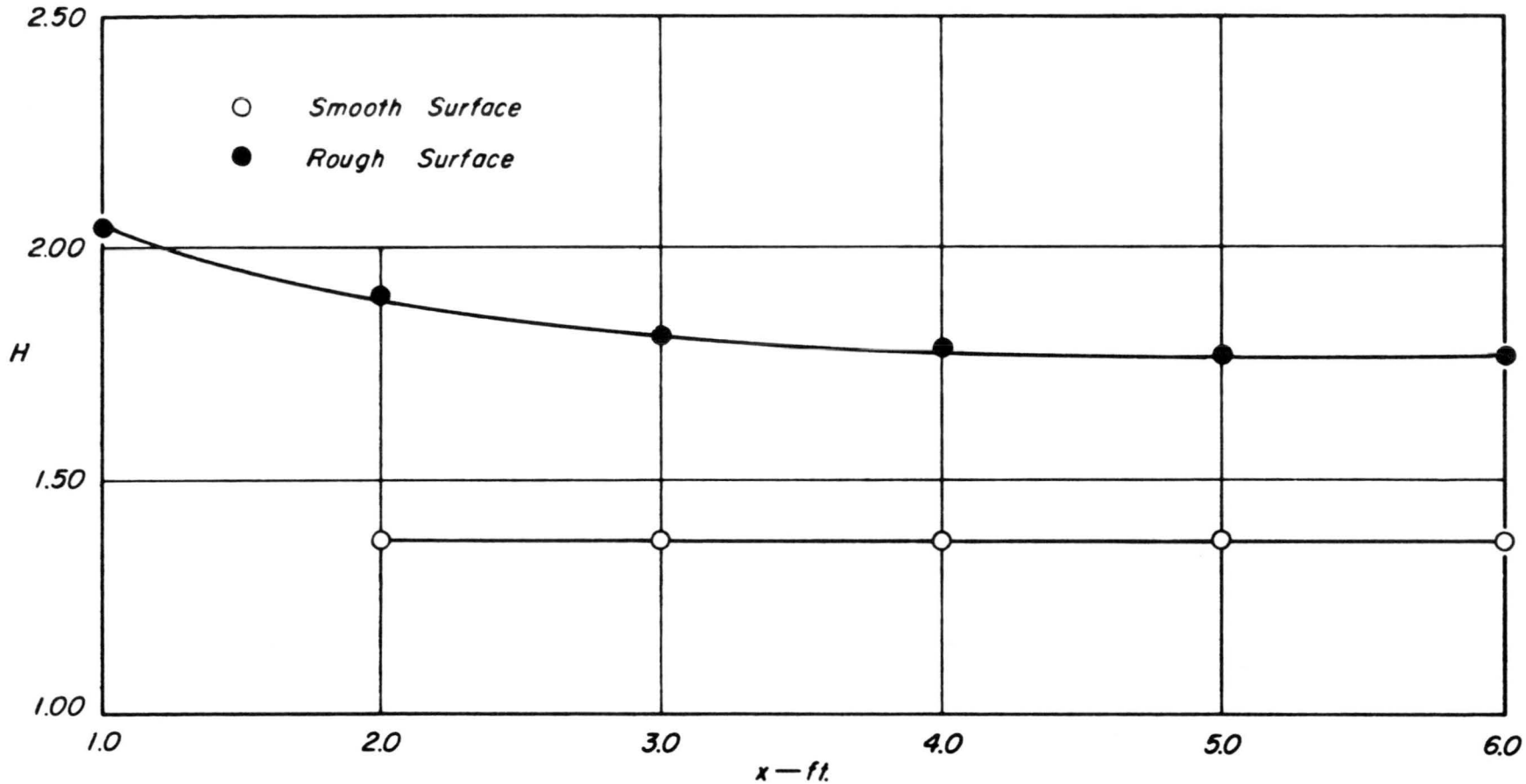

Fig. 19 Variation of form factor with distance.

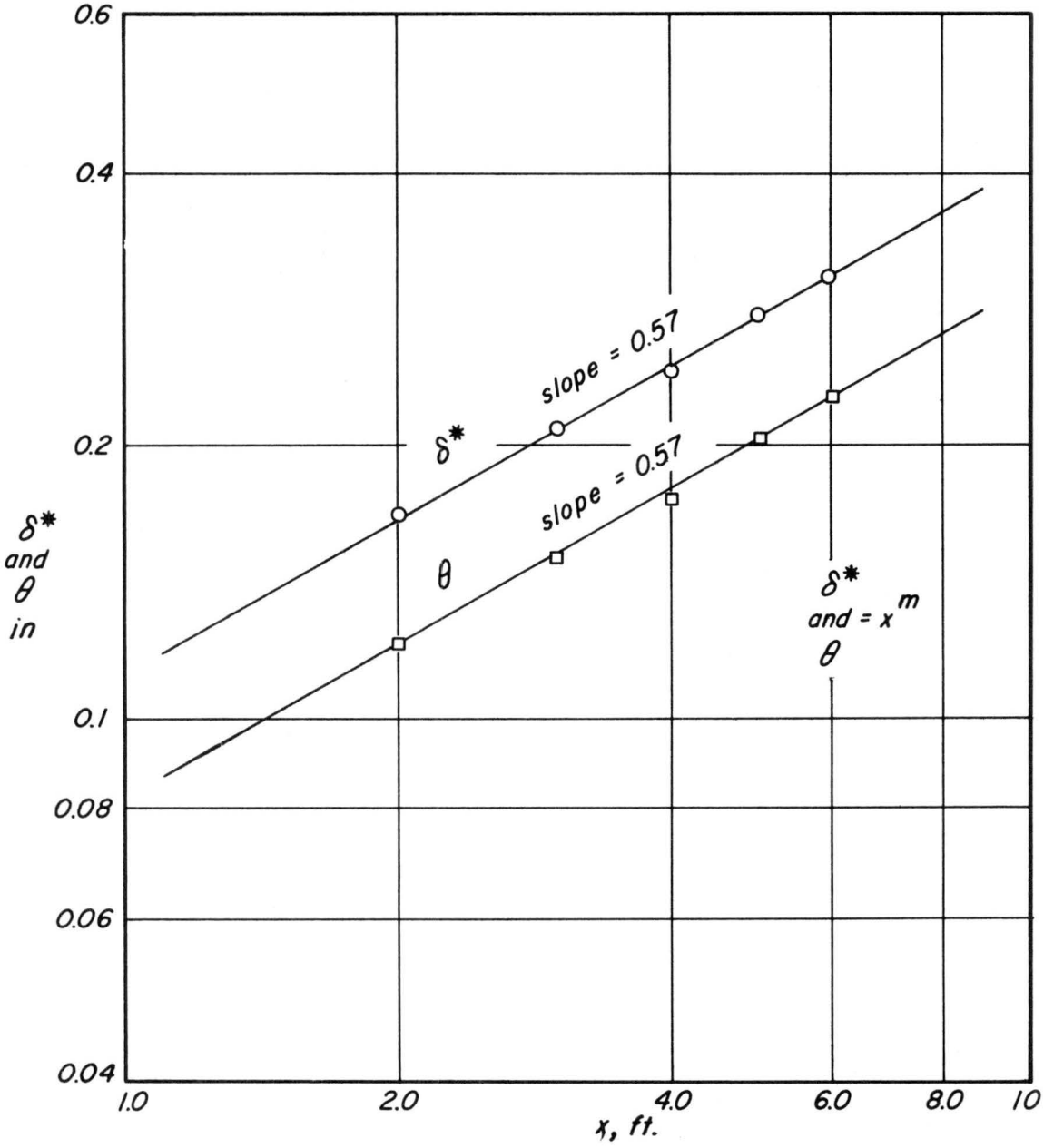

Fig. 20 Determination of slope (m) from values of δ and θ (℄) on smooth plate.

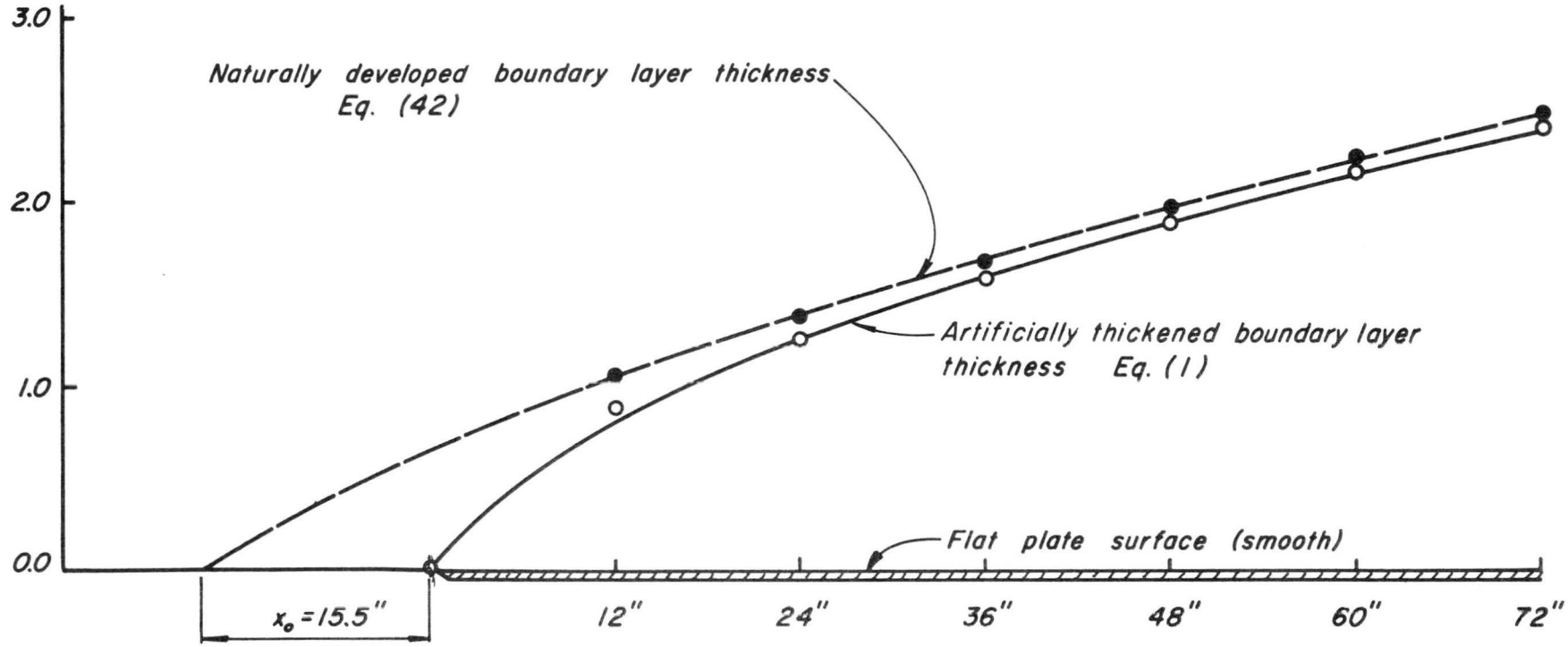

Fig. 21 Comparison of artificially and naturally developed boundary layer thickness.

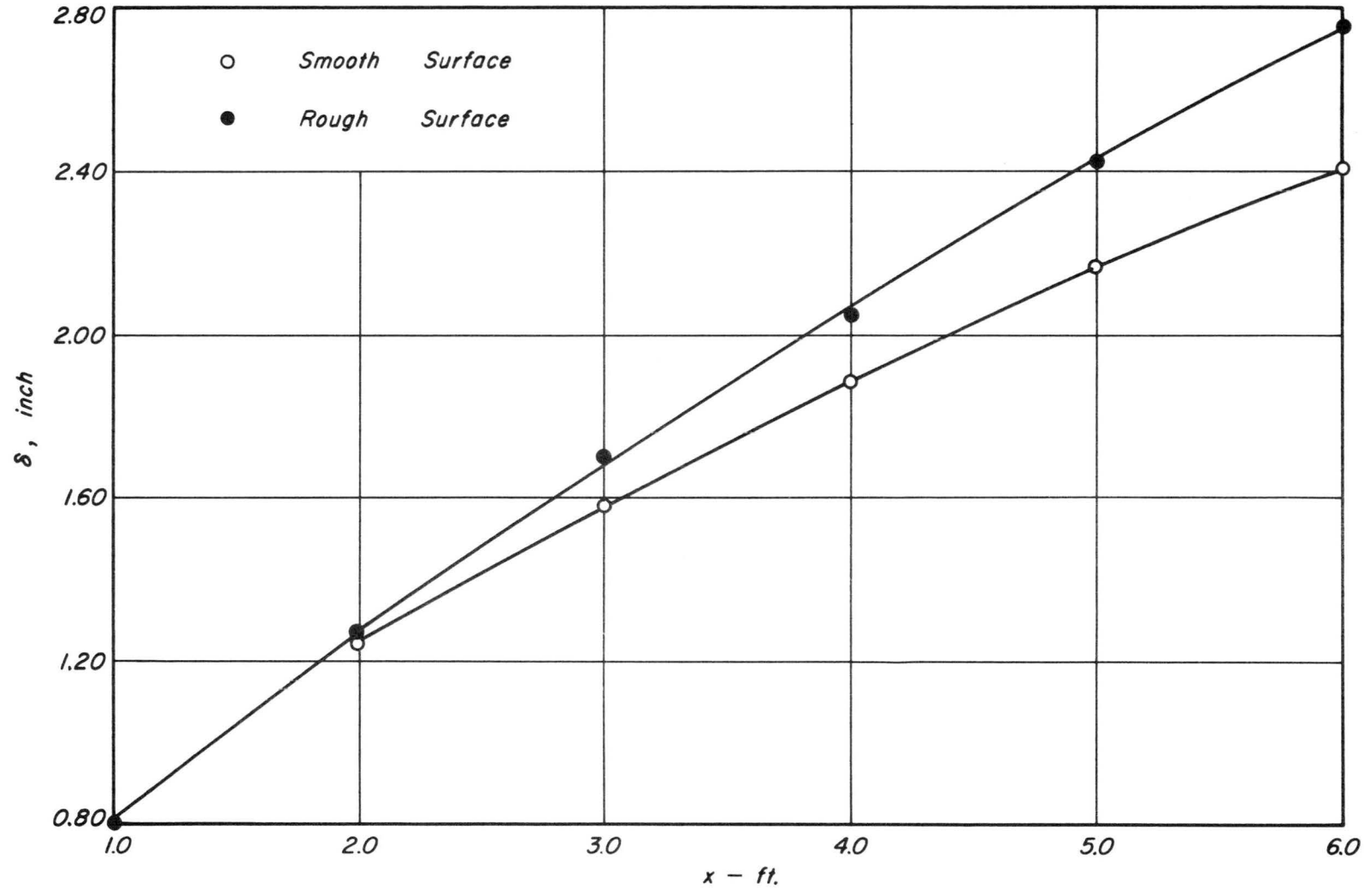

Fig. 22 Development of boundary layer thickness.

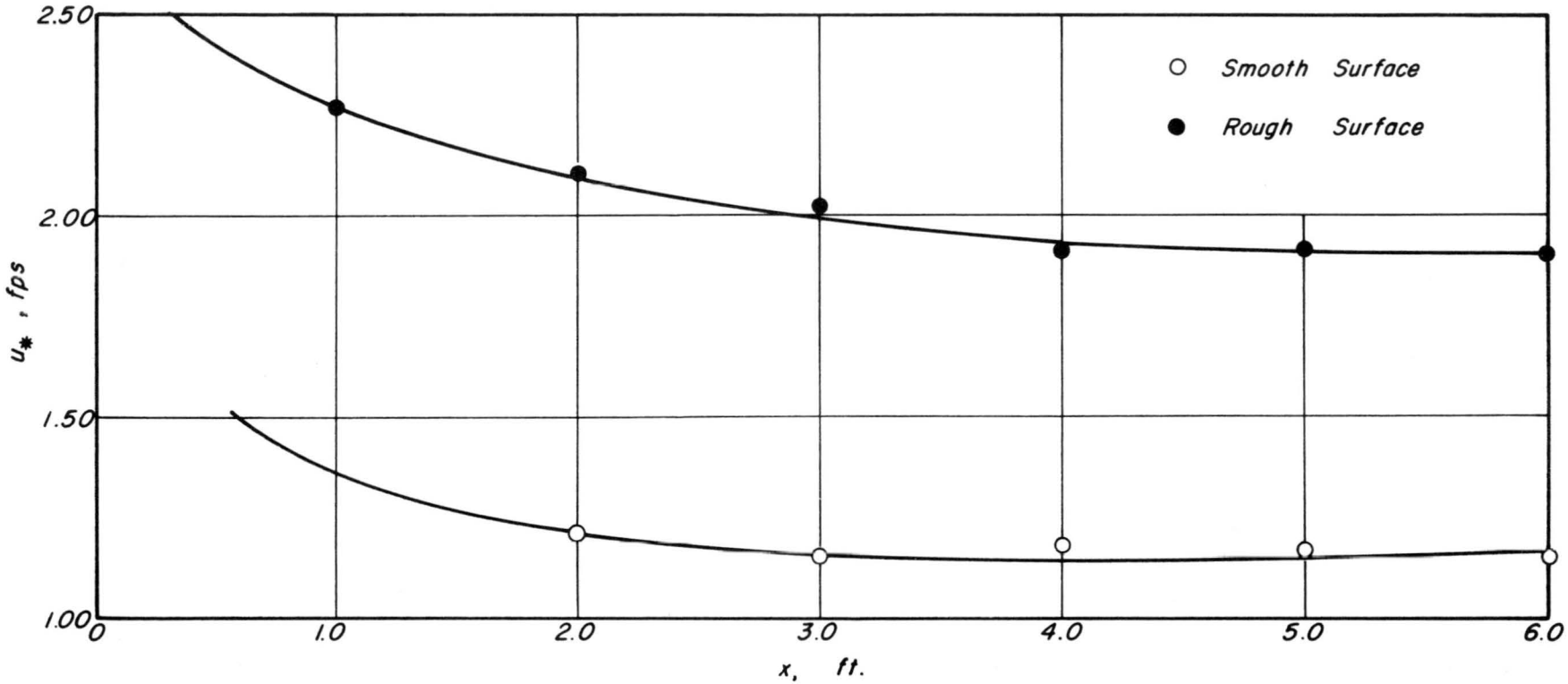

Fig. 23 Distribution of shear velocity along ℄

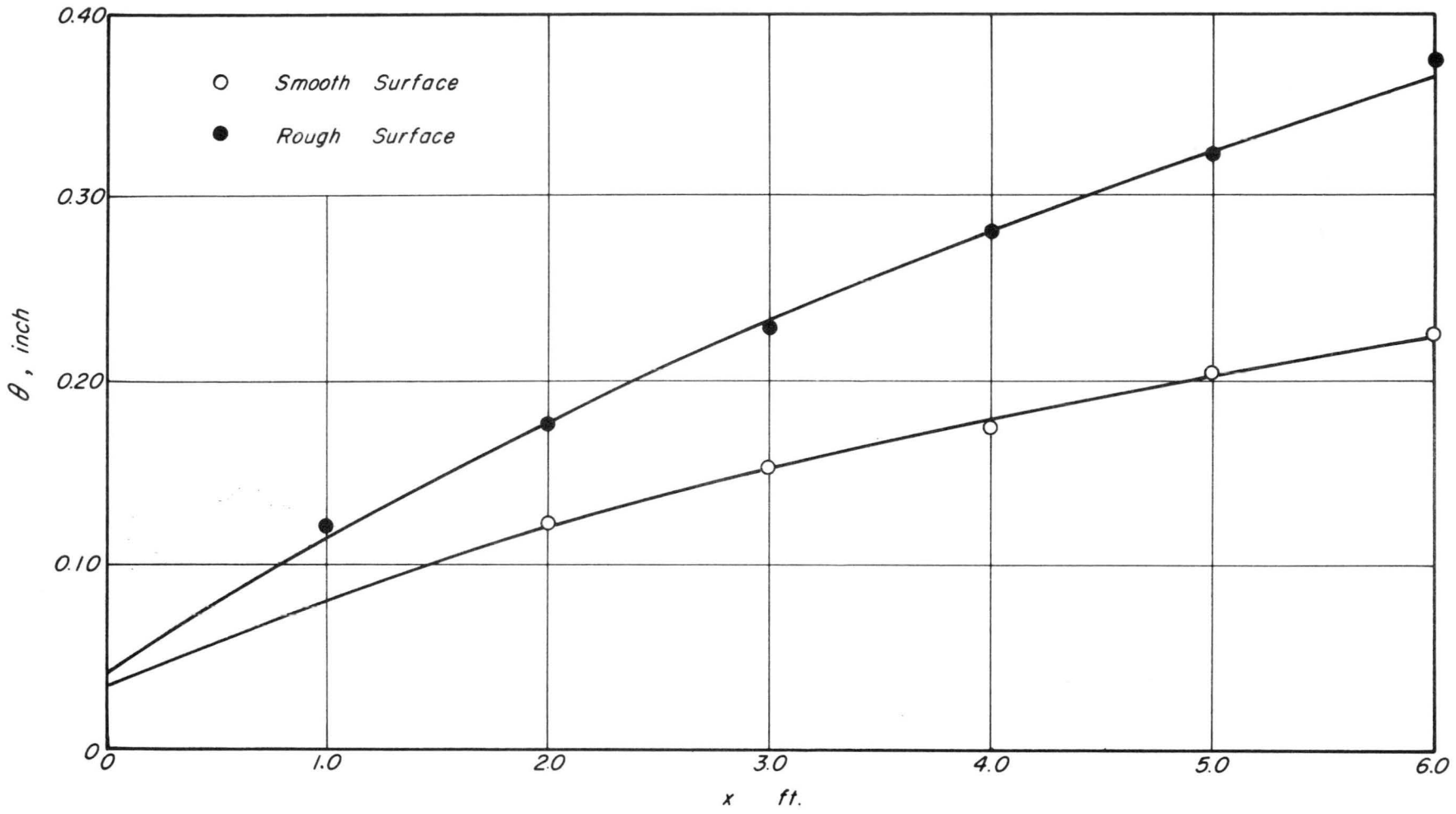

Fig. 24 Development of momentum thickness

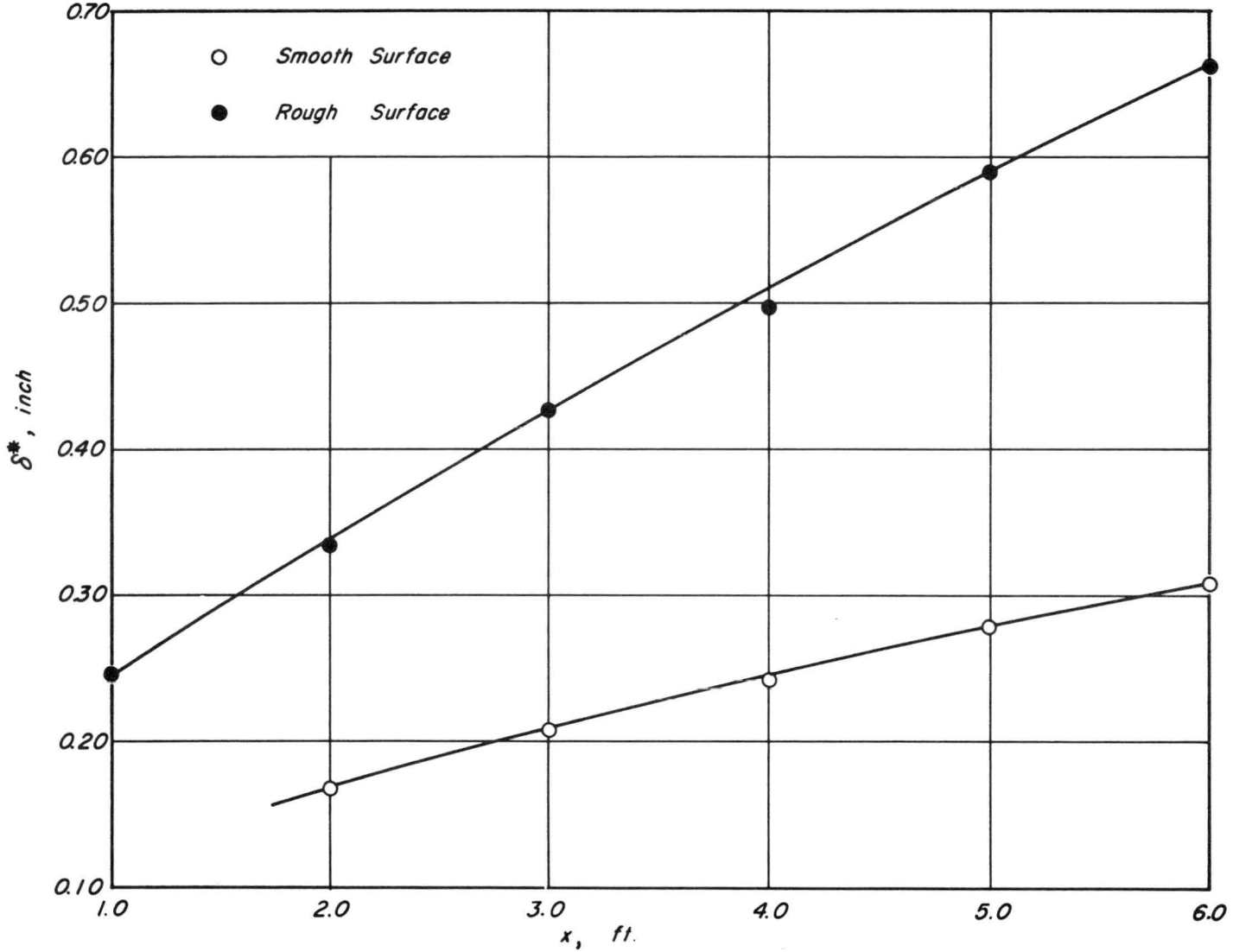

Fig. 25 Development of displacement thickness.

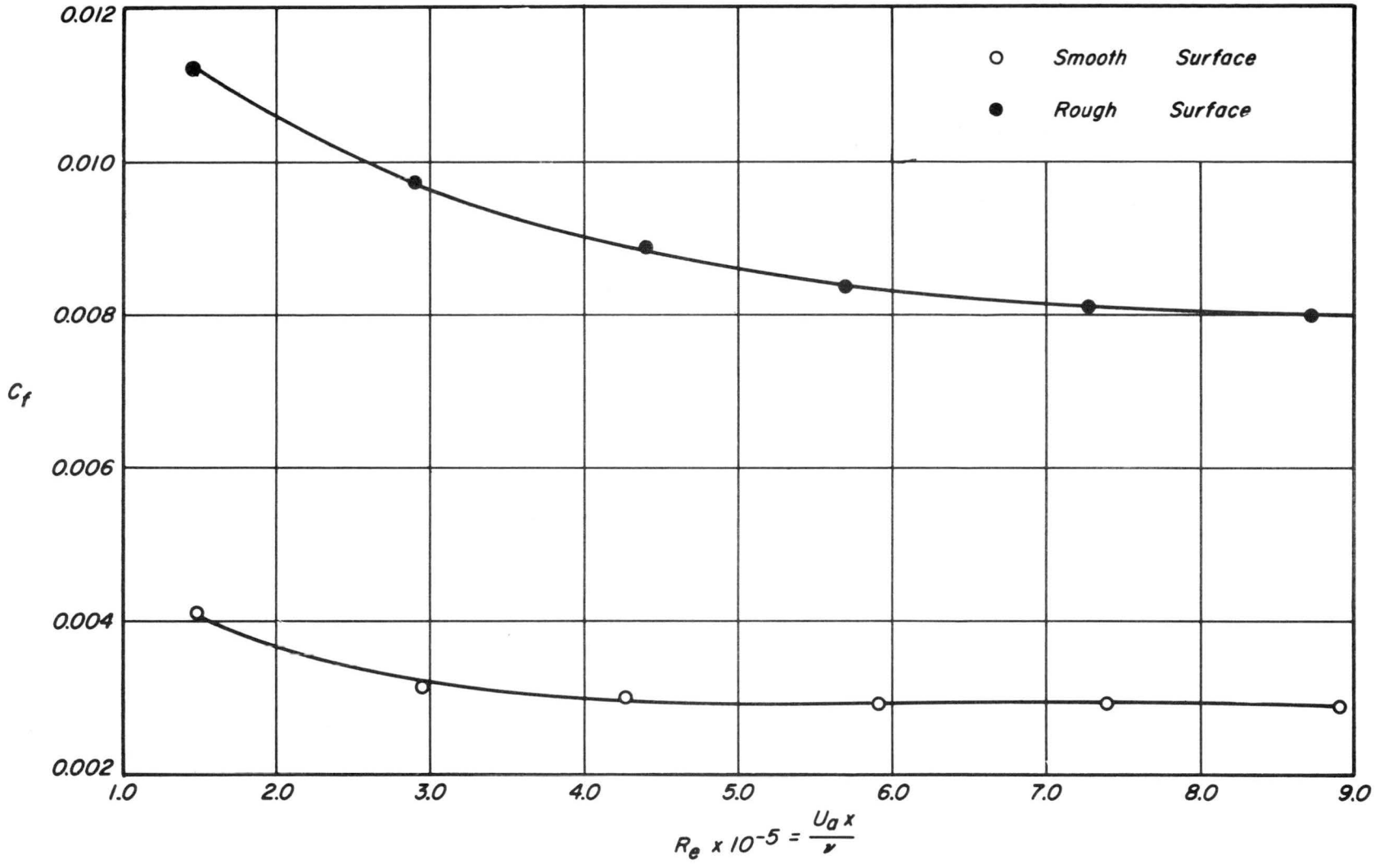

Fig. 26 Development of wall friction with Reynold's number.

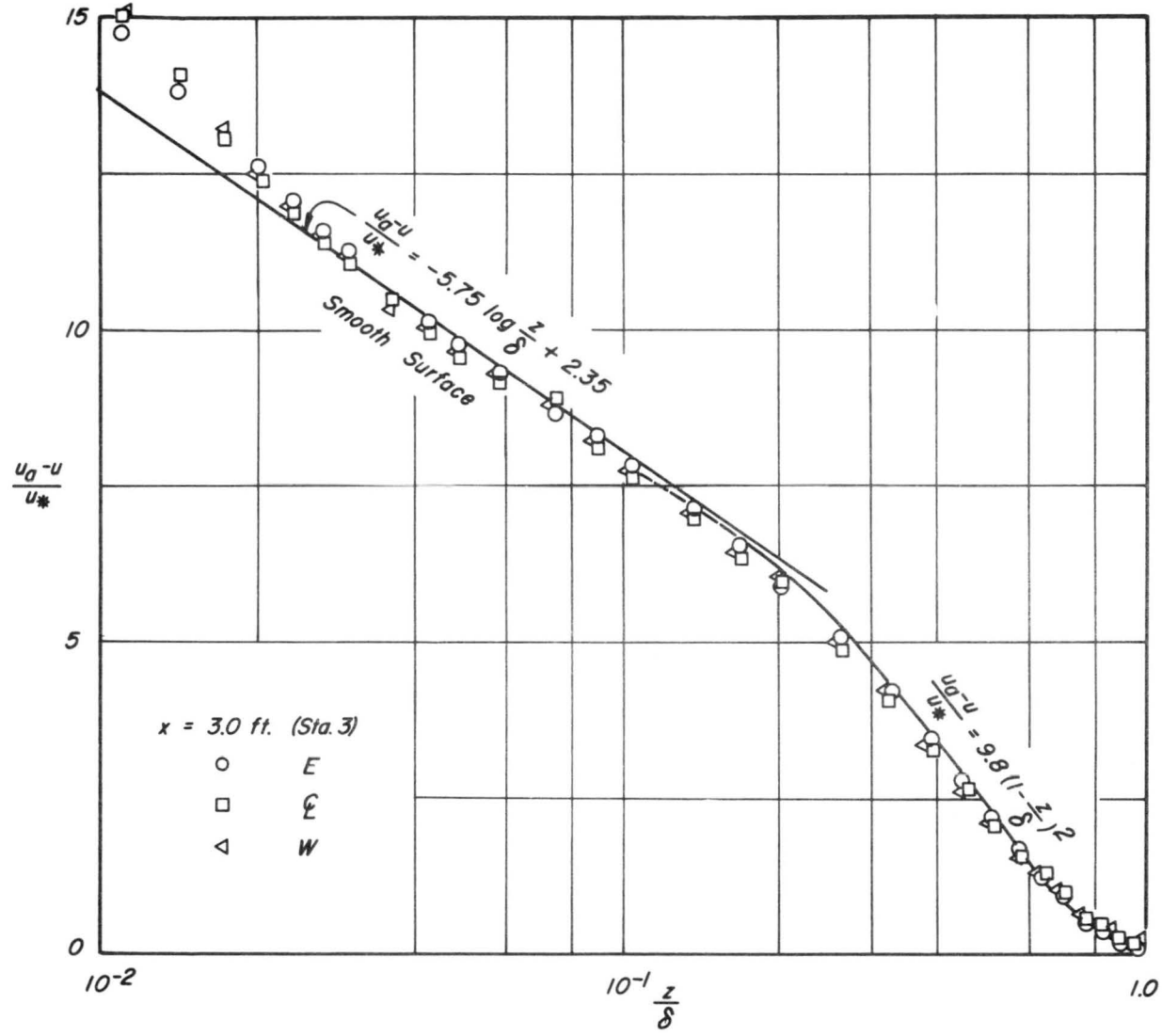

Fig. 27 Velocity defect law on smooth flat plate

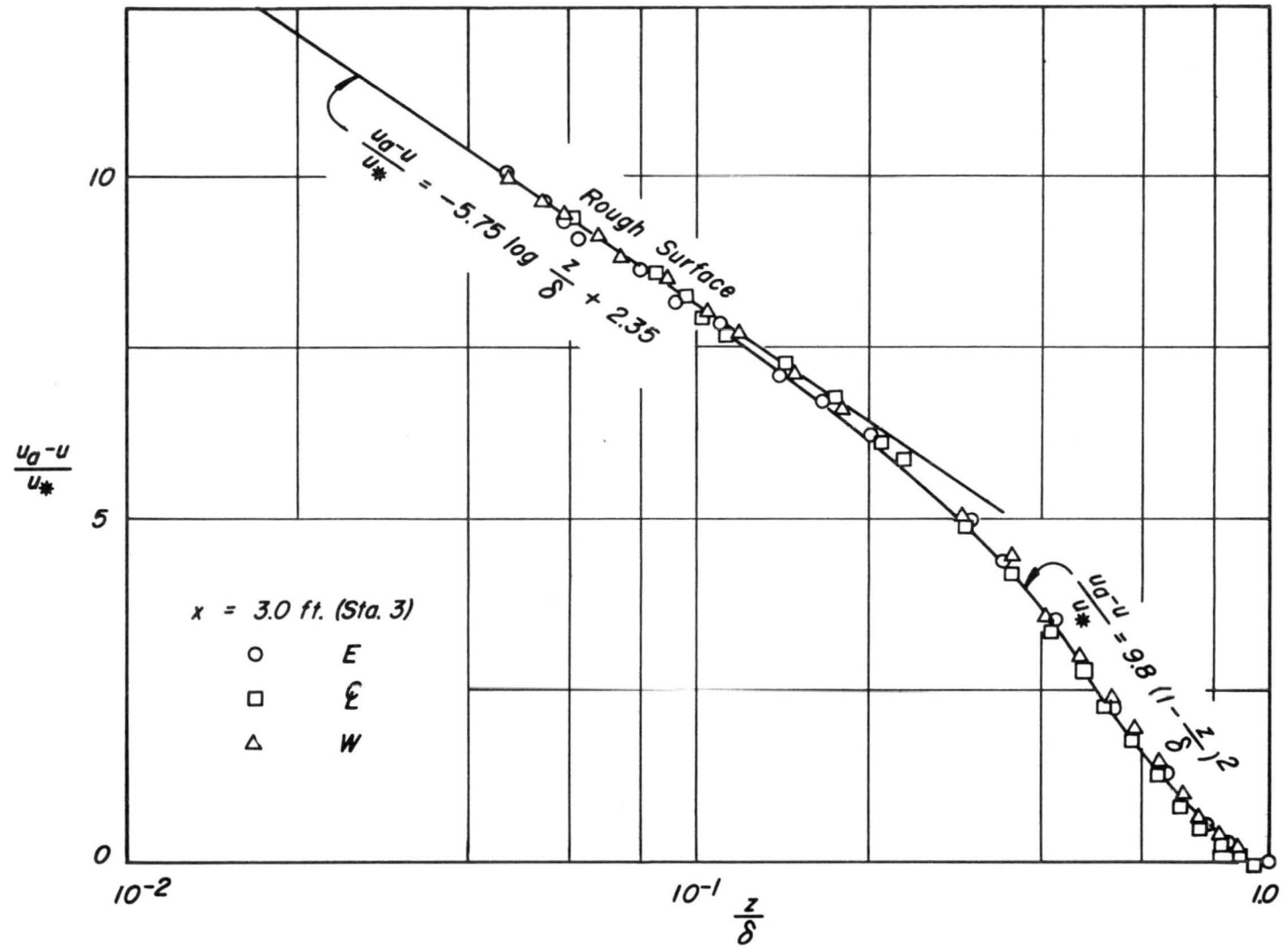

Fig. 28 Velocity defect law on rough flat plate

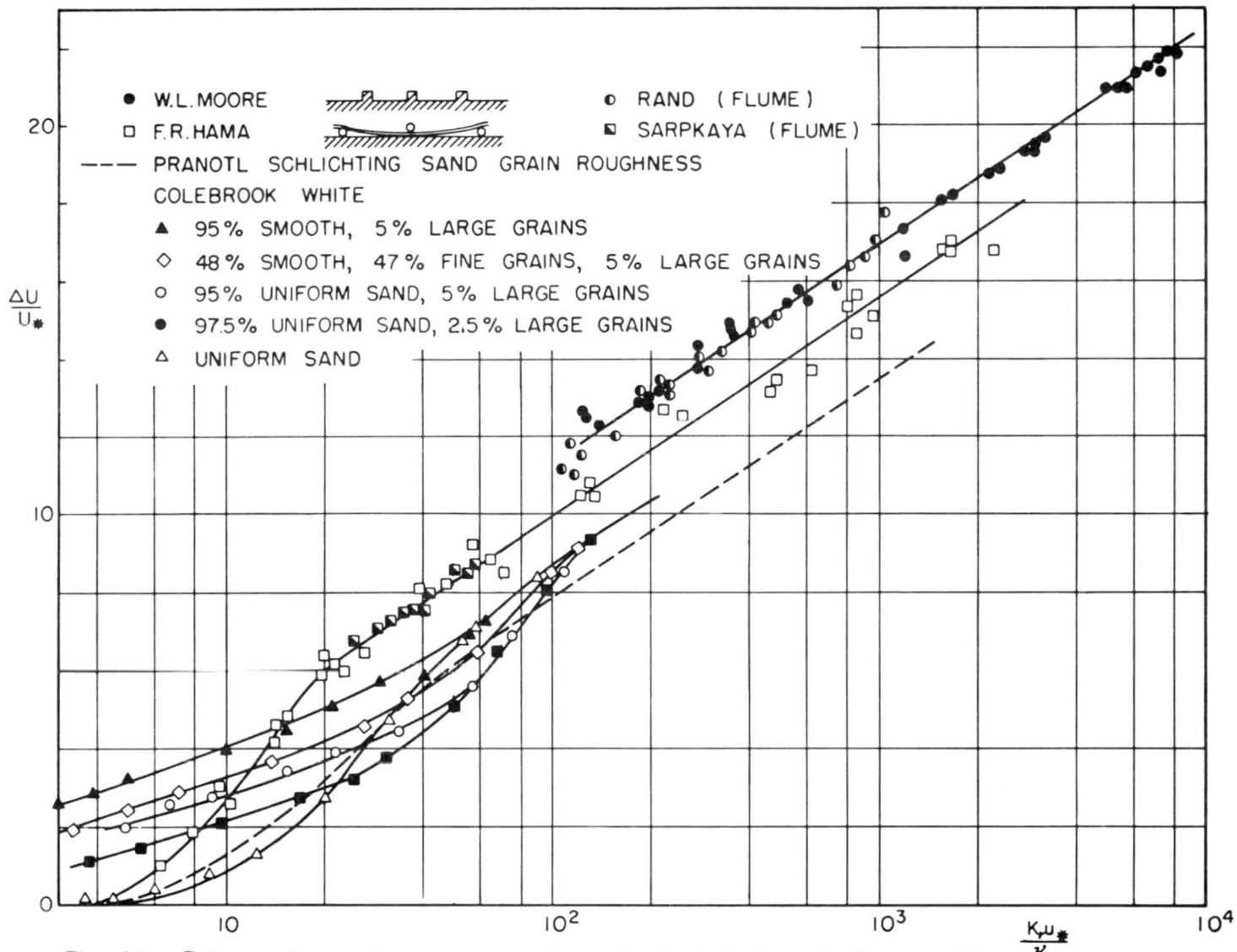

Fig. 29 Effect of roughness on universal turbulent velocity profiles.

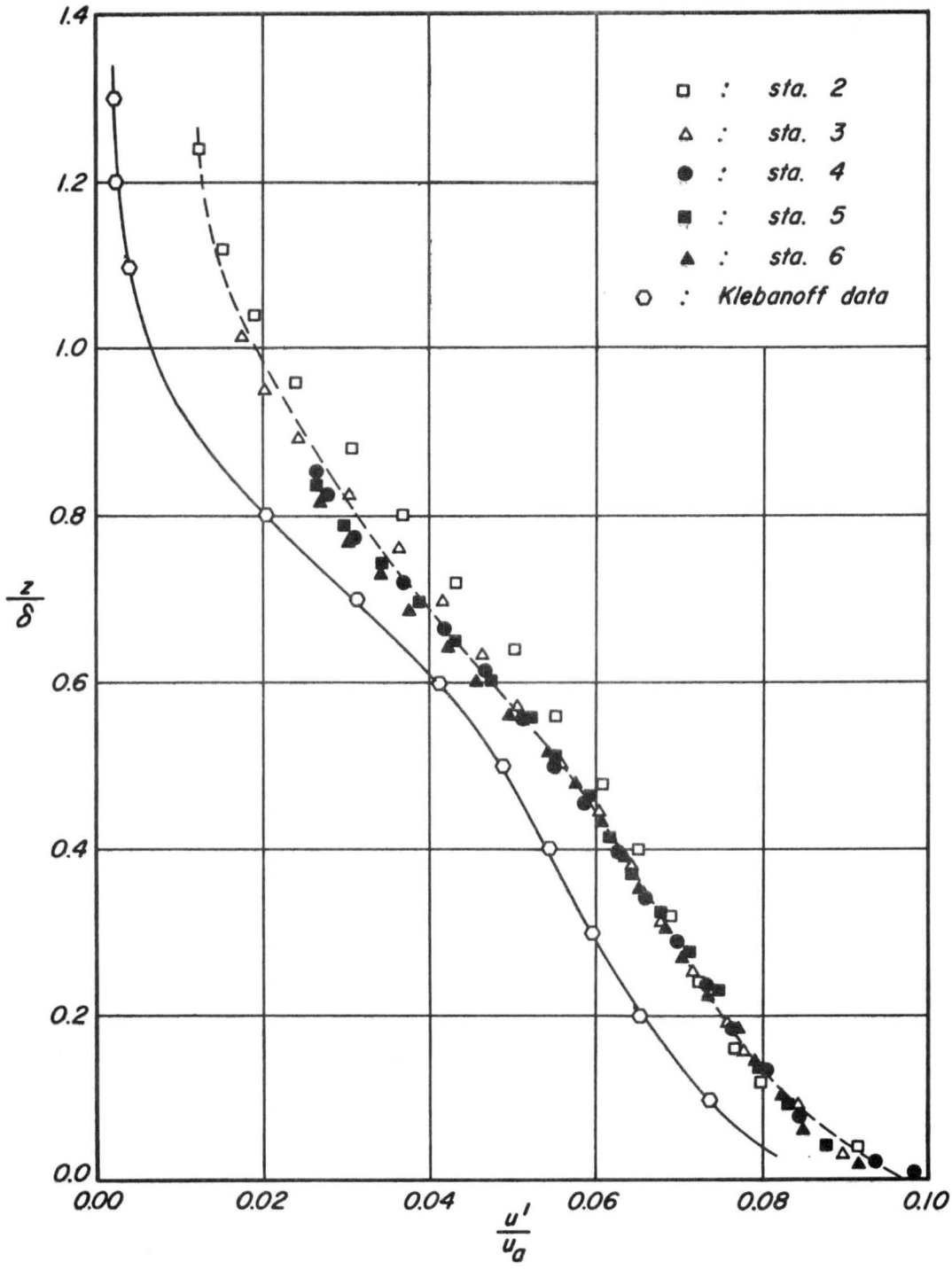

Fig. 30 Distribution of turbulence intensities on smooth flat plate.

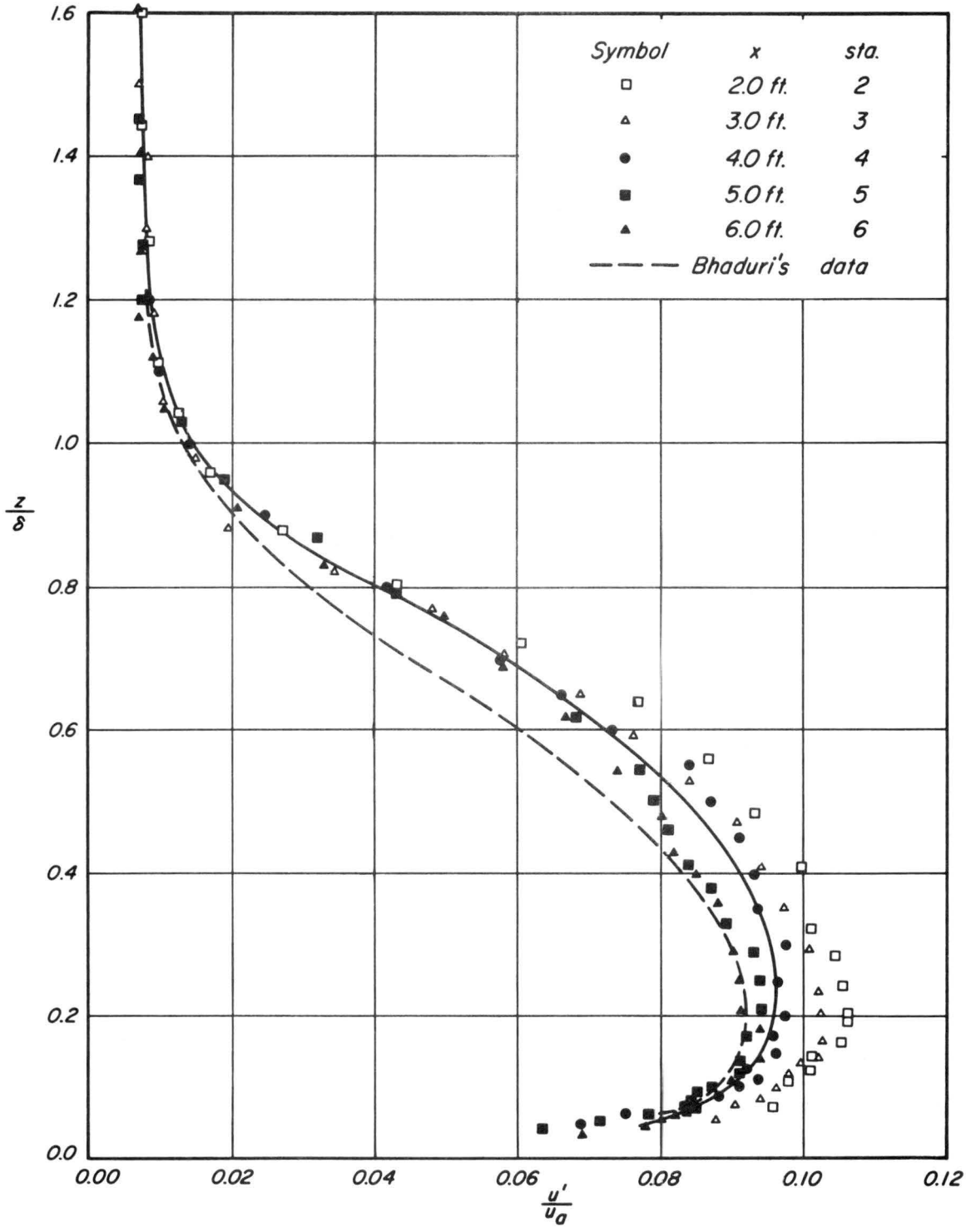

Fig. 31 Distribution of the turbulence intensities on rough flat plate.

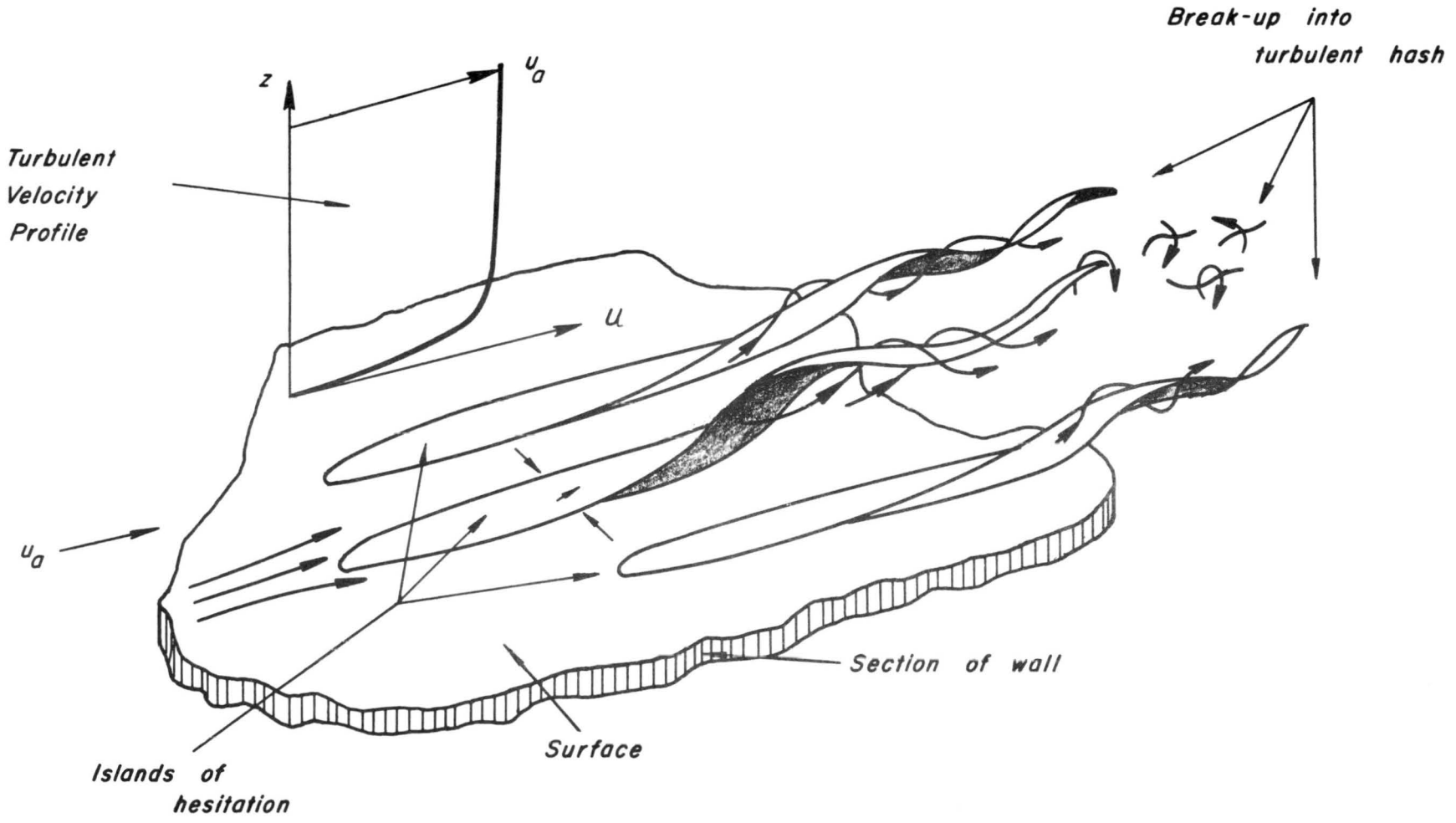

Fig. 32 Diagrammatic sketch of the flow model in the wall layers of the fully developed turbulent boundary layer after Kline and Runstadler.

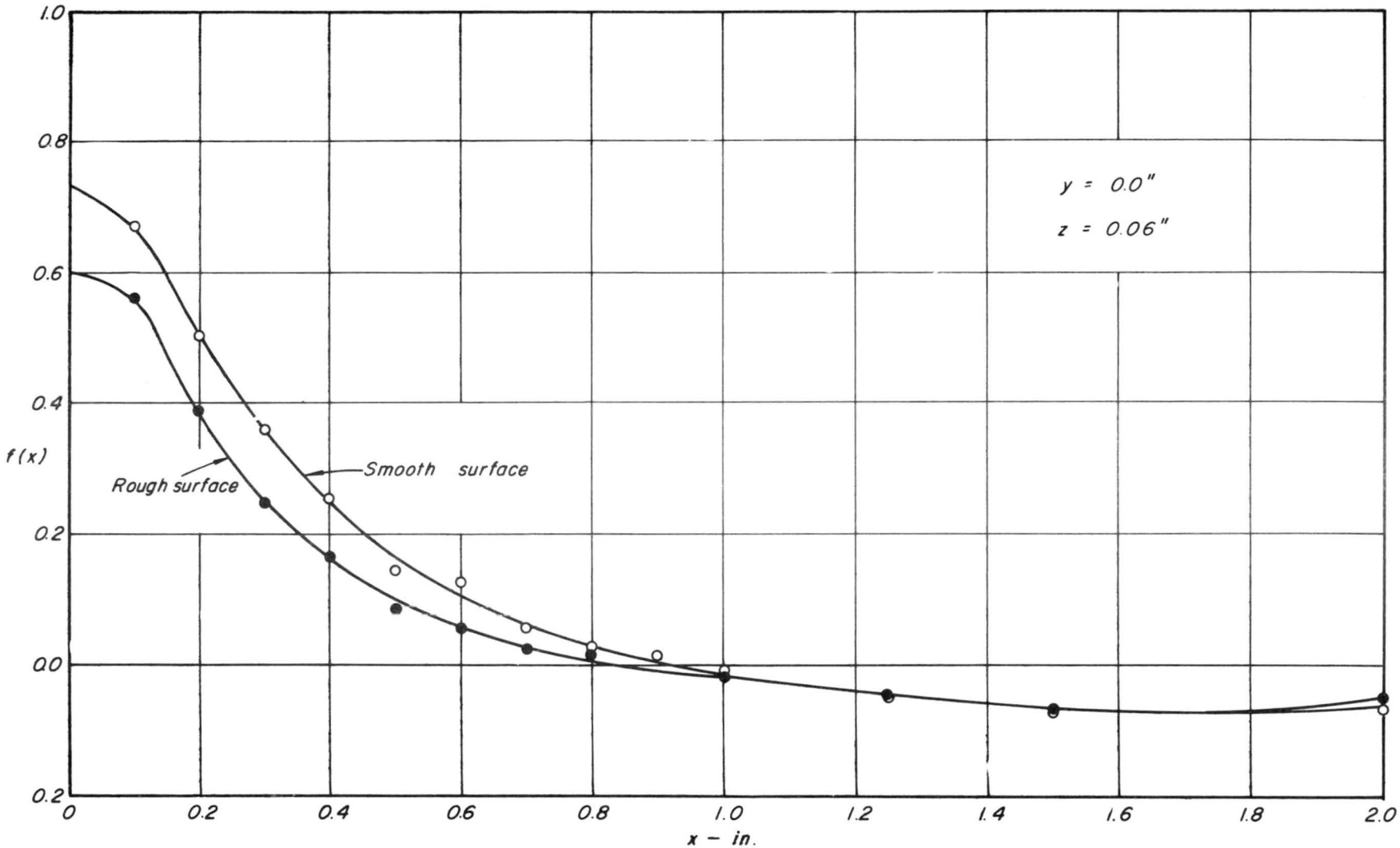

Fig. 33 Non-dimensional longitudinal space correlations on flat plate.

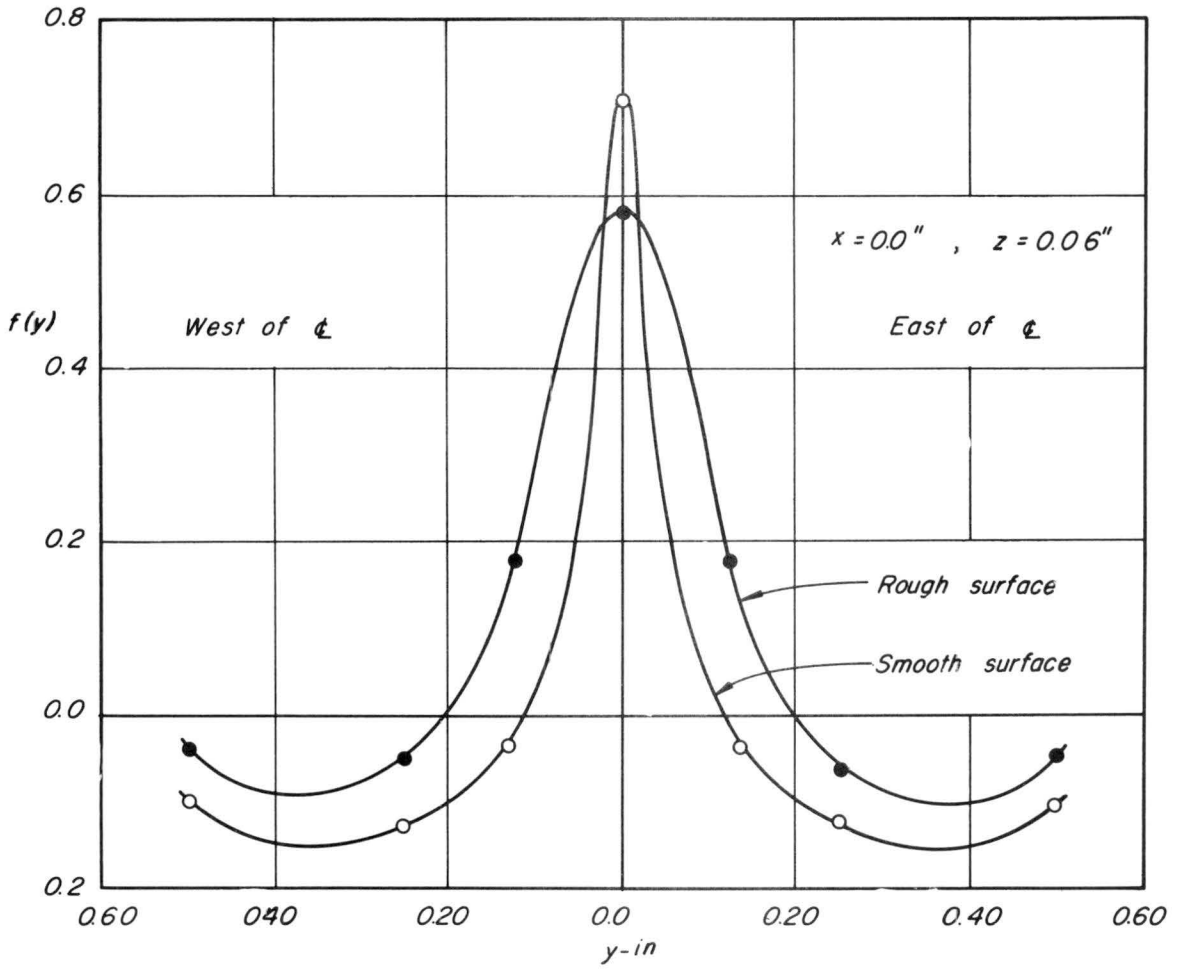

FIG. 34 Non-dimensional transverse space correlations on flat plate

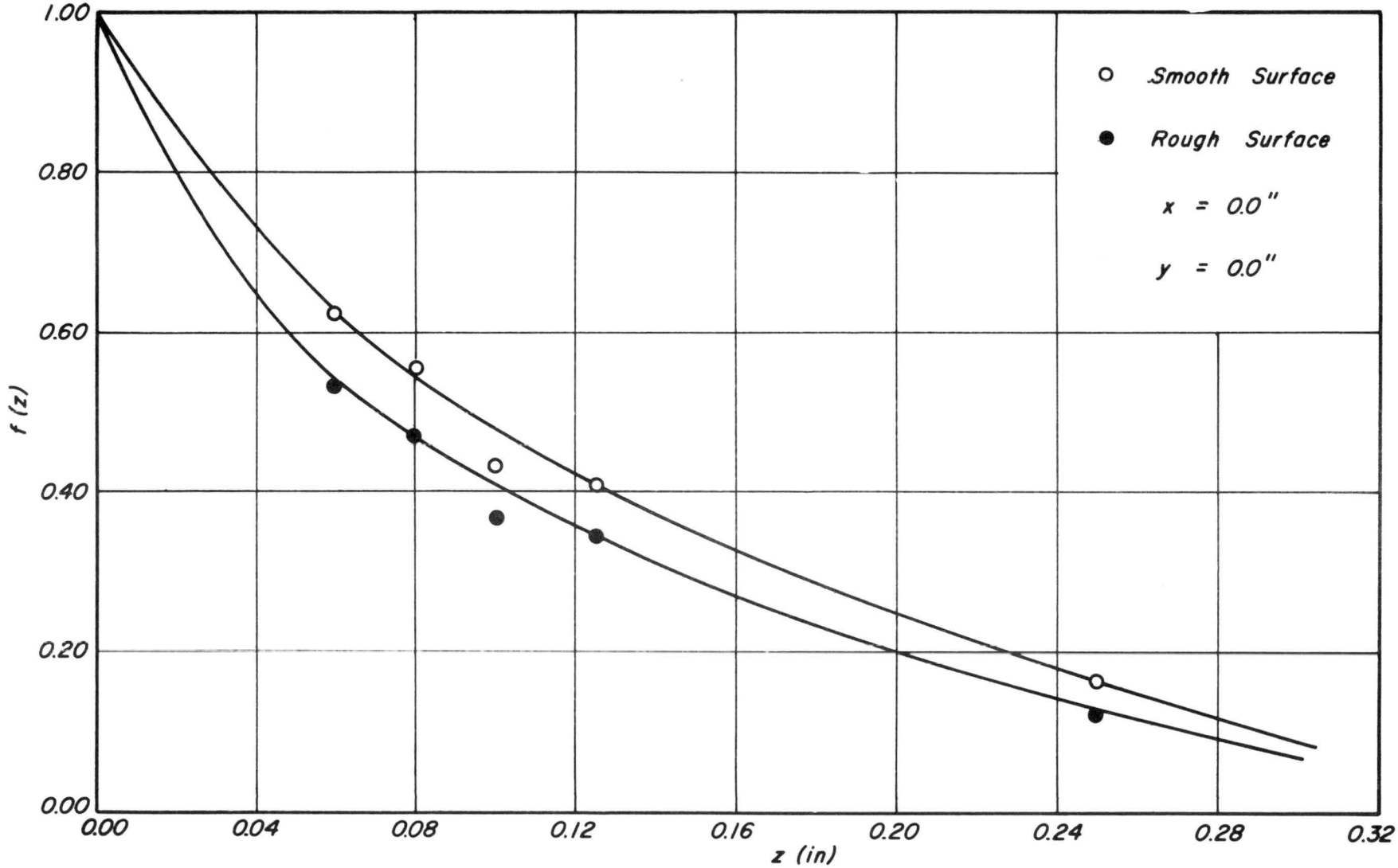

Fig. 35 Non-dimensional vertical space correlations on flat plate

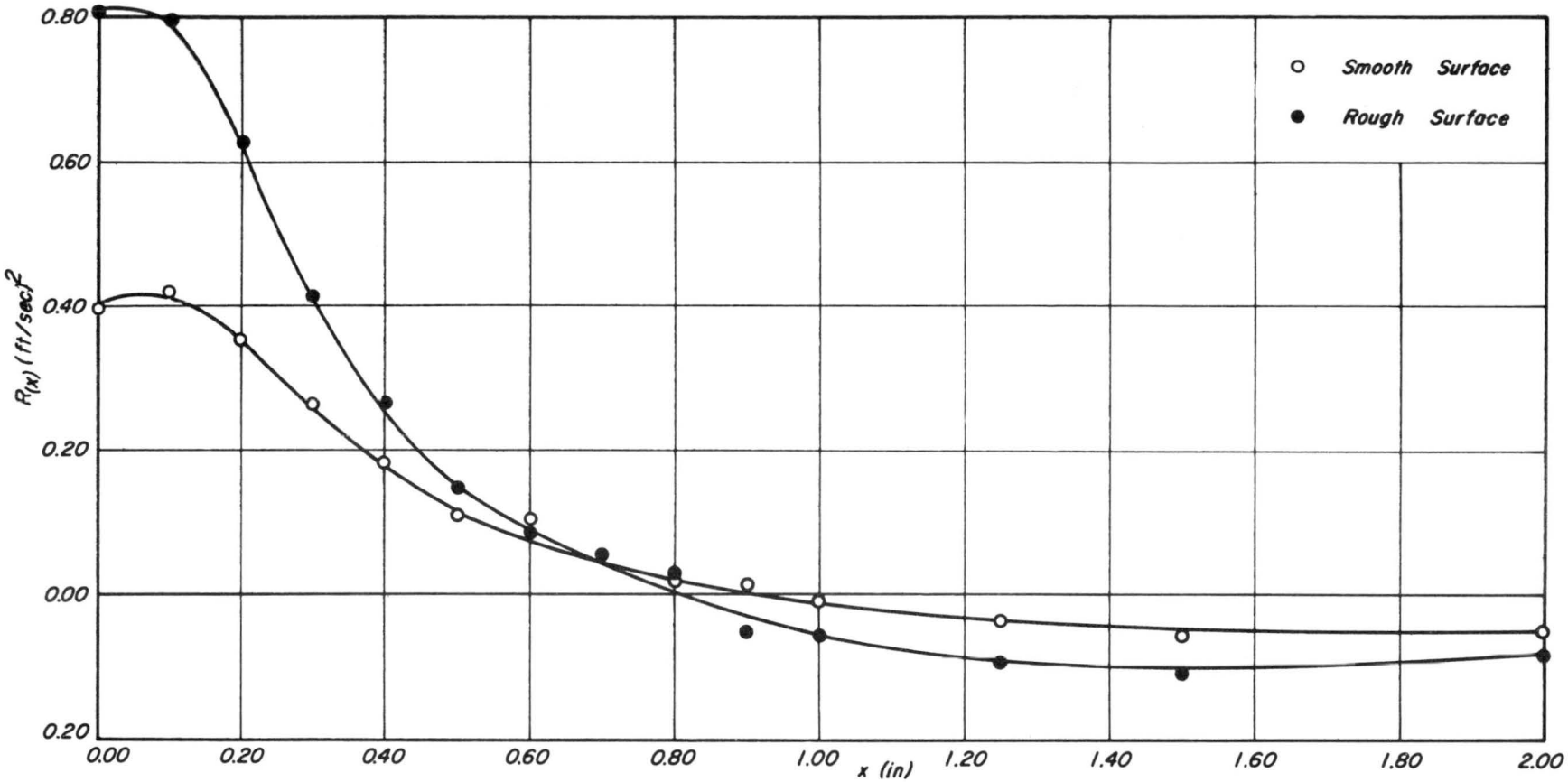

Fig. 36 Dimensional longitudinal space correlations on flat plate.

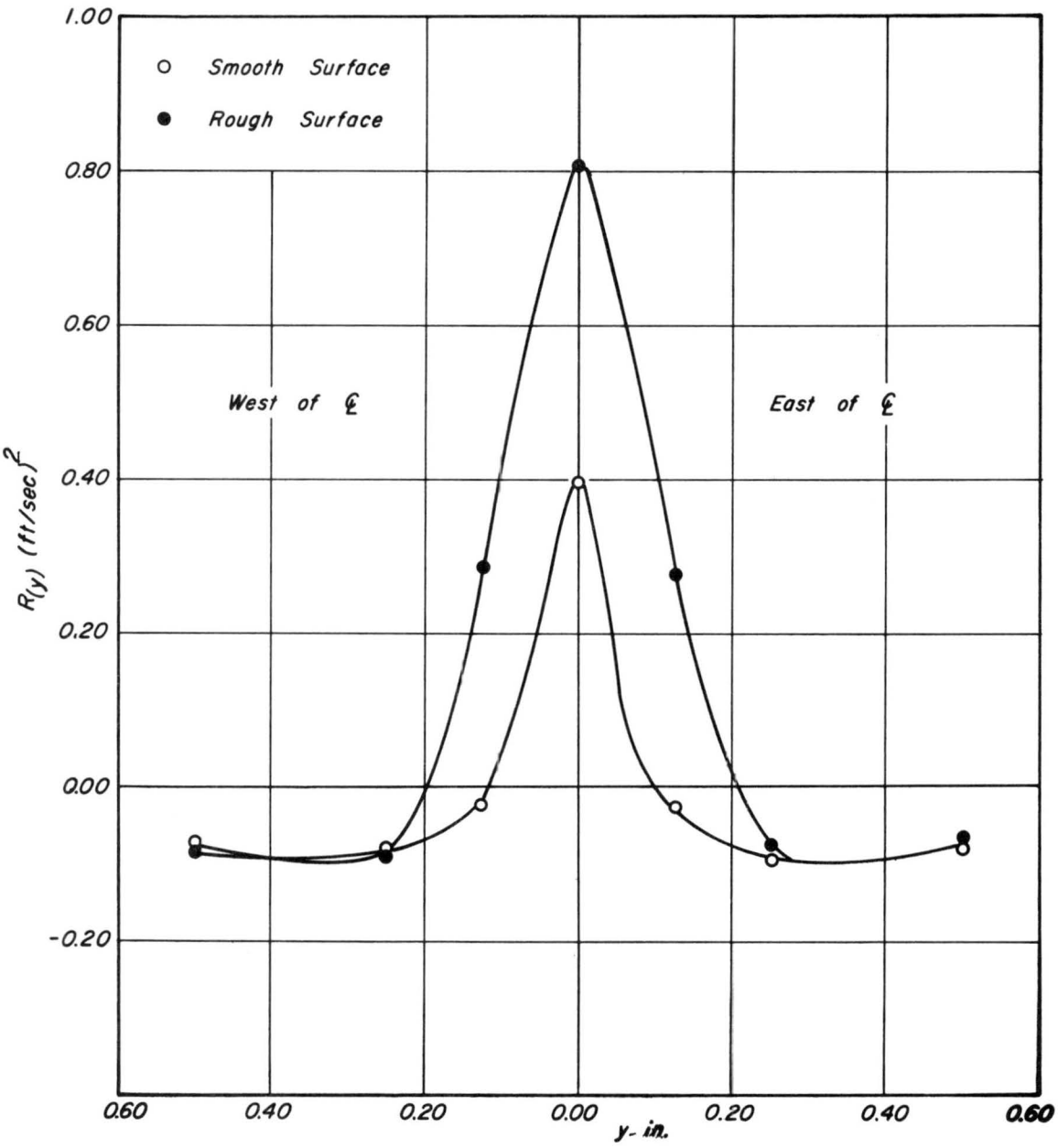

Fig. 37 Dimensional transverse space correlations on flat plate.

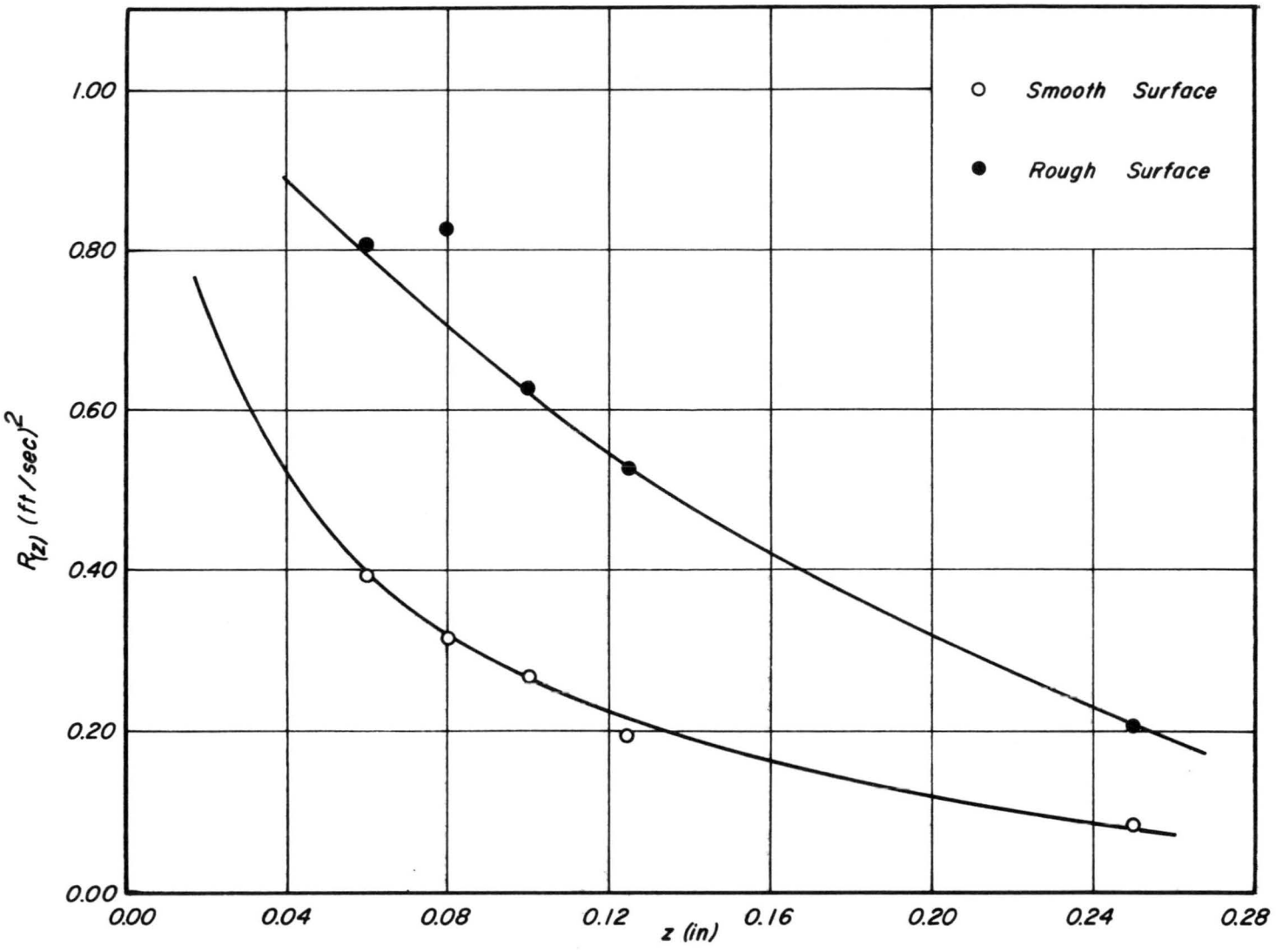

Fig. 38 Dimensional vertical space correlations on flat plate.

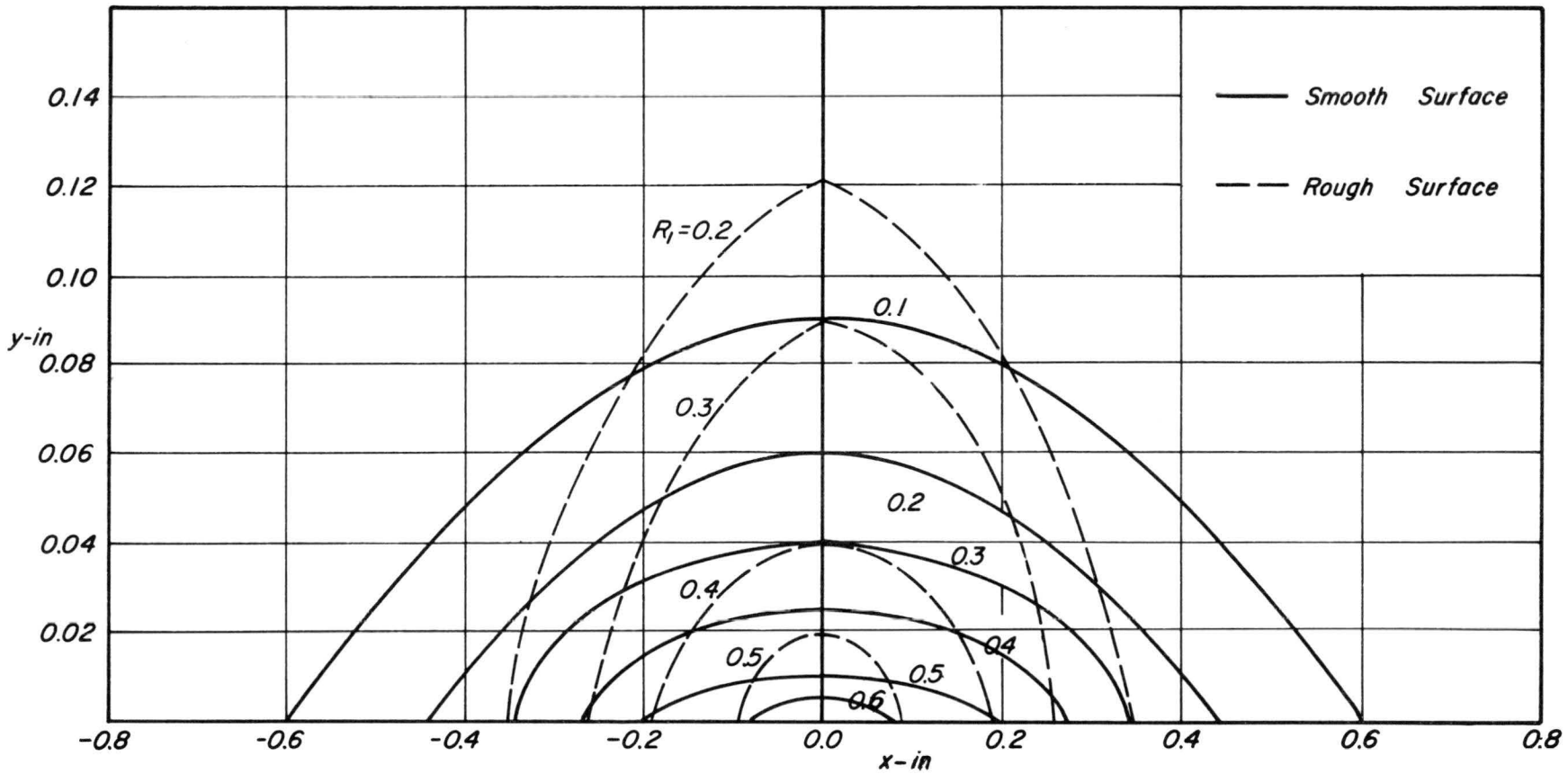

Fig. 39 Surfaces of total iso-correlations in x-y plane.

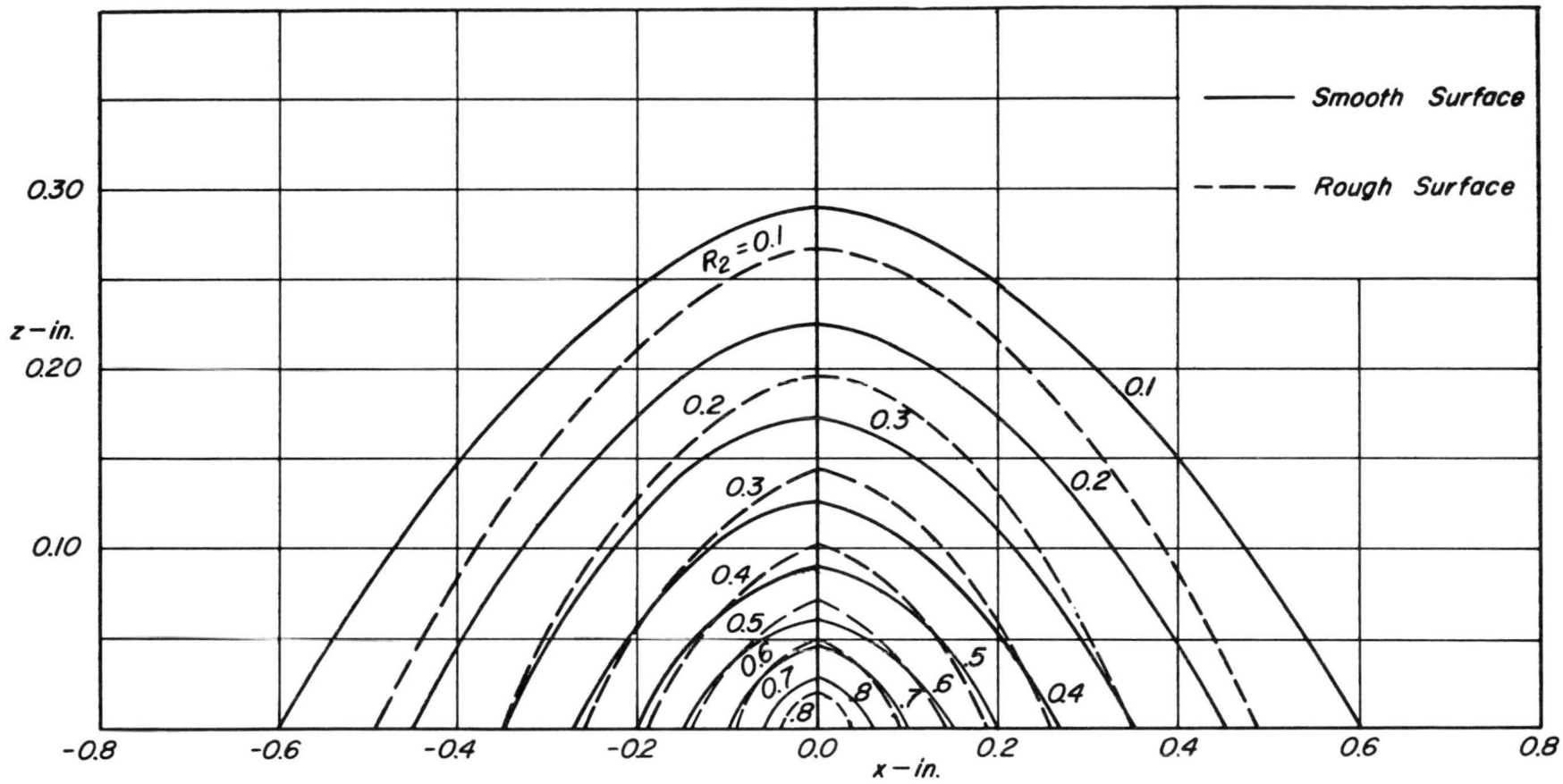

Fig. 40 Surfaces of total iso-correlations in x – z plane

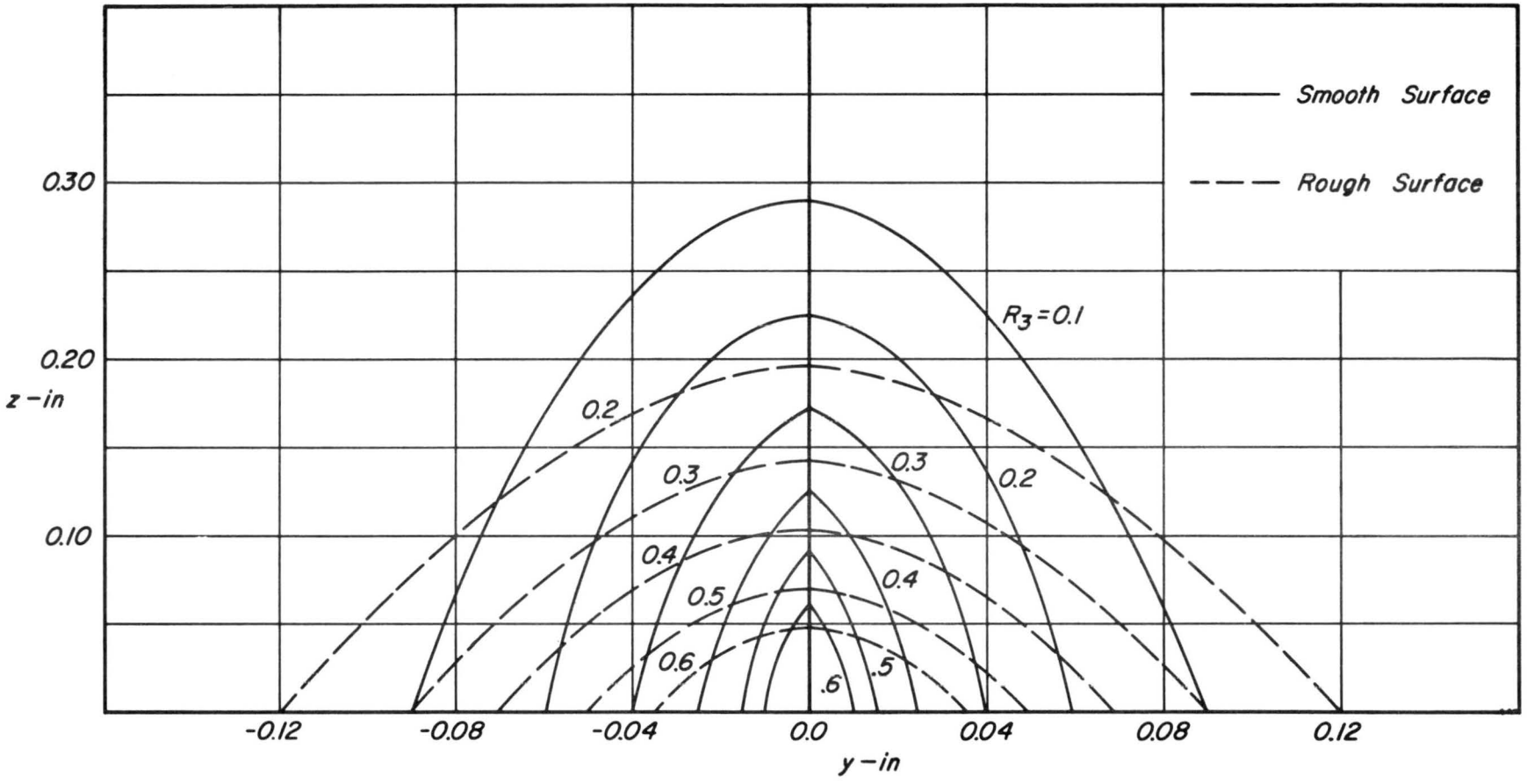

Fig. 41 Surfaces of total iso-correlations in y − z plane.

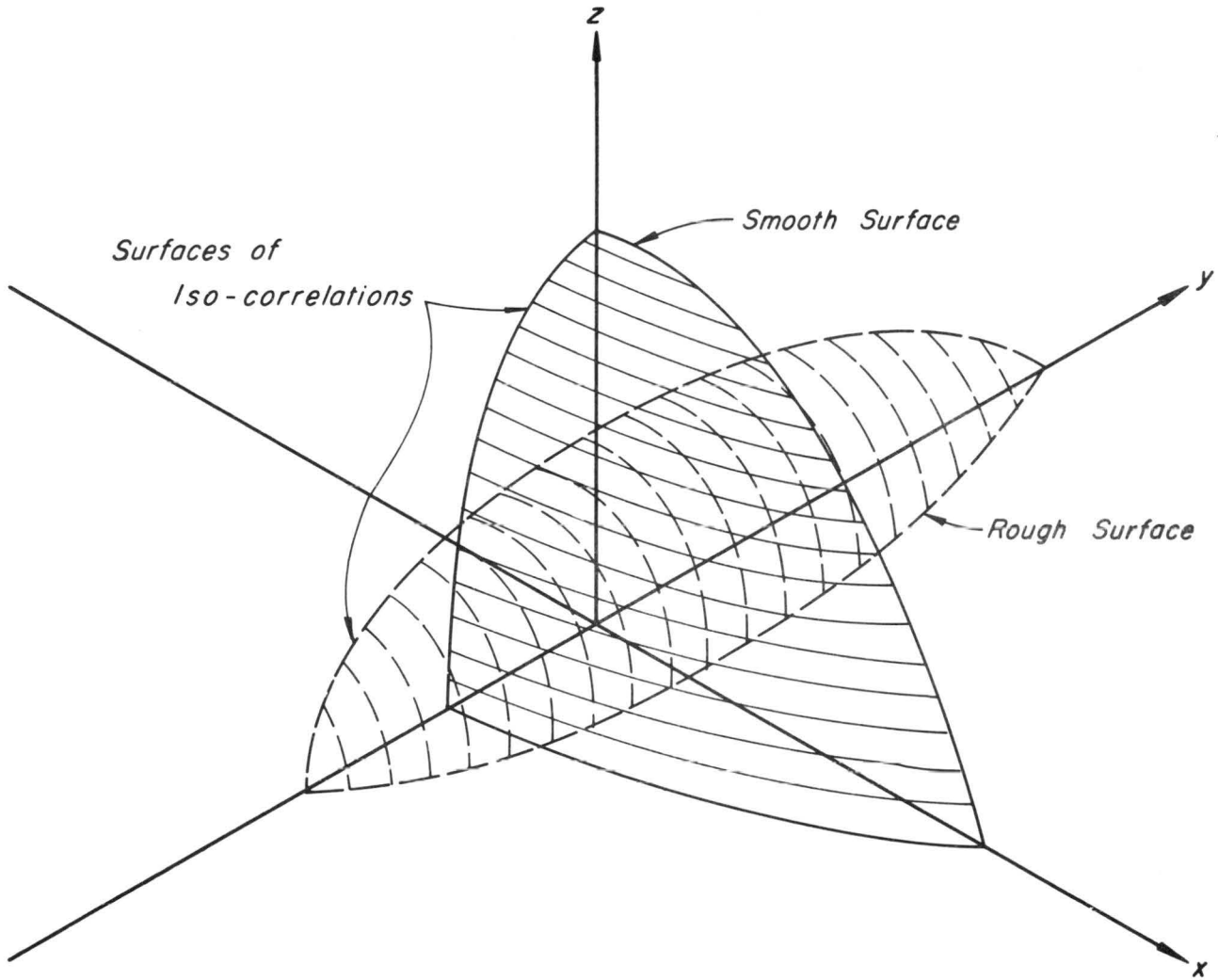

Fig. 42 Picture of the eddy structure in (x, y, z) plane on the flat plate.

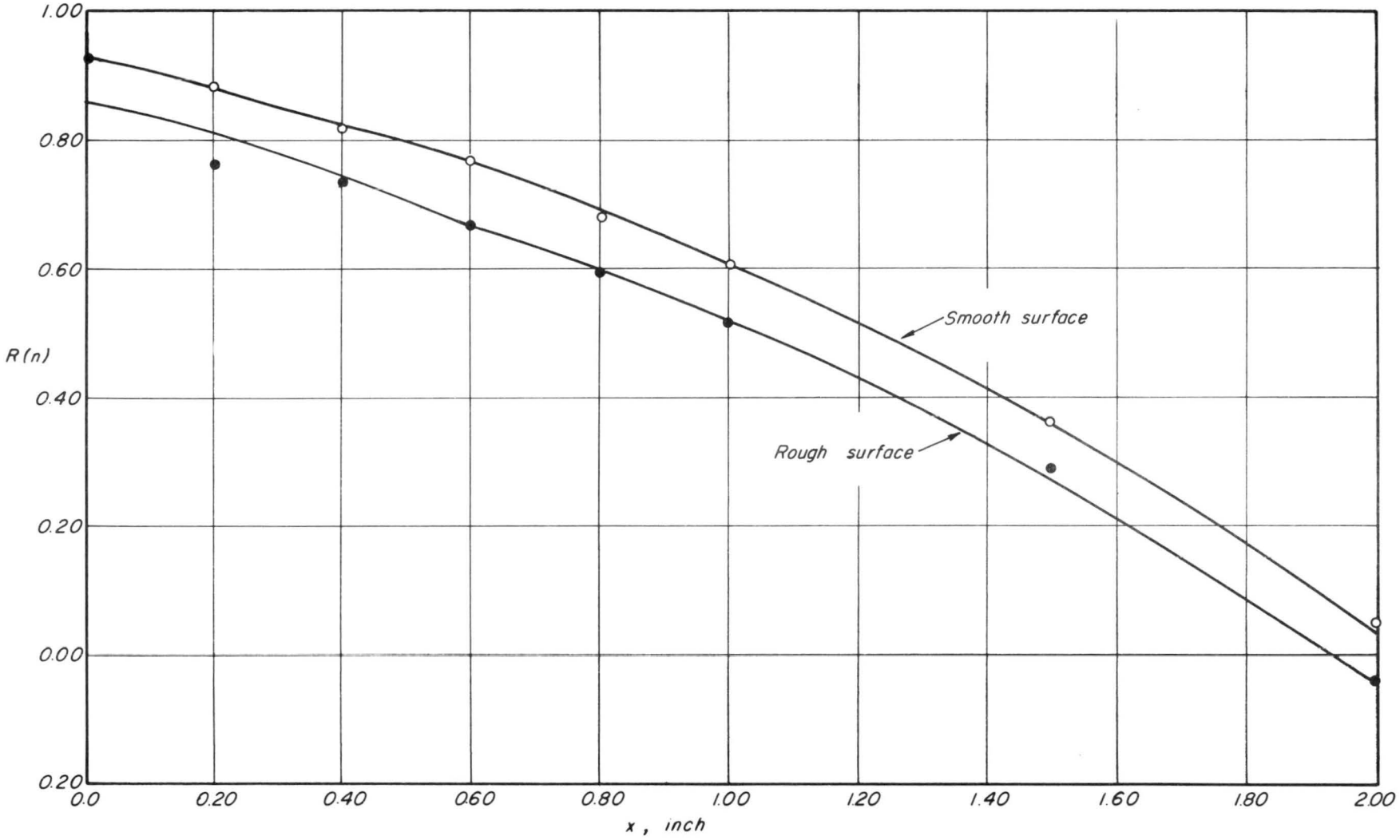

Fig. 43 Non – dimensional longitudinal filtered space correlations on flat plate. n = 20 C/S.

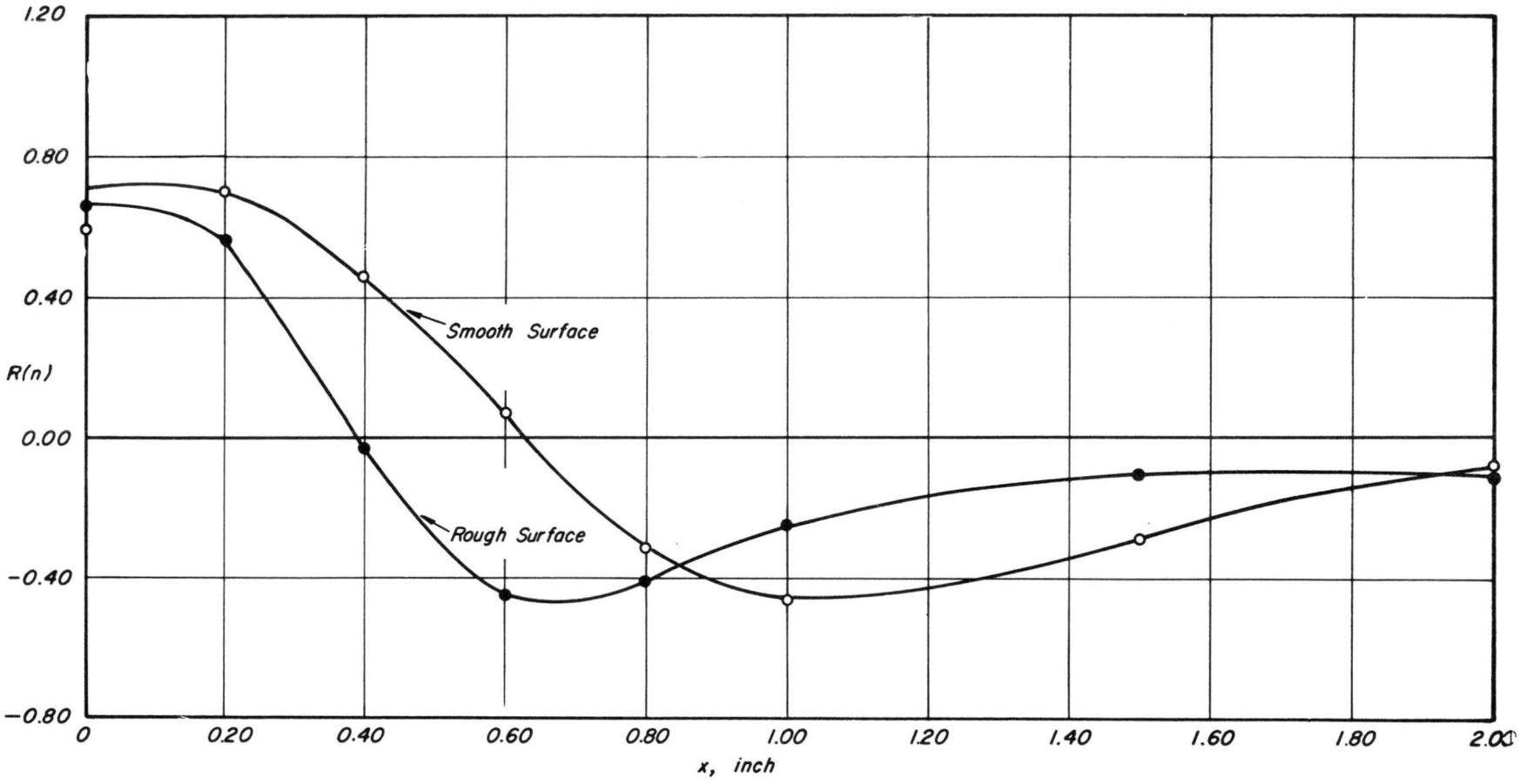

Fig. 44 Non – dimensional longitudinal filtered space correlations on flat plate. n= 100 C/S.

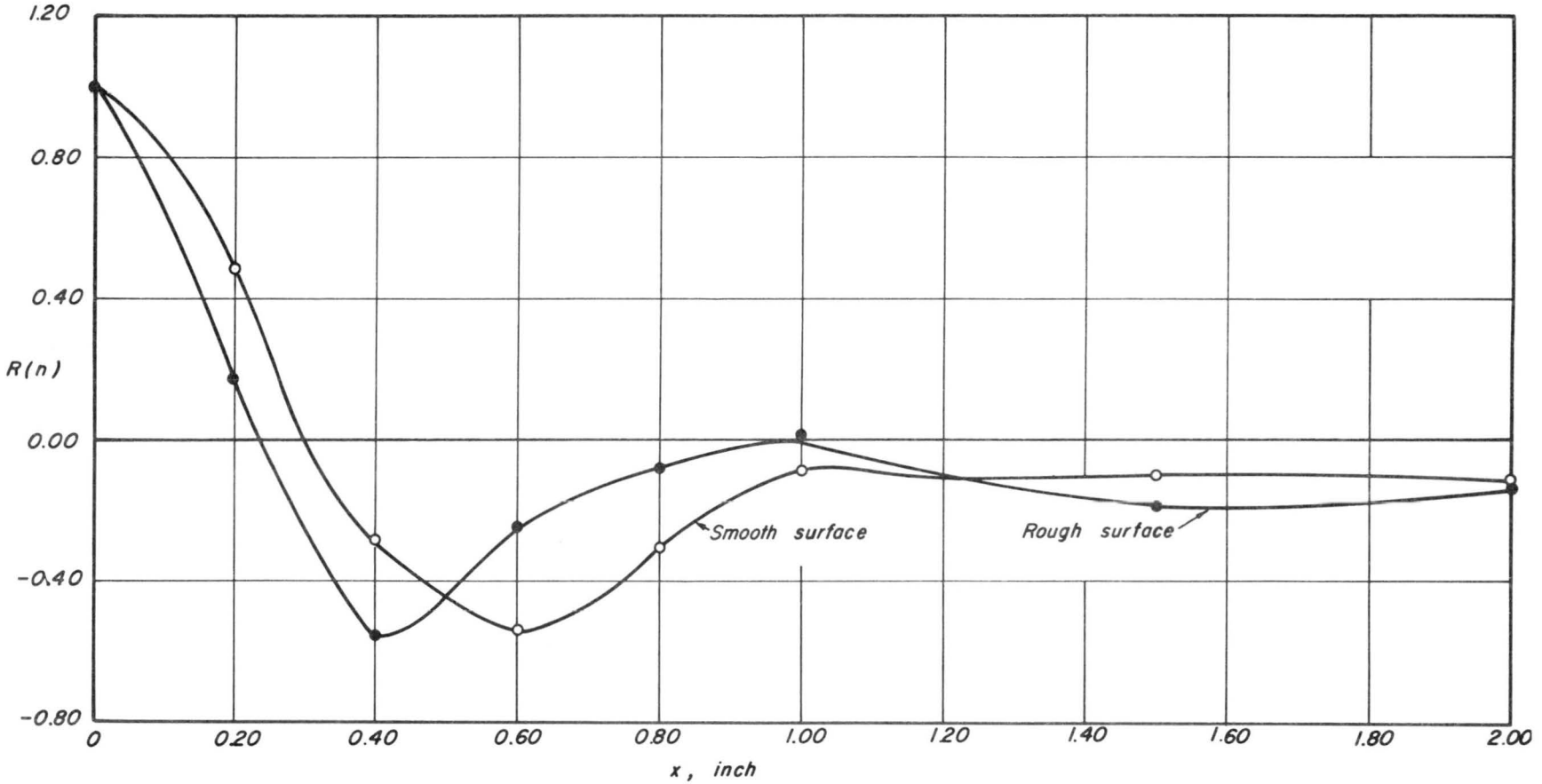

Fig. 45 Non-dimensional longitudinal filtered space correlations on flat plate. n=200 C/S.

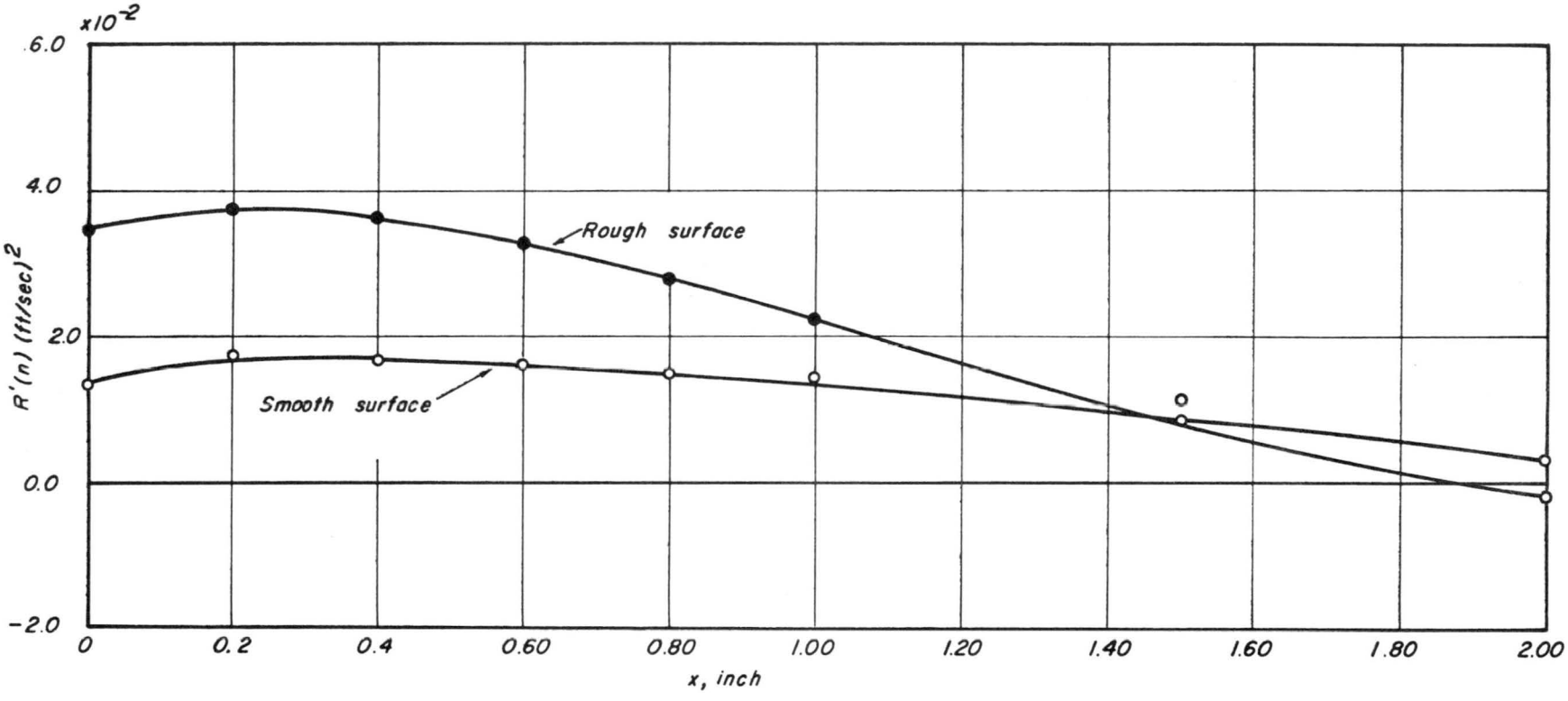

Fig. 46 Dimensional longitudinal filtered space correlations on flat plate. n = 20 C/S.

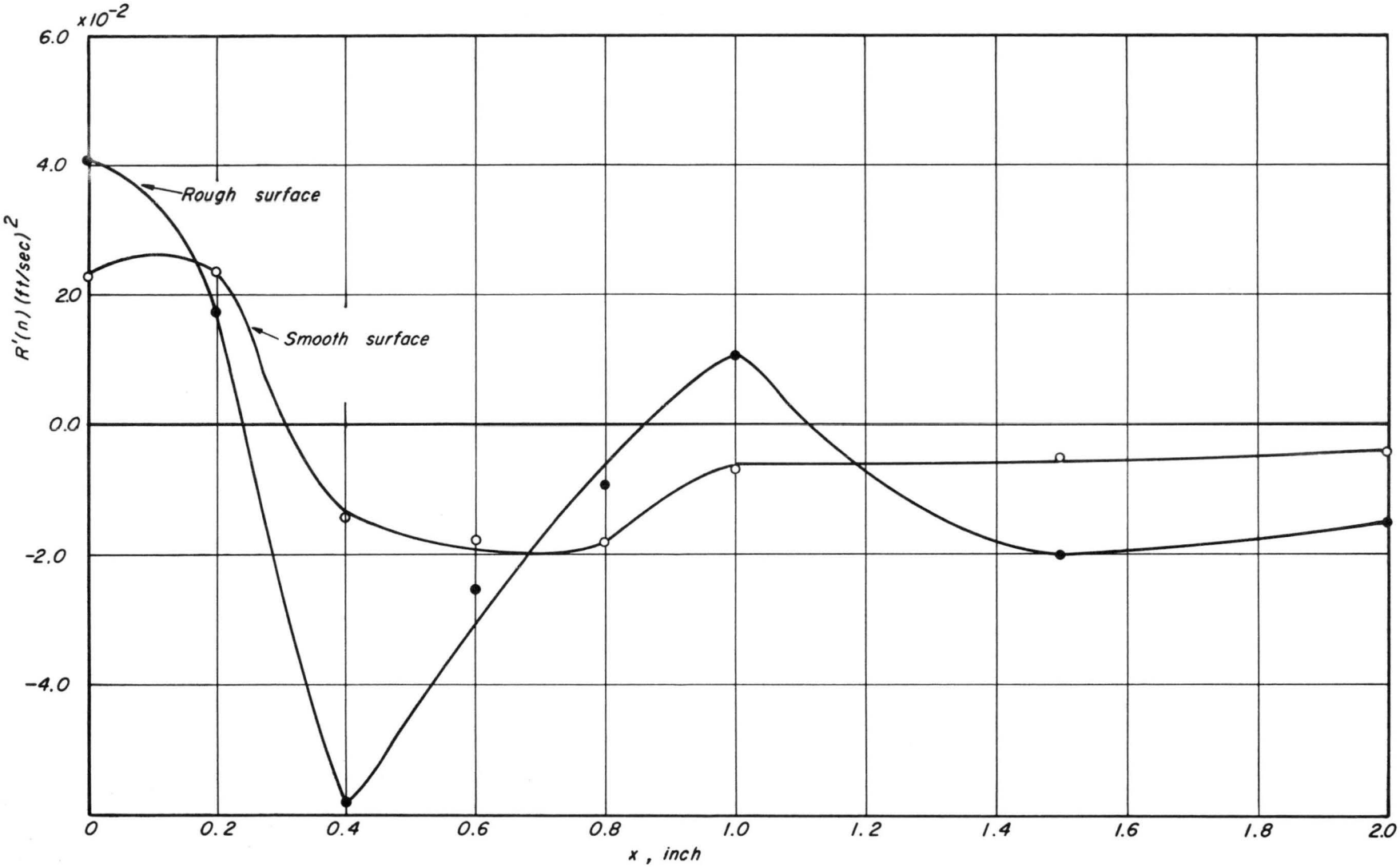

Fig. 47 Dimensional longitudinal filtered space correlations on flat plate n = 200 C/S.

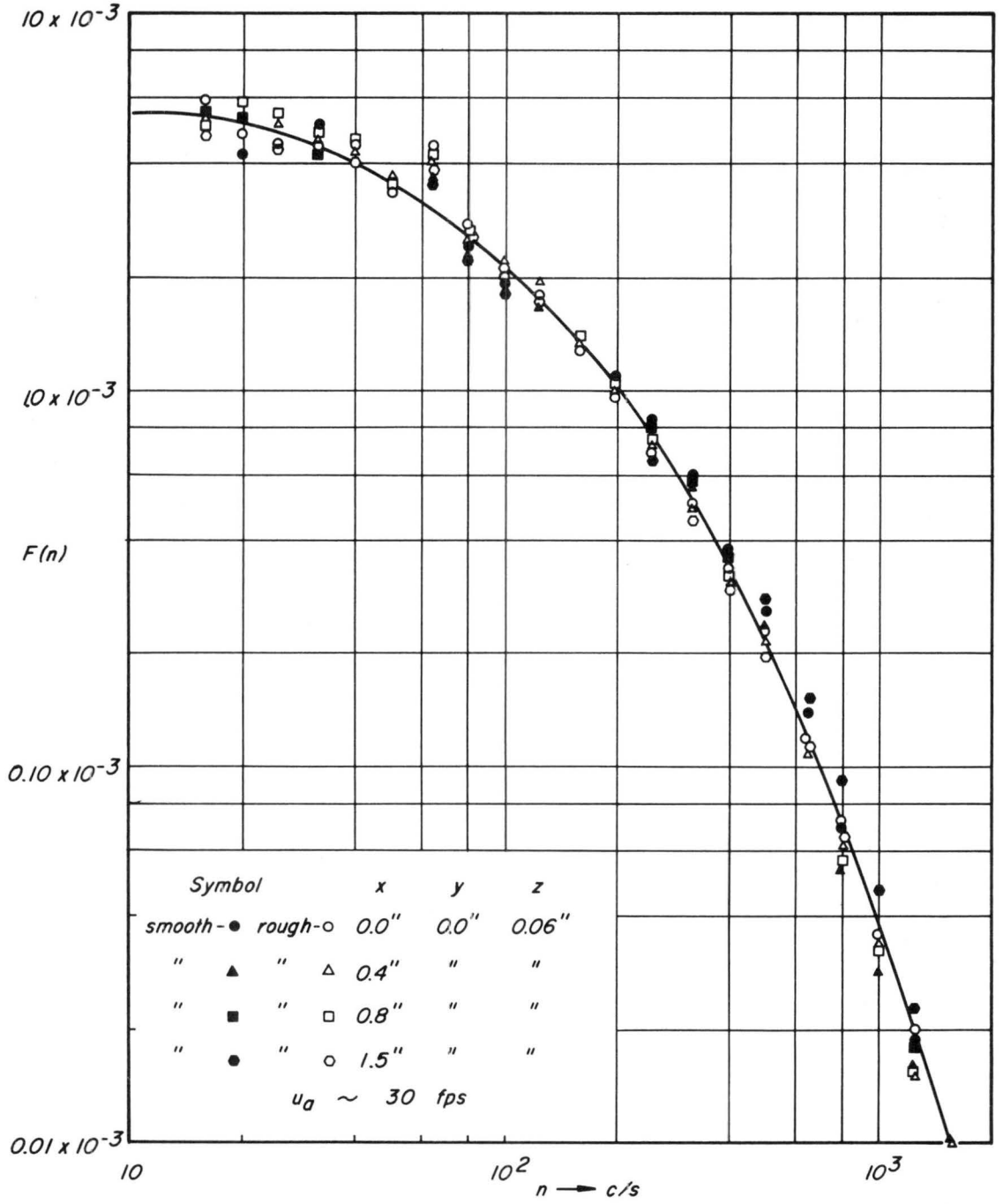

Fig. 48 Non-dimensional spectrum of turbulence signal (no. 1) on flat plate.

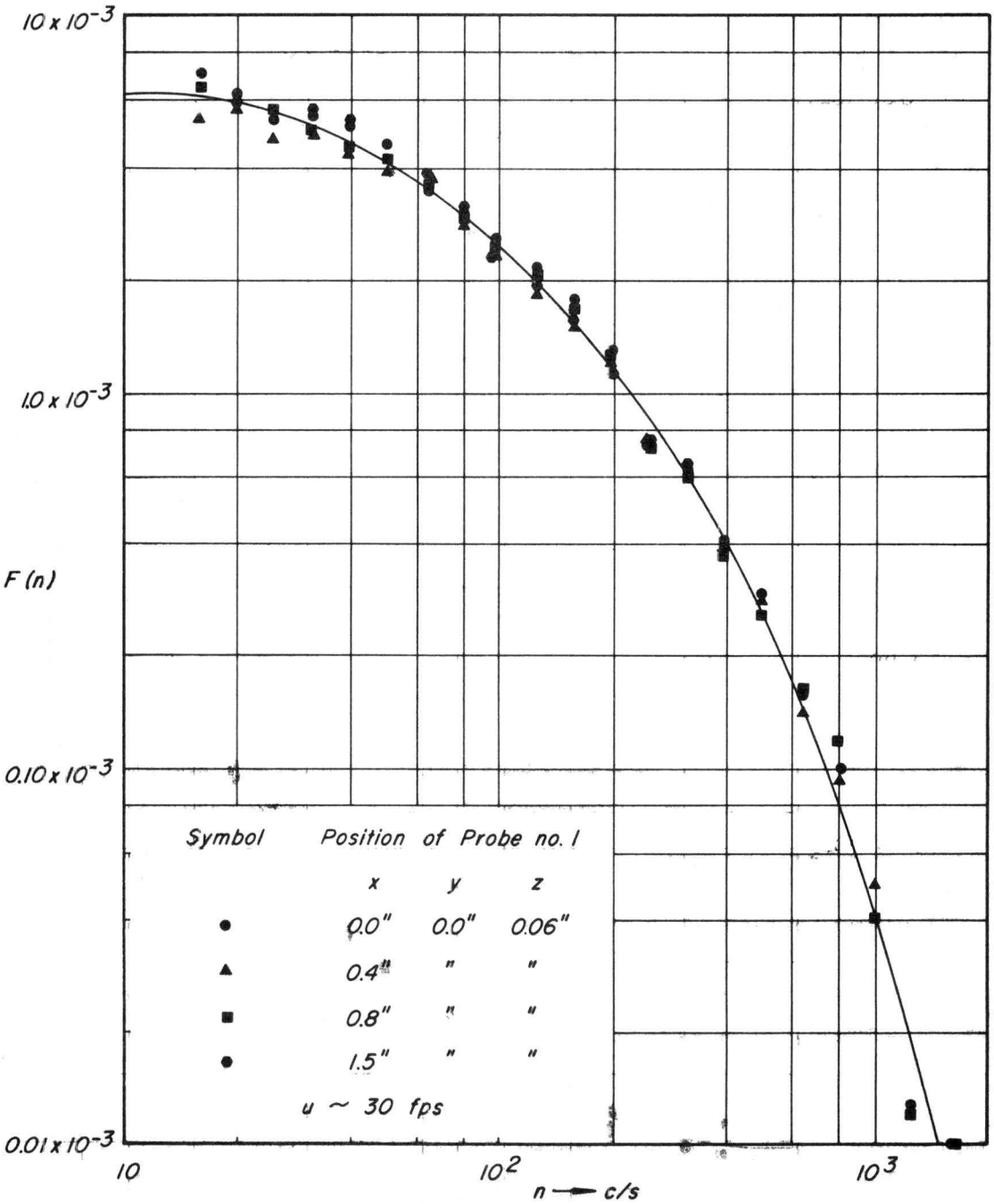

Fig. 49 Non-dimensional spectrum of turbulence signal (no. 2) on smooth flat plate.

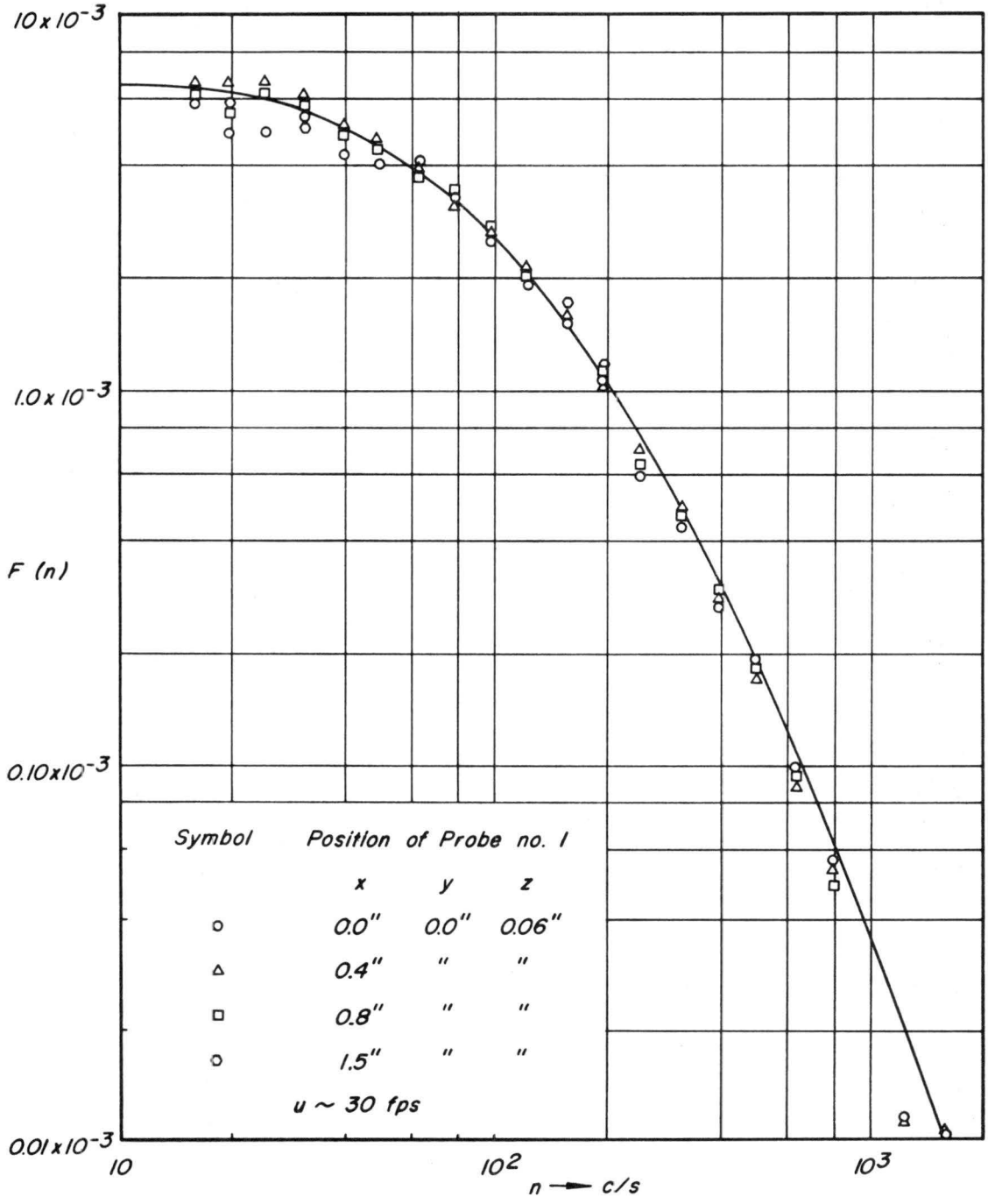

Fig. 50 Non-dimensional spectrum of turbulence signal (no. 2) on rough flat plate.

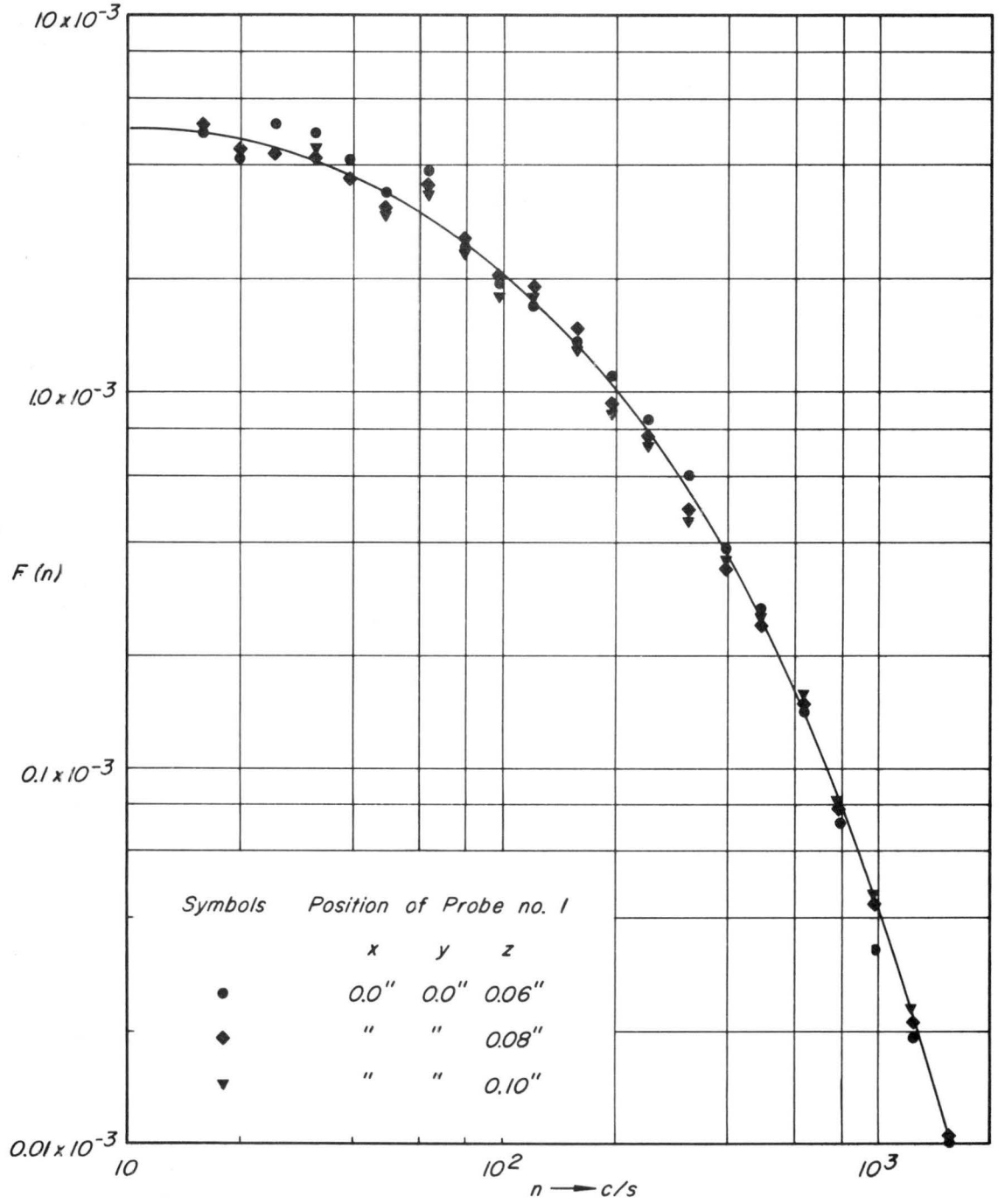

Fig. 51 Non-dimensional spectrum of turbulence signal (no. 1) on smooth flat plate.

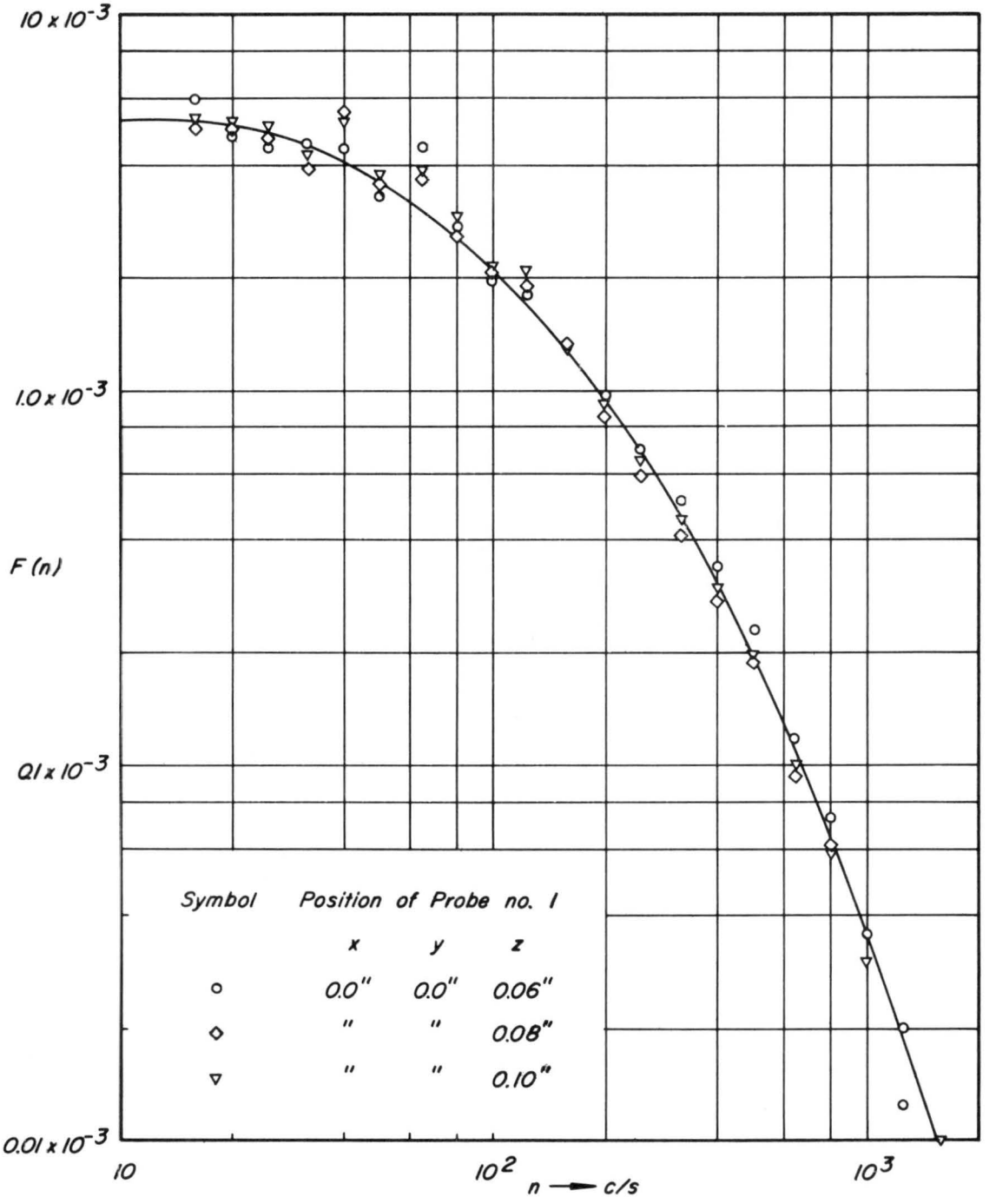

Fig. 52 Non-dimensional spectrum of turbulence signal (no. 1) on rough flat plate.

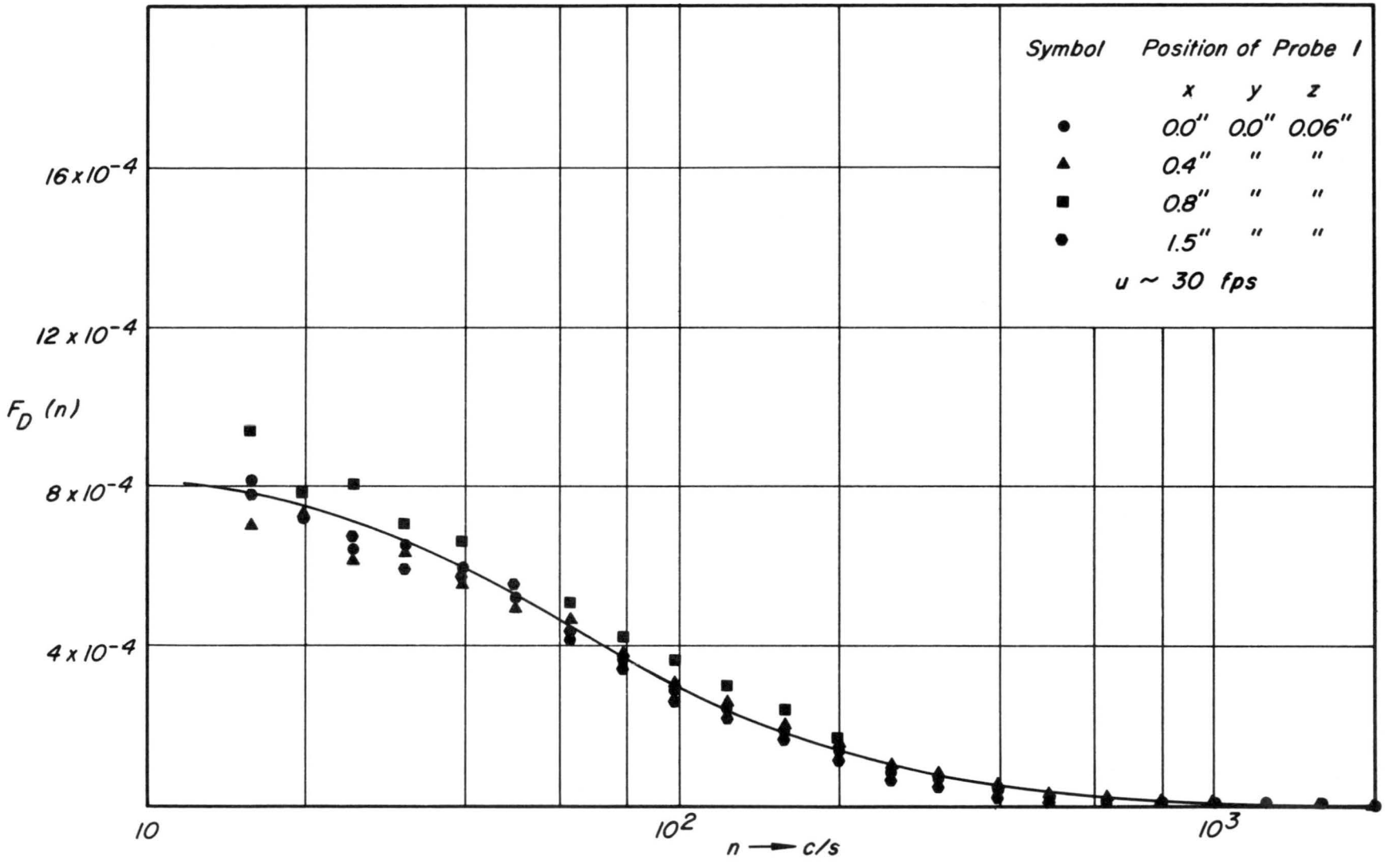

Fig. 53 Dimensional spectra of turbulence signals (no. 2) on smooth flat plate.

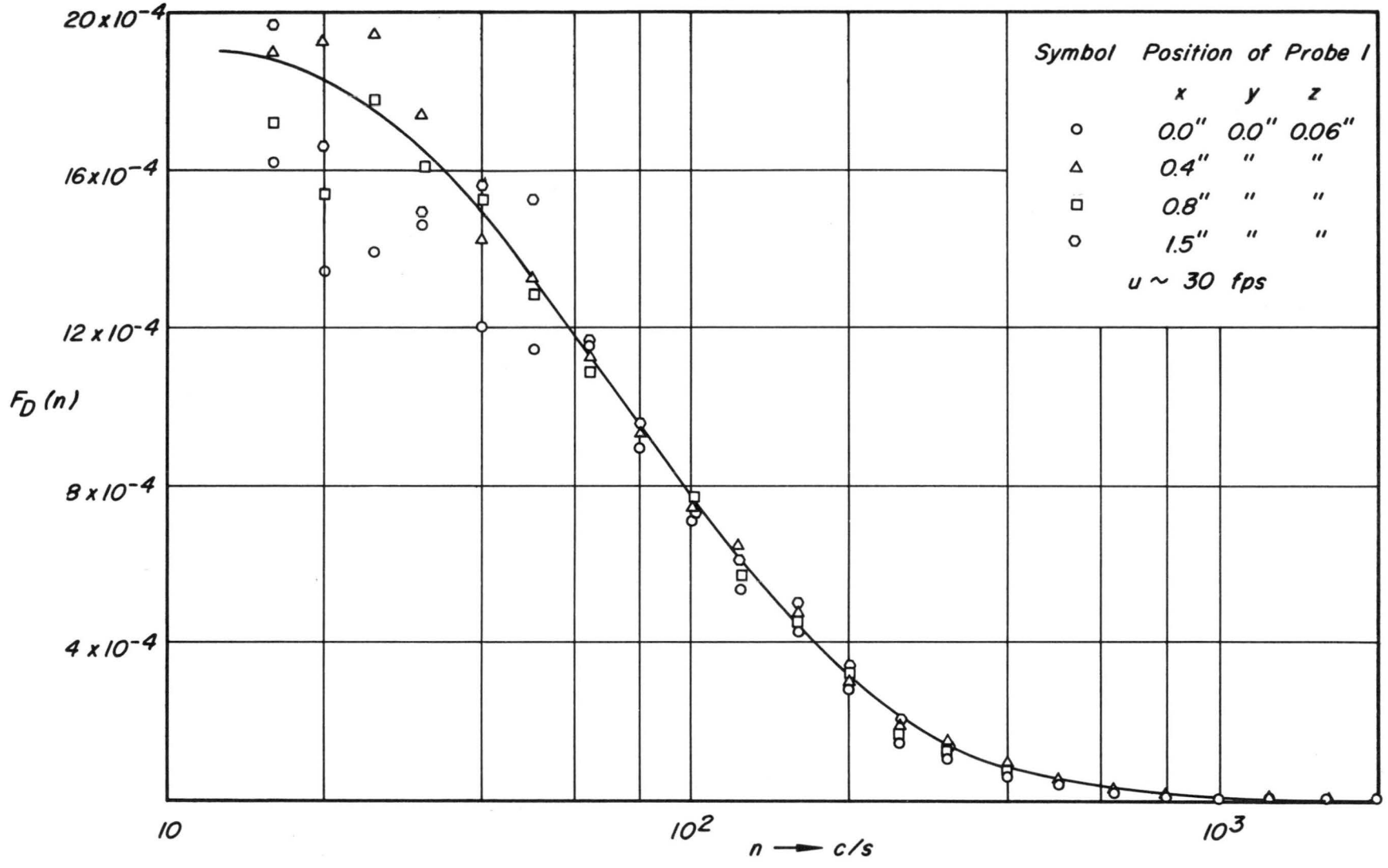

Fig. 54 Dimensional spectra of turbulence signals (no. 2) on rough flat plate.